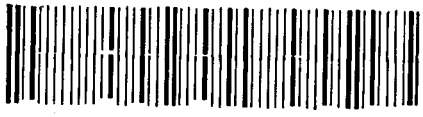

STUDIES OF THE DOUBLE LAYER AND EXCHANGE REACTIONS AT COPPER AND CADMIUM ELECTRODES

by

Roger James Latham

Supervisor: Dr. N.A. Hampson

Submitted for the degree of Doctor of Philosophy
of Loughborough University of Technology, April 1971.

SUMMARY

The structures of the electrical double layers at some metal/aqueous solution interphases have been studied. The kinetics of the exchange reactions at copper and cadmium electrodes have been investigated in selected electrolytes using a.c. impedance and galvanostatic techniques. The contributions by various possible steps to the overall exchange process have been investigated.

In nitrate electrolyte (NO_3^- not adsorbed) the component process controlling the rate of exchange at copper electrodes is shown (at ~ 40°C) to change from crystallisation (and dissolution of the lattice) to charge transfer. In sulphate electrolytes (SO_4^{2-} adsorbed at the electrode) the control is solely by the processes of crystallisation (and dissolution of the lattice).

The exchange process at a cadmium electrode system was found to be difficult to study in aqueous solution. The system is very susceptible to interference from impurities in the electrolyte. In $NaClO_4$ electrolyte the exchange process is controlled by crystallisation (and dissolution) effects. In alkaline electrolytes the exchange reaction is a very rapid process. In this case however, it is likely that the exchange proceeds via a surface film and there is no evidence for any crystallisation effects. For some metals, the mechanism of the exchange process (i.e. whether the reaction proceeds by surface diffusion or direct transfer to a kink site across the double layer) has been discussed in connection with the crystal structure.

ACKNOWLEDGEMENT

I would sincerely like to thank my supervisor, Dr. N.A. Hampson, for the help, encouragement and inspiration given to me during the past three years.

My thanks are also expressed to my fellow research students for their help and companionship; to Professor R.F. Phillips for providing the facilities for this research; to members of the technical staff of the Chemistry Department for their assistance and co-operation; to the Science Research Council for the provision of a research studentship; and finally to Miss E. Field for the care taken in typing this thesis.

CONTENTS

CHAPTER 1

INTRODUCTION

In recent years some progress has been made, both experimentally and theoretically, in the study of the electrochemical behaviour of solid metals. The use of experimental techniques which have been successfully employed in the study of amalgam systems, has been extended to the investigation of solid metal systems and the theory of the overall exchange process between atoms in the ordered lattice and ions in solution has been refined.

The study of rapid electrode processes requires the use of relaxation techniques, i.e. the behaviour of the electrode is studied during a relatively short time after departure from equilibrium caused by a change in the electrode potential. Electrochemical relaxation techniques may be classified as follows:-

1. galvanostatic,
2. potentiostatic,
3. a.c. impedance,
4. rotating disc and ring-disc electrodes.

Of the transient methods, the galvanostatic method was selected for use in this study since the results are easily abstracted and the instrumentation problems encountered are considerably less than those of the potentiostatic technique. Considerable experience in the use of the a.c. impedance technique has been accumulated in this laboratory and therefore this method of study was chosen for use in this investigation.

Many metal/metal ion exchange reactions at amalgam electrodes have been successfully studied using relaxation techniques. However, in addition

to charge transfer and diffusion in solution, the overall electrode process at a solid metal electrode is complicated by the processes of inclusion and release of metal atoms into and from the ordered lattice. Studies of solid metal systems are also further complicated by the difficulties of reproducing clean electrode surfaces.

The marked effect on electrode processes of trace impurities in solution was first discussed by FRUMKIN and PROSKURNIN (1). The presence of traces of organic compounds in solution usually markedly reduces the value of the differential capacitance. Exchange reactions at solid metal electrodes proceed via a relatively low number of active sites on the surface, and the adsorption of impurities must therefore be avoided. Hence throughout this experimental work particular attention was paid to cleanliness of glassware and solution purification.

FRUMKIN (2-4) has also discussed the importance of studies of the double layer and the significance of the potential of zero charge. Consequently the studies of the kinetics of exchange reactions in this work were preceeded by an investigation of the electrode/electrolyte interphase.

It is important to extend the range of studies of exchange reactions at solid metal electrodes. The Cd(II)/Cd exchange at solid electrodes has been little studied and has been shown (5) to be particularly sensitive to solution impurities and nature of the electrolyte. As a comparison it was decided also to study the kinetics of exchange at a solid copper electrode, for which considerably more experimental data was available. A preliminary investigation showed that the copper system was much less susceptible to impurities in solution. This contrast in experimental behaviour,

coupled with the differences in metallurgical character, makes the cadmium and copper electrode systems a suitable choice for study.

CHAPTER 2

THEORETICAL PRINCIPLES

2.1. THE ELECTRICAL DOUBLE LAYER

The earliest and most simple model of the electrical double layer at an electrode/electrolyte interphase is due to HELMHOLTZ (6). GOUY (7) and CHAPMAN (8) developed the concept of the diffuse layer rather than the compact layer of HELMHOLTZ (6) since this considers that there is thermal motion of the ions in the electrolyte. However, comparison of experimental results with values calculated from the GOUY-CHAPMAN (7, 8) theory reveals discrepancies due to the fact that ions are considered as point charges and thus may approach to within infinitely small distances of the electrode surface. STERN (9) postulated that the model should include a plane of closest approach for the ions and consequently the overall double layer has a compact layer and then a diffuse layer extending into the bulk of the electrolyte. GRAHAME (10) improved the STERN (9) model and represented the compact layer as:-

(a) The inner Helmholtz plane which is governed by the plane of closest approach of solvent dipoles and specifically adsorbed ions.

(b) The outer Helmholtz plane which is determined by the plane of closest approach of solvated cations.

Figure 1 shows the generally accepted model (10) of the electrical double layer. Using this model GRAHAME (10) has shown that the total double

FIG. 1 Model of the electrical double layer.

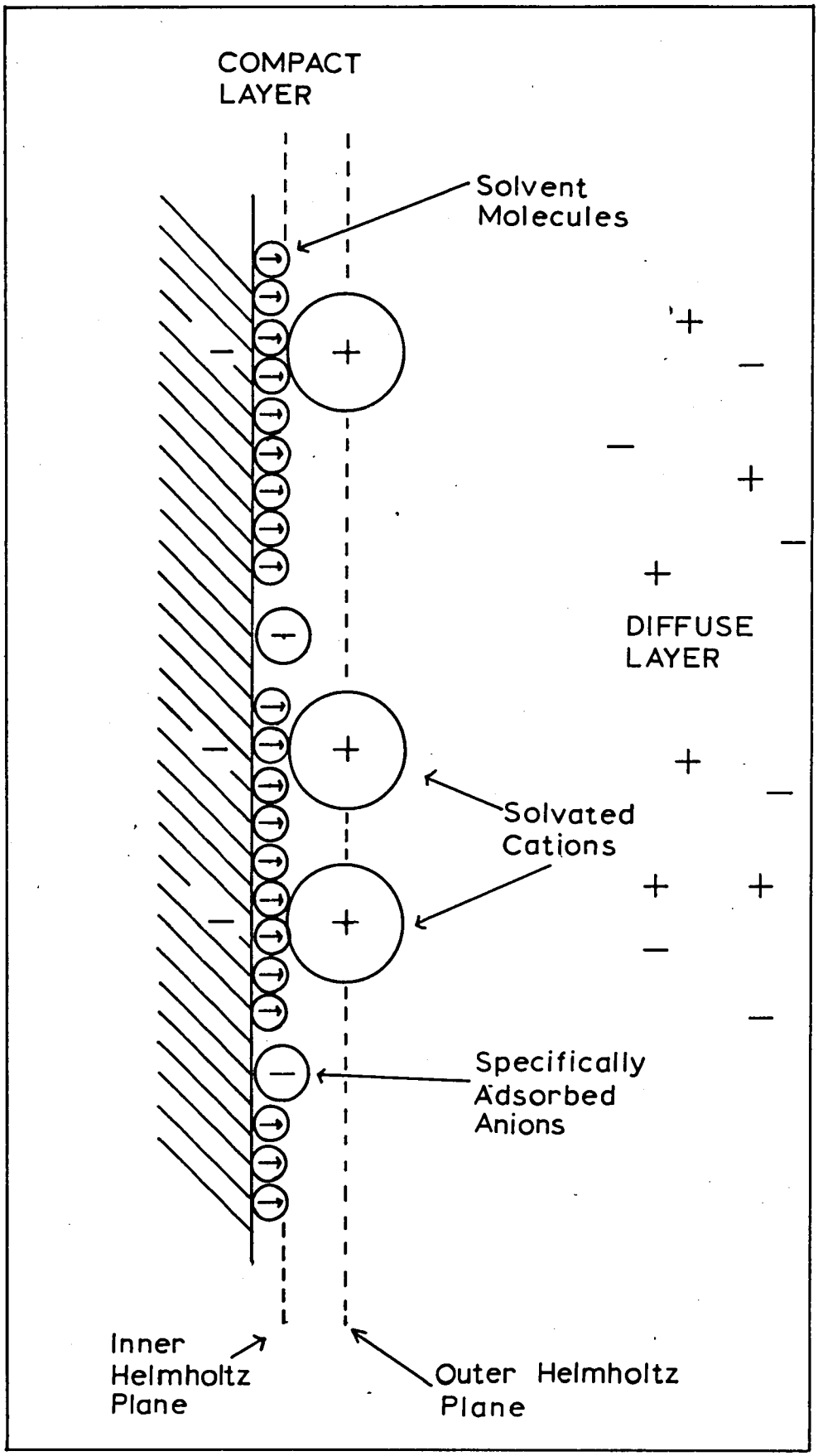

layer capacitance could be represented by:-

$$\frac{1}{C_L} = \frac{1}{C_{diff.}} + \frac{1}{C_{comp.}} \qquad [1]$$

where C_L = total double layer capacitance

$C_{diff.}$ = capacitance of diffuse layer

$C_{comp.}$ = capacitance of compact layer,

and a relationship for the diffuse layer capacitance is found to be given by:-

$$C_{diff.} = \left(\frac{\varepsilon^2 F^2 \epsilon_{2-s} C^S}{2\pi RT}\right)\left[\cosh\left(\sinh^{-1} \frac{\pi}{2 RT \epsilon_{2-s} C^S} qn\right)\right] \qquad [2]$$

where ε, F, R and T have the usual significance

ϵ_{2-s} = dielectric constant of diffuse layer

C^S = bulk concentration of electrolyte

This expression predicts that the magnitude of $C_{diff.}$ increases or decreases with the corresponding change in electrolyte concentration. GRAHAME (11, 12) has shown that, using this model, calculated and measured values of the double layer capacitance are in reasonable agreement.

More recently LEVINE et al. (13) and BARLOW and MACDONALD (14) have considered discreteness of charge effects in the double layer. A much better comparison of experimental data and theoretical curves is obtained when discreteness effects are considered. As yet, however, discreteness of charge effects have only been considered for the diffuse double

layer and there is no complete treatment (involving all discreteness effects) available. However, at present there appears to be no way of applying the more sophisticated calculations to the experimental situation (15).

The importance of the potential of zero charge has been thoroughly discussed by FRUMKIN (2-4). Equation [2] predicts that as the charge on the electrode, q_n, passes through zero, the value of $C_{diff.}$ passes through a minimum. Thus the value of the p.z.c. (or E_z) can be obtained from differential (double layer) capacitance vs. potential curves. The charge on the electrode plays an important role in determining which species may be adsorbed at the surface. The magnitude of the charge is determined by the quantity $(E - E_z)$, which is referred to as the rational potential, E_r. At positive E_r, adsorption of negative ions is favoured and at negative E_r positive ions are attracted to the interphase. Likewise when there is little or no charge on the electrode, when the magnitude of E_r is small, adsorption of neutral molecules competes favourably with ionic adsorption. Thus a study of the differential capacitance and a knowledge of the p.z.c. is an important precursor to the study of an exchange reaction at an electrode/electrolyte interphase, since the most favourable experimental conditions may then be predicted.

2.2. THE CHARGE TRANSFER PROCESS

The transference of charge across the double layer gives rise to an overpotential, η_D. The equation for the current-overpotential relationship in the presence of excess supporting electrolyte was first derived by ERDEY-GRUZ and VOLMER (16)

$$i = i_o \left[\exp - \frac{\alpha\ z\ F\ \eta_D}{RT} - \exp \frac{(1-\alpha)\ z\ F\ \eta_D}{RT} \right] \qquad [3]$$

HORIUTI and POLANYI (17) have also verified that this relationship follows from a quantum mechanical treatment*.

For low overpotential ($|\eta_D| << \frac{RT}{zF}$), the overpotential-current curve is linear and the proportionality between overpotential and current corresponds to an electrical resistance:- the charge transfer resistance, R_D.

$$R_D = -\left(\frac{d\eta_D}{di}\right)_{i \longrightarrow 0} \qquad [4]$$

Differential of the ERDEY-GRUZ and VOLMER (16) equation and putting $\eta_D = 0$ gives:-

$$\left(\frac{di}{d\eta_D}\right)_{\eta = 0} = -\frac{zFi_o}{RT} \qquad [5]$$

Hence:-

$$R_D = \frac{RT}{zF} \cdot \frac{1}{i_o} \qquad [6]$$

Thus the exchange current density may be obtained from the charge transfer

---

*Footnote

MARCUS (19) has shown that the transfer coefficient is a function of several terms which are not independent of potential. However, α becomes independent of potential if the double layer effects are small and the potential is not far removed ($\pm$ 250 mV) from the equilibrium. In the present work the potential excursion from the equilibrium does not exceed this limit and the double layer effects can be considered constant in the presence of a large concentration of supporting electrolyte.

resistance at the equilibrium ($\eta = 0$).

The ERDEY-GRUZ and VOLMER (16) equation for high cathodic overpotentials gives the TAFEL (18) relationship.

$$\eta_D = \frac{RT}{\alpha zF} \log i_o - \frac{RT}{\alpha zF} \log i \qquad [7]$$

and for high anodic overpotentials*

$$\eta_D = \frac{RT}{(1-\alpha)zF} \log i_o + \frac{RT}{(1-\alpha)zF} \log i \qquad [8]$$

Hence the magnitude of the exchange current density may also be obtained from high overpotential measurements extrapolated back to the equilibrium potential.

The dependence of exchange current on reactant concentration has also been established (20). In the case of the reaction:-

$$O + ze = R \qquad [9]$$

we have

$$i_o = zFK^o \; a_R^{\alpha} \; a_O^{1-\alpha} \qquad [10]$$

a_R and a_O are usually replaced by the corresponding concentrations, since activities are unknown.

2.3. INTERPRETATION OF IMPEDANCE DATA

When a faradaic reaction occurs at the interphase the impedance

---

*Footnote · Throughout this work α corresponds to the cathodic process.

FIG. 2 Electrical analogues of the electrode interphase.

(a) Charge transfer and diffusion control.

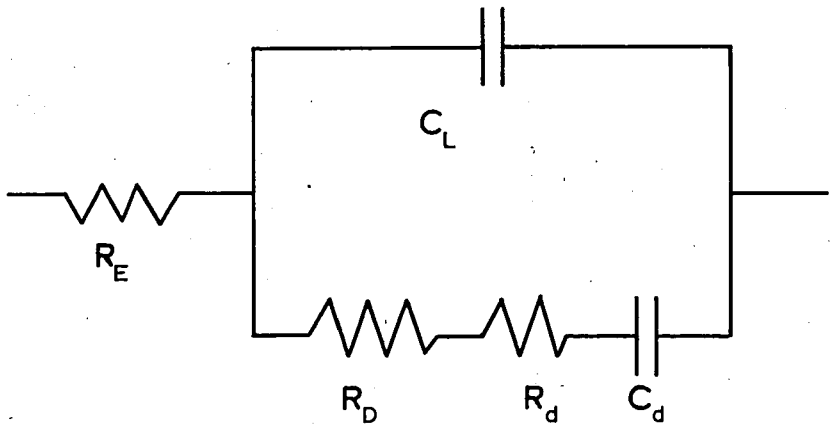

R_E , Ohmic resistance of electrolytic system.

C_L , Double layer capacitance.

R_D , Charge transfer resistance.

R_d , Diffusion resistance.

C_d Diffusion capacitance.

(b) Charge transfer, diffusion and crystallisation contol.

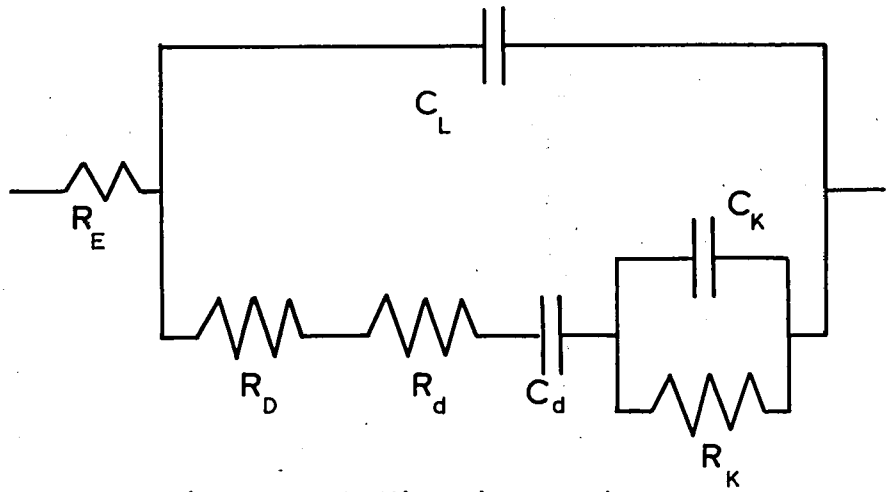

R_K, Lattice crystallisation resistance.

C_K, Lattice crystallisation capacitance.

FIG. 3 Theoretical impedance curves.

(a) charge transfer and diffusion control.

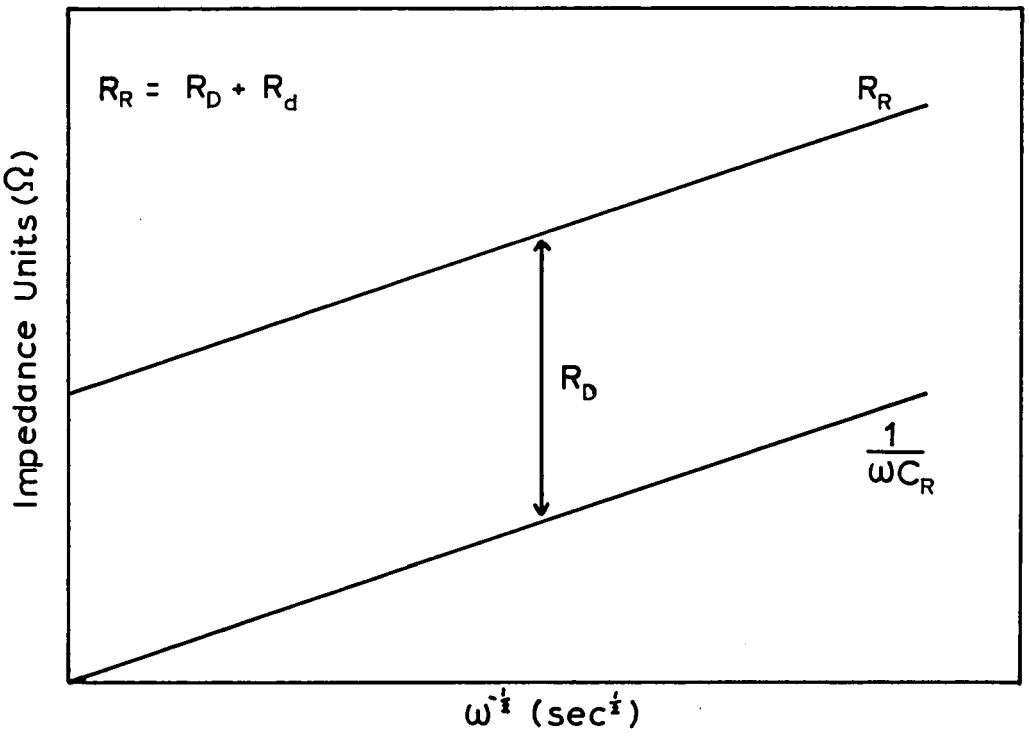

(b) charge transfer diffusion and crystallisation control.

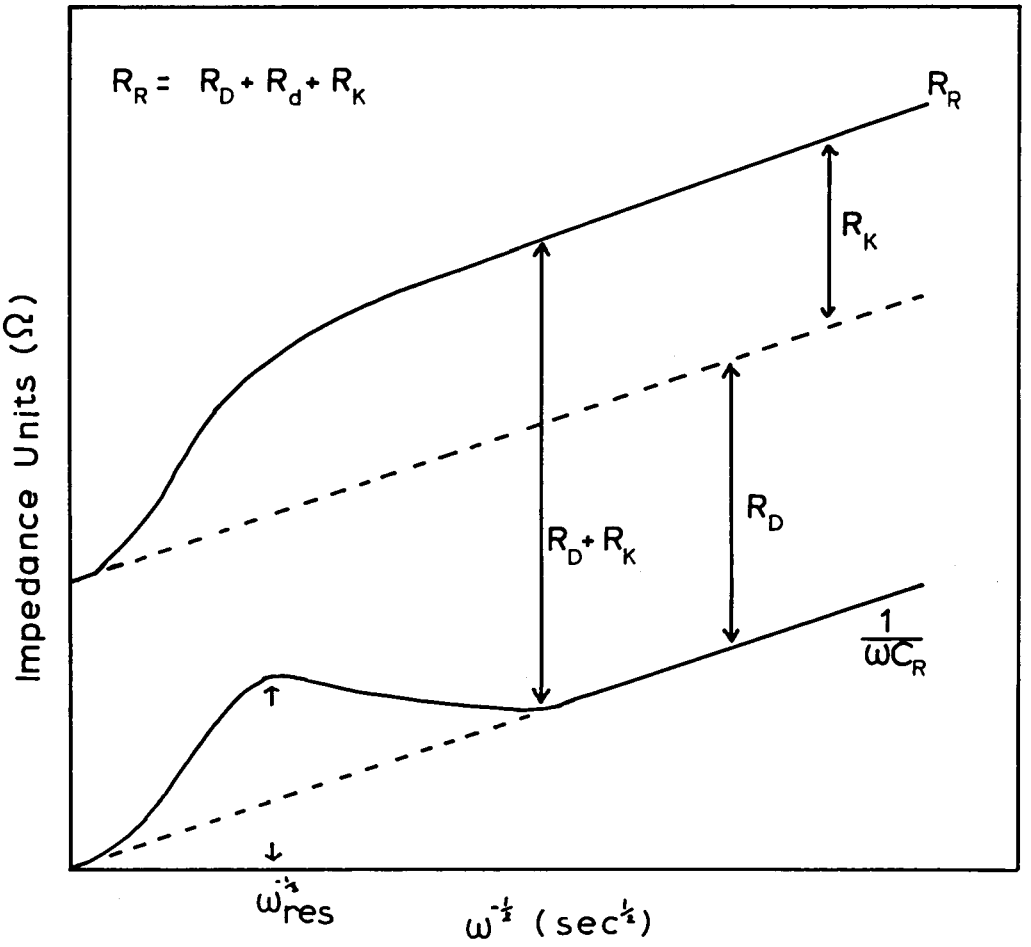

analogue of the electrode system comprises of the differential capacitance shunted by a faradaic impedance, Z_f. For amalgam systems the faradaic impedance is a combination of terms due to the charge transfer process and diffusion of products and reactants in solution. Solid metal systems are more complicated since the processes of inclusion and release of atoms into and from the ordered lattice must also be considered.

For a reaction controlled only by charge transfer and diffusion in solution, RANDLES (21) showed that the electrode system may be represented by the analogue shown in Figure 2a. RANDLES (21) theory also predicts that plots of R_R and $\frac{1}{\omega C_R}$ vs. $\omega^{-\frac{1}{2}}$ should be linear and parallel and that the latter line should pass through the origin (see Figure 3a). For the case of charge transfer and diffusion in solution:

$$R_R = R_D + R_d \qquad [11]$$

and the difference between the in-phase and out-of-phase components gives the charge transfer resistance:-

$$\Delta = R_D \qquad [12]$$

$\frac{1}{\omega C_R}$ corresponds only to the diffusion process and thus conforms to the behaviour originally formulated by WARBURG (22). The slope of the line of the out-of-phase component is determined by the WARBURG coefficient:-

$$\sigma = \frac{RT}{n^2 F^2 \sqrt{2}} \sum \left[\frac{1}{C_i D_i^{\frac{1}{2}}} \right] \qquad [13]$$

The original model (23-25) of a system involving the inclusion or release of atoms from the ordered lattice considered the single step:-

$$M_{ad} = M_{lat} \qquad [14]$$

Thus an extra resistance and capacitance must be included in the electrical analogue (Figure 2b) to represent this "crystallisation" process. Using this model an impedance plot of the type shown in Figure 3b is obtained. With this model:-

$$\Delta_{\omega \rightarrow \infty} = R_D \qquad [15]$$

and

$$\Delta_{\omega \rightarrow o} = R_D + R_K \qquad [16]$$

where

$$R_K = \frac{RT}{z^2F^2V_g^o} \qquad [17]$$

In the early work the adatom flux, V_g^o, was identified with:-

$$V_g^o = \frac{D_a}{l^2} \qquad [18]$$

The presence of the adatoms on the surface gives rise to an adsorption capacitance:-

$$C_K = \frac{z^2F^2}{RT} \times \Gamma_o \qquad [19]$$

in parallel with R_K (see Figure 2b). As the frequency of the applied a.c. increases through the resonant frequency,

$$\frac{1}{\omega_{res}} = \frac{\Gamma_a}{V_g^o} \qquad [20]$$

the in-phase component decreases and the out-of-phase component passes through a local maximum as the "crystallisation" process is relaxed out. This variation is superimposed on the "normal" WARBURG behaviour.

More recently (26, 27) the process [14] has been separated into two components:-

$$M_{ad}\ (\text{planar surface}) = M_{ad}\ (\text{edge}) \qquad [21]$$

$$M_{ad}\ (\text{edge}) = M_{lat.} \qquad [22]$$

Diffusion of the ion in solution is linked with diffusion of the adsorbed species on the electrode surface from the point of deposition to a growth site. As a consequence of this the exchange current, i_o, is related to the impedance component representing the surface diffusion process; whereas for the lattice incorporation step [22] the value of the component representing the process in the electrode analogue is independent of i_o. It has been pointed out that any interpretation of experimental results using this treatment would be extremely difficult (28). However, with polycrystalline metal systems where the metal surface will have a high density of dislocations, diffusion to a growth site is not likely to be a slow process. Comparison between the early and more modern treatments (in the case of polycrystalline metals) indicates that factors representing charge transfer and crystallisa-

tion are identifiable in each case. In the more modern theory the lattice incorporation resistance is given by:-

$$R_{lat} = \frac{RT}{zFi_o} \times \frac{k_2'}{k_3} \qquad [23]$$

where

$$k_2' = \frac{i_o}{zFT_0} \qquad [24]$$

and k_3 is a rate constant. R_{lat} can therefore be identified with R_k in the older theory and thus:-

$$V_g^o = \frac{\Gamma_o k_3}{1} \qquad [25]$$

RANGARAJAN (29) has also discussed the crystallisation step as a multi-step process. However, a complete description of the electrode reaction in terms of the model in which the crystallisation process is split into two processes [21] and [22] would be extremely difficult. The newer theory does provide two criteria that can be applied to decide which of [21] and [22] is predominantly rate controlling:

(a) If surface diffusion is rate controlling the magnitude of V_g^o is a function of i_o.

(b) The presence in the electrode analogue of a significant impedance representing surface diffusion forces the frequency response to be very different from that indicated by GERISCHER (23, 24) and LORENZ (25).

It should be noted that RANGARAJAN's (29) treatment when simplified to the case of control only by the process of lattice building (adatom diffusion effects assumed to be absent) leads to the types of curves originally predicted by GERISCHER (23, 24).

Other methods of treatment of impedance data have also been developed. Components of the electrode analogue may be abstracted using the complex impedance plane method of SLUYTERS (30) and the more recent method developed by de LEVIE (31, 32) in which the capacitance complex plane is plotted. Although both methods have proved to be satisfactory in the study of the kinetics of exchange at amalgam electrodes, it was considered that in the case of solid metal exchange reaction no advantage was offered over the method of RANDLES (21), GERISCHER (23-24) and LORENZ (25).

2.3. INTERPRETATION OF GALVANOSTATIC DATA

2.3. (a) Single Impulse Data

Numerous attempts (33-37) have been made to explain the overpotential-time curve after a current step function has been applied to the electrode. When a Luggin system is employed a correction must be made for the potential difference between the Luggin capillary and the electrode surface. This usually appears as a gap in the initial rise of the transient since this ohmic overpotential is overcome faster than can be measured oscillographically.

The diffusion overpotential, η_d, is zero at time t = 0 and thus the initial overpotential after correction for the ohmic overpotential η_Ω, corresponds to the charge transfer overpotential η_D. SAND (38) and

KARAOGLANOFF (39) showed that for the case of no convection in solution:-

$$\eta_{\alpha} = \frac{RT}{zF} \sum V_j \ln\left(1 \pm \sqrt{\frac{t}{\tau_j}}\right) \qquad [26]$$

BERZINS and DELAHAY (40) have also considered the case of diffusion overpotential but also take account of double layer charging. For low overpotentials a plot of η vs. $\sqrt{t}$ yields a straight line, of which the intercept gives η_D. This latter theory, however, only concerns the case for charge transfer and diffusion in solution. The additional process of adatom diffusion is present in the case of solid metals and straight lines are not obtained from $\sqrt{t}$ plots. GERISCHER (41, 42) has shown that a simple linear extrapolation to zero time can be successfully used.

In addition to overpotential data, using the single impulse technique, approximate values of the differential capacitance can be obtained from the initial rise of the transient:-

$$C_L = -i\left(\frac{dt}{d\eta}\right) \quad t \to 0 \qquad [27]$$

2.3. (b) Double Impulse Data

GERISCHER and KRAUSE (43) developed the double impulse technique in order to eliminate the effects of double layer charging which are encountered when using the single impulse technique. The first short pulse is of sufficient length to charge the double layer capacitance to the overpotential equivalent to the current density of the second pulse (Figure 4). At the beginning of the second pulse $d\eta/dt$ is zero and consequently η_D may be

FIG.4 Schematic diagram for double impulse technique.

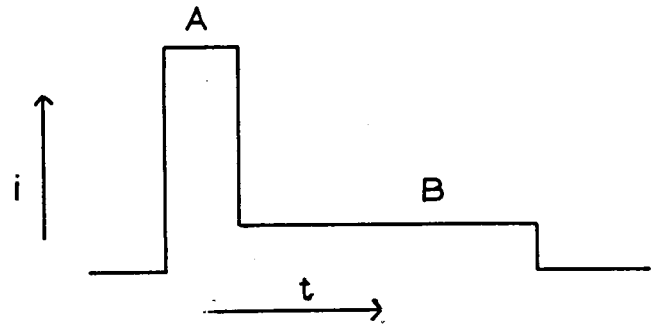

A, Double layer charging pulse.

B, Driving pulse.

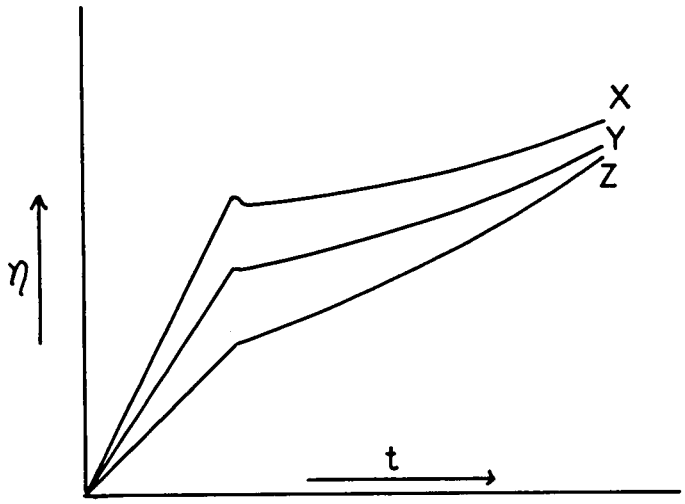

X, Pulse 'A' too large.

Y, Pulse 'A' correctly balanced.

Z, Pulse 'A' too small.

obtained directly with no extrapolations. Figure 4 shows the effects of different magnitudes of the current density of the initial pulse. The ratio of the pulses must be found by trial and error such that at the beginning of the second pulse $d\eta/dt$ is zero.

2.4. THE RATE DETERMINING PROCESS

According to the theory of reaction rates the factor determining the rate of the reaction is not the enthalpy of activation but the free energy of activation. Enthalpies of activation may be deduced using the Arrhenius rate equation:-

$$k = A \exp(-\Delta H/RT) \qquad [28]$$

According to the theory of absolute reaction rates of GLASSTONE et al. (44) for electrochemical charge transfer processes:-

$$I_o = B \exp(-\Delta H/RT) \qquad [29]$$

where I_o is the standard exchange current density. The value of I_o used in this calculation depends on the value of the charge transfer coefficient according to:-

$$i_o = I_o \; C_M^{\alpha} \; C_{M^{z+}}^{1-\alpha} \qquad [30]$$

The magnitude of the pre-exponential term in equation [29] is given by:-

$$B = 9.6 \times 10^{8} \exp(\Delta S/R) \qquad [31]$$

The choice of the value of B depends on the size of the electroactive species at the electrode surface. The value giving [31] is that of GLASSTONE et al. (44) and was originally considered for the case of proton transfer from water molecules. It corresponds to an effective diameter of 3 - 4 Å. The effective radius of metal ionic species in the "critical state" is unknown; however, from ionic radii and the size of water molecules, a value of 2 Å appears to be reasonable.

Hence ΔG_D can be obtained and by similar calculations (for the crystallisation process, say) the free energies of activation for other electrode processes may also be derived.

True enthalpies of activation cannot be obtained from electrochemical measurements since the variation of the reversible potential of the system varies with temperature (45). This could only be assessed by measuring against a reference electrode at constant potential and such measurements fail due to the presence of an unknown thermo-liquid junction potential.

However, a comparison of the experimentally determined quantities may be used to elucidate the rate determining process.

CHAPTER 3

EXPERIMENTAL

3.1. ELECTROLYTIC SYSTEMS

3.1. (a) Electrolytic Cells

Various designs of glass cells were used and are described in the relevant sections. Electrolytic cells and all glassware were cleaned by steeping for ten days in a 50/50 mixture of concentrated nitric and sulphuric acids. The acid was removed by numerous washings with deionised water, after which the cell was allowed to stand in bidistilled water for a day.

3.1. (b) Electrolytes

Electrolytes were made up from A.R. grade chemicals using water bidistilled from deionised stock. (Analyses of electrolytes are described in APPENDIX 1).

Electrolytes were purified by constantly pumping over specially prepared activated charcoal (46). Nitrogen, deoxygenated by passing over copper at 400°C and prehumidified, was used to circulate electrolytes in the cells. (The preparation of the charcoal is described in APPENDIX 1). Electrolyte purity was judged by the stability of the a.c. impedance of a sitting mercury drop electrode; in general about five weeks circulation was considered necessary to achieve a satisfactory level of cleanliness.

3.1. (c) Electrodes

Polycrystalline test electrodes were prepared from wires cast in glass under an atmosphere of nitrogen. All metals used were of 99.999% purity (Johnson Matthey Company or Societe de la Vielle Montagne). The wires were sheathed in polythene and then cut at right angles to the long axis (Figure 5). The polythene used was additive-free powder; a quantity was added to a cell containing a mercury drop electrode and no reduction in the differential capacitance was observed.

For galvanostatic measurements, counter and reference electrodes were constructed of the same material as the test electrode. These electrodes were either constructed from metal rod or sheet and were sealed in glass with polythene.

For differential capacitance and faradaic impedance studies the counter electrode was made from platinum gauze (~ 80 cm^2). In these studies the reference used was a saturated calomel electrode.

3.2. DOUBLE LAYER AND FARADAIC IMPEDANCE STUDIES

3.2. (a) Electrical Circuit

A Schering bridge (47) (Figure 6) was used to match the interphase as a series combination of resistance and capacitance (48). The a.c. generator and detector: Two types of generator and detector have been used in the circuit.

(1) The a.c. was obtained from an audio-frequency generator (Solartron, Type CO 546.2). The out of balance signal was passed via a filter (Muirhead, Type D. 925.B), set to reject 50 Hz, to a tuned amplifier

FIG.5 Test electrode construction.

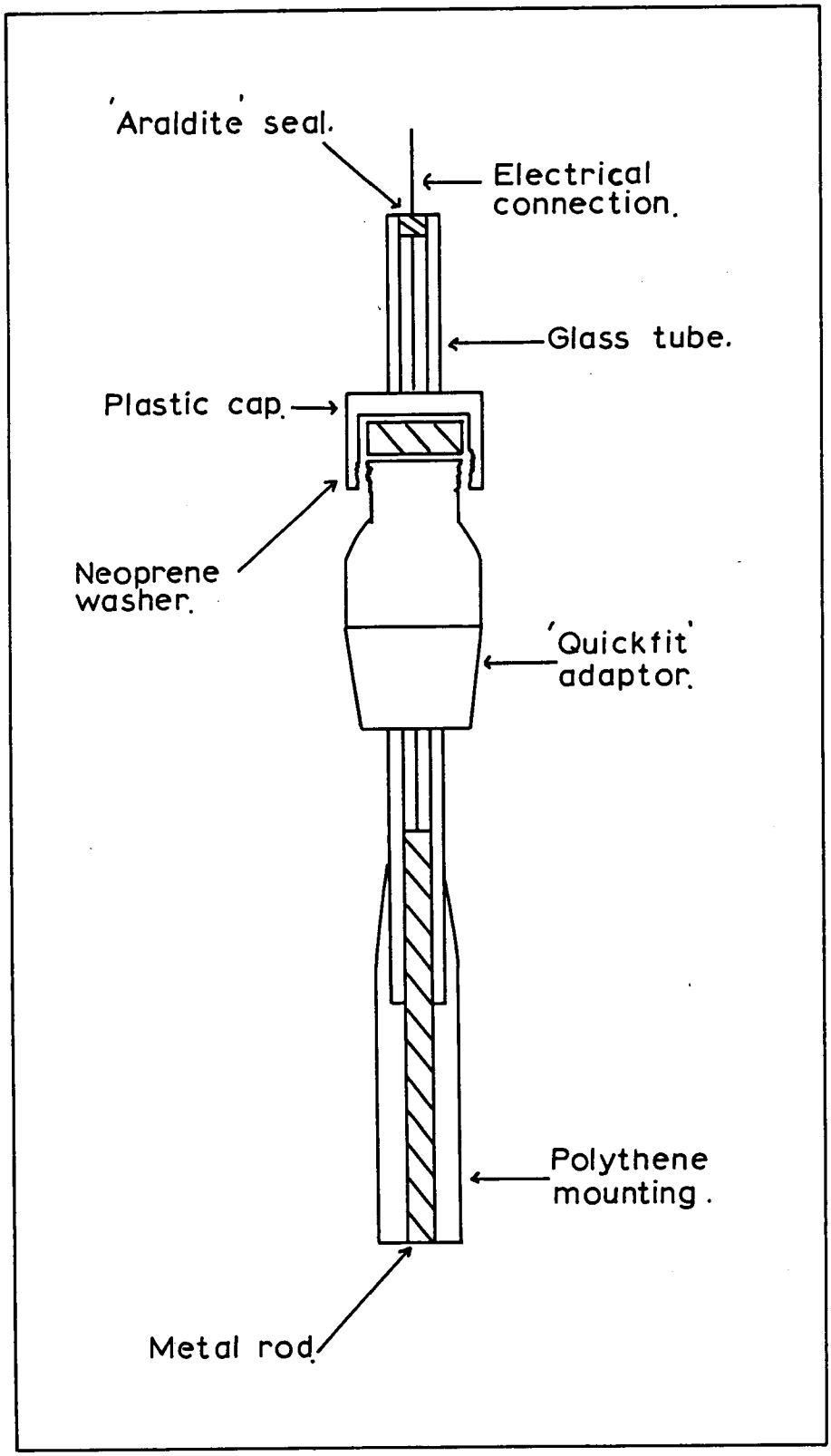

FIG.6 Electrical circuit for double layer and faradaic impedance studies.

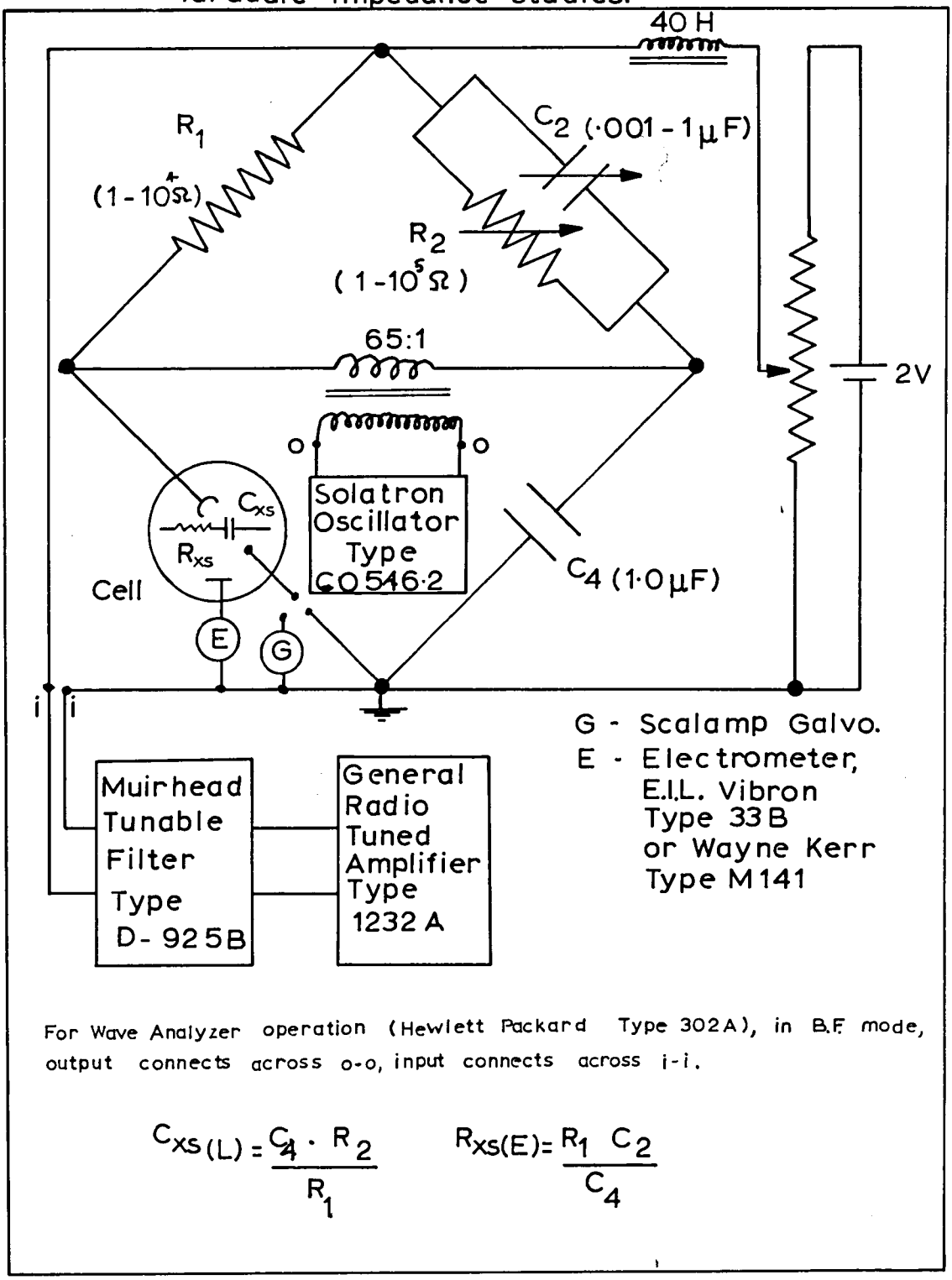

For Wave Analyzer operation (Hewlett Packard Type 302A), in B.F mode, output connects across o-o, input connects across i-i.

$$C_{xs(L)} = \frac{C_4 \cdot R_2}{R_1} \qquad R_{xs(E)} = \frac{R_1 C_2}{C_4}$$

(General Radio, Type 1232-A). The amplifier was continuously tunable in the frequency range 20 Hz - 20 kHz. The dial accuracy was ± 3% and the meter sensitivity 1μ V.F.S.D.

(2) A wave analyser (Hewlett Packard, Type 302A) was used as an a.c. generator and tuned voltmeter for null detection (B.F.O. mode). The generator had a frequency range of 10 Hz - 50 kHz. in divisions of 10 Hz. A single control tuned both the oscillator and the voltmeter. The voltmeter had a narrow pass band with meter ranges from 30 V - 300 V.F.S.D.

In both cases the output from the generator was applied to the bridge through an isolated 65:1 step down transformer. The amplitude of the perturbing a.c. was adjusted to 6.5 mV peak to peak. Bridge components: Variable capacitances and resistances were Muirhead 0.1% grade or Sullivan 0.1% grade. Polarising circuit: The bridge was polarised symmetrically. During all experiments the test electrode was connected to earth in order to avoid screening difficulties. The a.c. and d.c. circuits were separated by a 40 H choke. Electrometer: The instruments (Wayne Kerr, Type 141M and E.I.L. Vibron, Type 33B) used had high input impedances (greater than 10^{16} Ω and shunted by 3 pF) and consequently potentials could be constantly monitored. Frequency of the bridge: The impedance of a cell analogue (a high stability resistance and a standard capacitance in series) was measured over a range of frequencies. The discrepancy between bridge readings and known values are shown in Table 1.

TABLE 1.

Frequency	10 Hz - 1 kHz	1-5 kHz	5-10 kHz	20 kHz
Error (better than)	1%	1%	5%	10%

Thus the bridge could be used in the frequency range 10 Hz - 10 kHz.

3.2. (b) Circuit Transformations and Computor Program for Faradaic Impedance Data

A number of series-parallel circuit transformations (given in APPENDIX 2) described by LAITINEN and RANDLES (49) were used to abstract the faradaic impedance terms R_R and $1/\omega C_R$ from the measured total series combination. A computor program (given in APPENDIX 2) was used to perform the circuit transformations. Since values of R_E and C_L cannot be obtained directly from faradaic impedance data selected values of these parameters were used and the results then reviewed for the best classical behaviour. Thus, using this method values of R_E and C_L may also be obtained.

3.3. GALVANOSTATIC SINGLE IMPULSE STUDIES

3.3. (a) Electrical Circuit

The circuit diagram is shown in Figure 7. A square current pulse was obtained from a pulse generator (Solartron, Type GO 1377 or Hewlett Packard, Type 214A). Using microelectrodes it was found convenient to include a load resistance to limit the current amplitude. The current amplitude was estimated by measuring the potential developed across a standard resistance. Measurements of the potential of the test electrode were made

FIG. 7 Electrical circuit used for galvanostatic single pulse measurements.

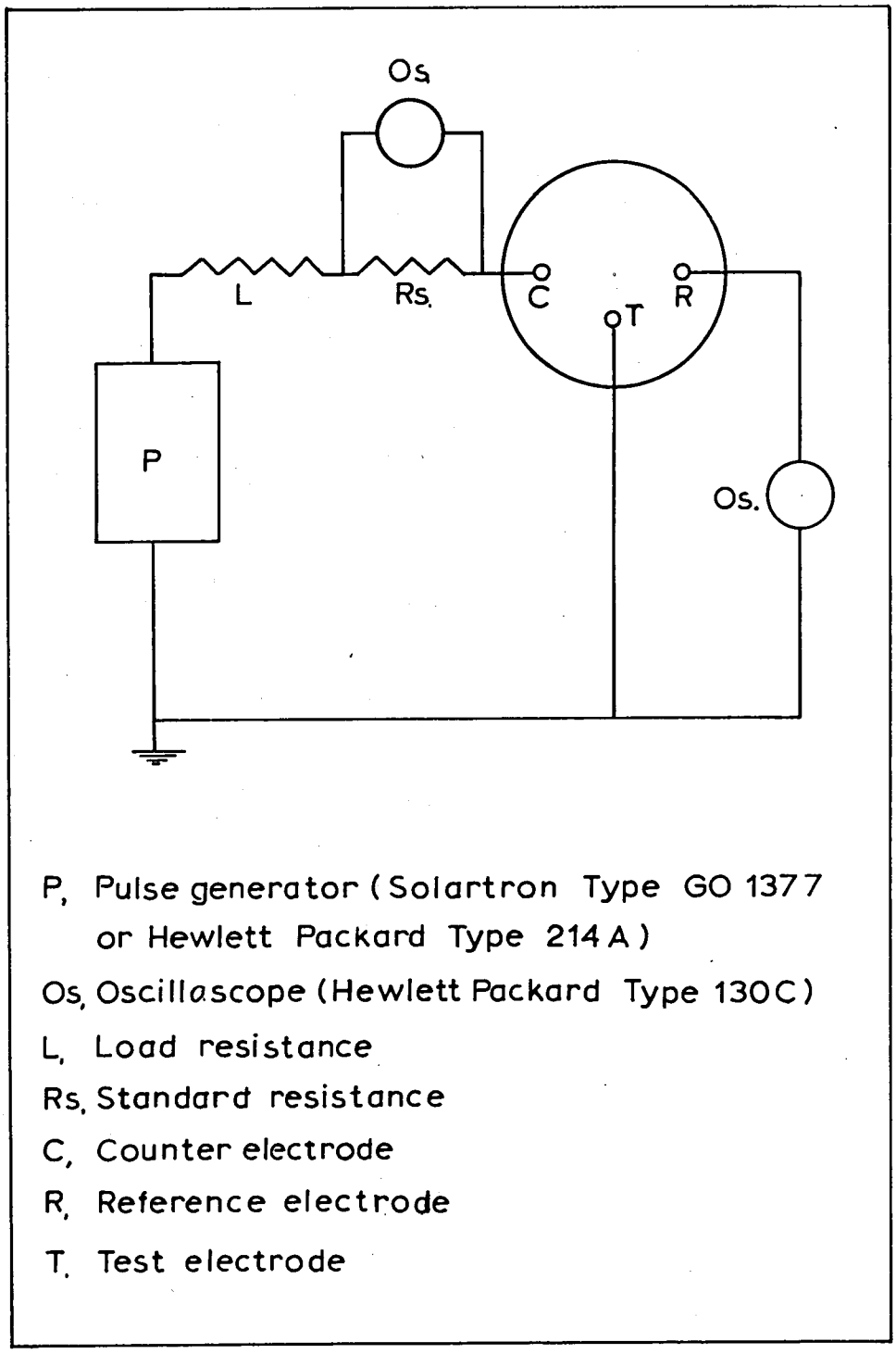

P, Pulse generator (Solartron Type GO 1377 or Hewlett Packard Type 214 A)

Os, Oscillascope (Hewlett Packard Type 130C)

L, Load resistance

Rs, Standard resistance

C, Counter electrode

R, Reference electrode

T, Test electrode

FIG. 8 A typical overpotential-time transient. Single impulse measurements.

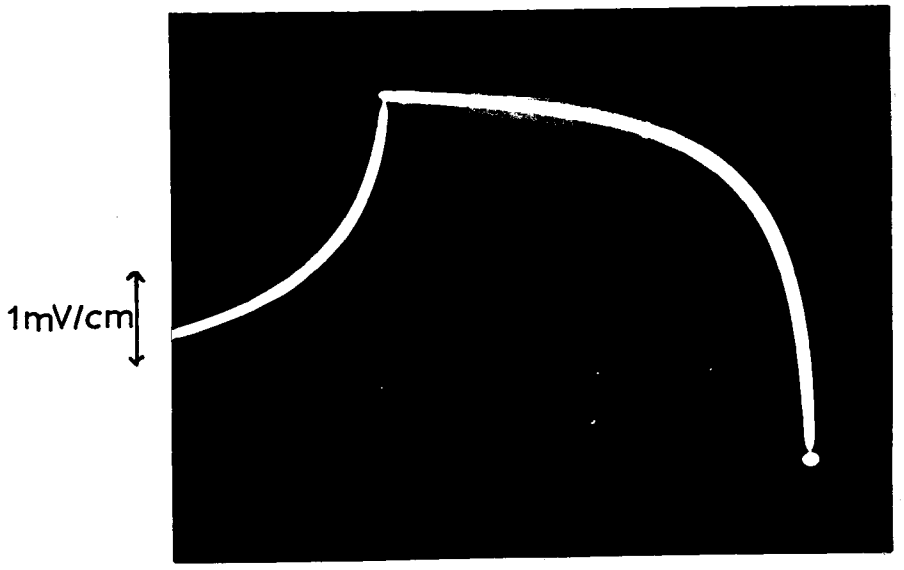

Polycrystalline Cu in KNO_3.
0·0365 mol l^{-1} Cu^{2+}, total $[NO_3^-]$ 1 mol l^{-1}
with KNO_3, pH 3, 23°C.

Cathodic pulse, current density 2·2 mA cm^{-2}.

against the unpolarised reference electrode using an oscilloscope (Hewlett Packard, Type 130C) fitted with an oscilloscope camera (Hewlett Packard, Type 196B). A typical oscilloscope trace is shown in Figure 8. The oscilloscope was triggered by a pre-pulse obtained from the pulse generator.

3.3. (b) Accuracy of Measurements

The rise time of the current pulse was about 0.5μ s. Potential measurements could be made to $\pm$ 0.01 mV in the range up to 2 mV, and $\pm$ 0.05 mV in the range up to 10 mV. Current measurements were $\pm$ 3%.

3.4. GALVANOSTATIC DOUBLE IMPULSE STUDIES

3.4. (a) Electrical Circuit

The L-shaped pulse was obtained from two pulse generators (Solartron, Type GO 1005 and Solartron, Type GO 1377) as shown in Figure 9. The pre-pulse from P2 triggered both P1 and the oscilloscope (Hewlett Packard Type 130C). The delay units were adjusted so that the oscilloscope was triggered just before the combined pulse rose. From this arrangement a complex negative pulse was obtained, either step of which was continuously variable in the range 0.5μs. to 10 ms. A load resistance was included to limit the current amplitude. Potential measurements were made using the method described for the galvanostatic single impulse technique. A typical oscilloscope trace is shown in Figure 10.

3.4. (b) Accuracy of Measurements

The measurements were subject to the same errors as the single impulse measurements, i.e. $\pm$ 3%.

FIG. 9 Electrical circuit for galvanostatic double impulse measurements.

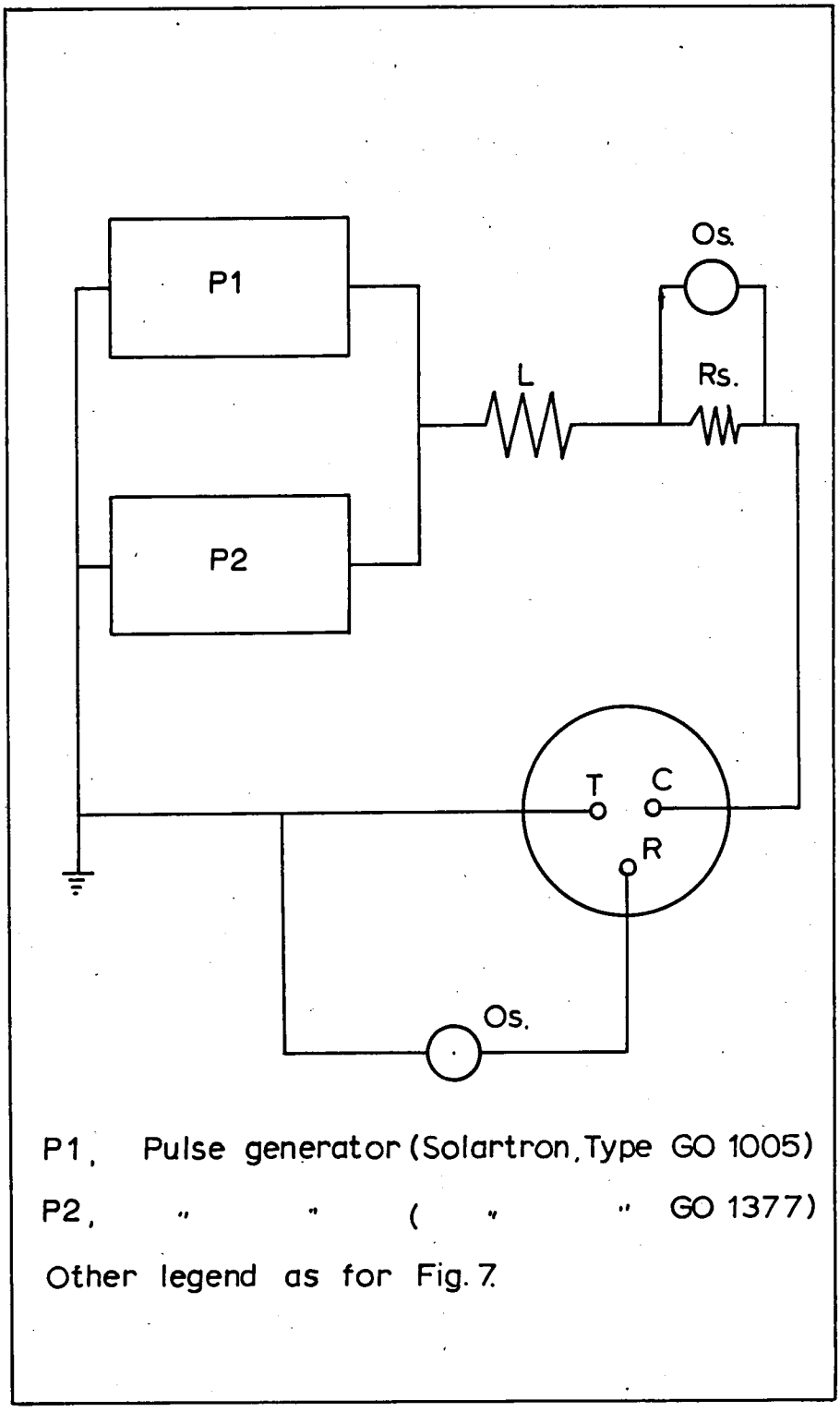

P1, Pulse generator (Solartron, Type GO 1005)

P2, " " (" " GO 1377)

Other legend as for Fig. 7.

FIG. 10 A typical overpotential-time transient. Double impulse measurements.

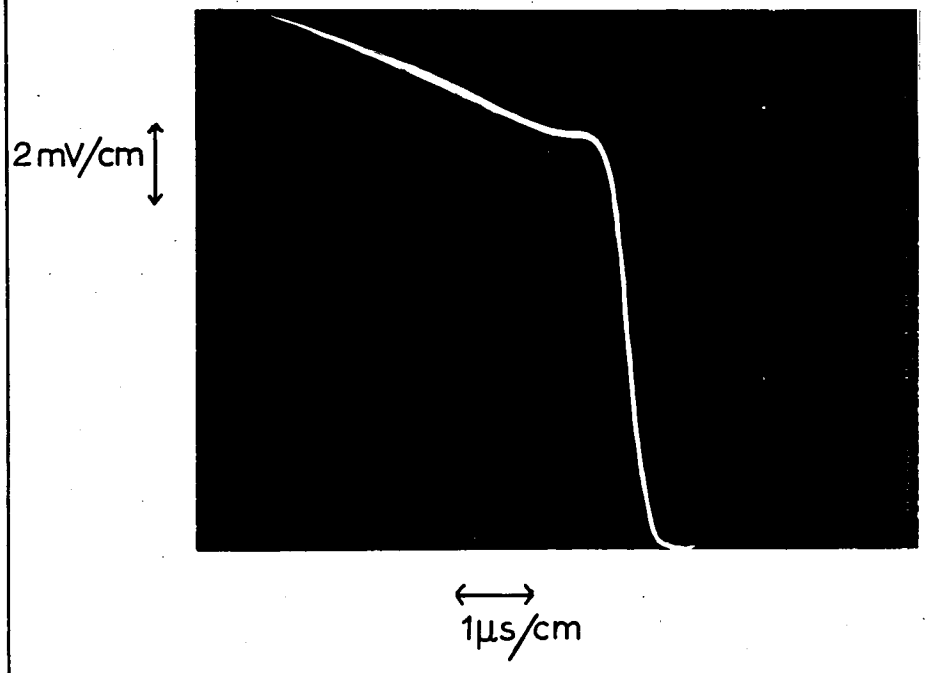

Polycrystalline Cd in NaOH.

0·0099 mol l^{-1} Cd^{2+}, total [OH] 7 mol l^{-1} with NaOH, 23°C.

Anodic pulse, current density 24 mA cm^{-2}.

CHAPTER 4

POLYCRYSTALLINE COPPER IN AQUEOUS SOLUTIONS - A LITERATURE REVIEW

4.1. POTENTIAL OF ZERO CHARGE

A number of investigations concerning the potential of zero charge of solid copper in aqueous solution have been reported. Contact angle (50), friction (51), immersion (52, 53), charging curves (54), capillary rise with contact angle (55), electroreduction (56) methods have been used to identify E_z. However, results have varied from 0.11 V (54) to -0.26 V (51). The spread of reported values is significant and indicates a greater magnitude than can be explained by minor differences in electrode preparation, electrolyte type, temperature and concentration.

The most convenient method of investigating the structure of the interphase established at an electrode is by studying the impedance of the system as a function of the d.c. bias potential. HILLSON (57) has recorded values of the differential capacitance of a solid copper electrode in KNO_3 + 0.05 mol l^{-1} H_2SO_4 electrolyte. BOCKRIS and CONWAY (58) measured C_L in H_2SO_4 electrolyte and obtained a capacitance minimum at 0.0 V (N.H.E.). PEARSON and SCHRADER (59), using identical electrolyte to BOCKRIS and CONWAY (58), obtained similar results but observed a greater dispersion of frequency. It is a point of dispute whether the frequency dispersion observed by both BOCKRIS and CONWAY (58) and PEARSON and SCHRADER (59), is due to dielectric relaxation in the double layer or poor electrode construction (60). The most recent investigation of the possible double layer relaxation

has been by PAYNE (61), who concluded that, at the frequency employed by BOCKRIS and CONWAY (58), and PEARSON and SCHRADER (59), such effects would not be observed. The only other reported measurements of the copper/aqueous solution interphase appear to be those of DERIAZ (62). Using impedance loci, values of C_L in H_2SO_4, K_2SO_4 and KF electrolytes were abstracted. However, it was reported that the potentials at which capacitance minima were observed changed with electrolyte and concentration. There is some conflict between BOCKRIS and CONWAY (58) and PEARSON and SCHRADER (59) on one hand, and DERIAZ (62) on the other, regarding the shape of capacitance curves, and the position of the capacitance minima.

4.2. THE Cu(II)/Cu EXCHANGE REACTION

The Cu(II)/Cu exchange has been extensively studied in sulphate electrolytes using a.c. impedance techniques, both at the equilibrium potential and also by experiments in which a.c. was superimposed on d.c. Of the early work at the equilibrium only LORENZ (63) provides evidence for the participation of adatoms but shows no evidence for the presence of a Cu(I) species as an intermediate in the exchange process. BOCKRIS and CONWAY (58) and also HILLSON (57) show no relaxation on impedance spectra, although HILLSON (57) shows some departure from linearity at low frequencies. BOCKRIS and CONWAY (58) provide no direct evidence for the presence of Cu(I), although they interpret the dependence of exchange current on $[Cu^{2+}]$ as evidence for Cu(I). This interpretation depends, however, on the assumption that α is 0.5. The more recent repetition of this work by PEARSON and SCHRADER (59) does not show evidence for the participation of adatoms or Cu(I). In contrast to the results of LORENZ (63), both BOCKRIS and CONWAY

(58) and PEARSON and SCHRADER (59) show impedance spectra as linear plots. The results of the recent Russian investigations using a.c. superimposed on d.c. are conflicting. TKACHIK et al. (64) show complex plane (30) diagrams which represent transformations of systems with no diffusion in solution, i.e. no faradaic reaction, and also report that R_D decreases with overpotential (and hence i_o increases). BEREZINA et al. (65) report the opposite trend of i_o with overpotential. They also show linear impedance plots for measurements taken at the equilibrium potential. It should be noted that a limited frequency range was employed (and did not extend far enough into the low frequency region to indicate unequivocally the absence of adatoms). The difference between impedance spectra obtained at the equilibrium and at high overpotential was interpreted in terms of the participation of a Cu(I) intermediate in the exchange reaction. A second paper of TKACHIK et al. (66) discusses the possibility of a Cu(I) intermediate and they calculate a diffusion coefficient for Cu(I) in solution. However, it should be noted that the calculation employed the use of a solution concentration of Cu(I) reported by BROWN and THIRSK (67). This latter concentration was calculated using an assumed diffusion coefficient. Recent impedance studies at the equilibrium potential by ICHIKAWA and HARUYAMA (68) showed no evidence for relaxation in the impedance spectra. However, the experimental procedure may have been influenced by the fact that R_E and C_L were compensated for in the bridge circuit. Values of these components were measured in the supporting electrolyte by keeping the potential at E^o for Cu(II)/Cu (in which case a faradaic circuit occurs). A second paper by HARUYAMA (69) reports the results of measurements for the superimposition of a.c. on d.c. for high overpotentials. The results are interpreted as evidence for the participation

of adatoms. However, plots of "crystallisation rate" vs. cathodic current do not show zero rate at zero current density. The results of these two investigations are therefore extremely conflicting.

The results of investigations using the galvanostatic technique have been reported by BOCKRIS and various co-workers (70-72), SEITER and FISCHER (73), MATTSSON and LINDSTROM (74) and also by HURLEN (75). A wide range of values of the exchange current density is reported. BOCKRIS and co-workers (70-72) obtained non-symmetrical (anodic and cathodic) Tafel plots and the results were interpreted as evidence for Cu(I). However, the interpretation assumes that α must be 0.5, although a recent review by BAUER (76) has shown that this is not necessarily correct. From the results of high overpotential measurements BOCKRIS and co-workers (70-72) also calculated values for the surface concentration of adatoms from the transients, although the values obtained ($\sim 10^{-9}$ mol cm^{-2}) were considerably higher than those of LORENZ (63) ($\sim 10^{-11}$ mol cm^{-2}) and values reported for other metals. SEITER and FISCHER (73) also provide some discussion of the possibility of adatoms taking part in the overall exchange but no data is provided. HURLEN (75) was unable to find evidence for either adatoms or Cu(I) but suggests that both phenomena may be observed by using suitable experimental conditions. It is worth noting that the galvanostatic experiments reported were made using relatively long current pulses ($\sim$ ms) which correspond to low frequency a.c. measurements. No data is reported for short time pulses ($\sim 100\,\mu s$) which correspond to high frequency a.c. measurements.

TINDALL and BRUCKENSTEIN (77-79) have investigated the Cu(II)/Cu exchange at a platinum ring-disc electrode. At high overpotentials they were unable to find evidence for Cu(I) in the deposition process but showed that

Cu(I) was present during the dissolution process. They were, however, able to establish the presence of Cu_{ad} in both processes. The most recent report of BREITER (80) in a study of chemisorption of copper atoms on platinum also confirms the presence of adatoms.

There is considerably less data available concerning the effect of temperature on the electrode processes. Using galvanostatic methods SEITER and FISCHER (73) obtained a value of 51.5 ± 8.0 k J mol^{-1} for the activation enthalpy of the charge transfer process; a value of 68-84 k J mol^{-1} was obtained by BARNES, STOREY and PICK (81), whereas MATTSSON and LINDSTROM (74) reported 38.5 k J mol^{-1}. Another relatively high value of 63.5 k J mol^{-1} was reported by HURLEN (82). Again it should be noted that long time pulses were used. Using the a.c. impedance technique, ICHIKAWA and HARUYAMA (68) obtained a value of ~ 25 k J mol^{-1} for the charge transfer process and ~ 84 k J mol^{-1} for the process of adatom diffusion on the surface. The latter value was obtained from the temperature dependence of D_{Cu}. This term was derived from the comparison of theoretical and experimental Warburg coefficients for this system. This procedure must be criticised since the Warburg impedance is related to diffusion in solution only and not on the surface.

A summary of some of the previously reported kinetic results is given in Table 2.

TABLE 2

Workers	Supporting Electrolyte	$[Cu^{2+}]$ mol l^{-1}	C_L $\mu F cm^{-2}$	i_o mA cm^{-2}	Γ_o mol cm^{-2}	Technique
Hillson (55)	1 mol l^{-1} KNO_3 + 0.05 mol l^{-1} H_2SO_4	0.05	67	36*		a.c. impedance
Bockris & Conway (56)	0.05 mol l^{-1} H_2SO_4	0.049	Min at 5kHz 60	73		a.c. impedance
Pearson & Schrader (57)	0.5 mol l^{-1} H_2SO_4	0.056	Min at 5kHz 28	10.6		a.c. impedance
Lorenz (61)	1 mol l^{-1} H_2SO_4	0.05		30	10^{-12}	a.c. impedance
Tkachik (62) et al.	0.5 mol l^{-1} H_2SO_4	0.5 mol l^{-1}	30			impedance complex plane
Berezina (63) et al.	0.2 mol l^{-1} H_2SO_4	0.3 mol l^{-1}		21.0		a.c. impedance
Tkachik (64) et al.	0.5 mol l^{-1} H_2SO_4	0.5 mol l^{-1}	17	0.4		a.c. impedance
Ichikawa (66) Haruyama	0.5 mol l^{-1} H_2SO_4	0.01 mol l^{-1}		9.9		a.c. impedance
Mattsson (68) & Bockris	0.5 mol l^{-1} H_2SO_4	0.15		Tafel Slope An 8.6 Cath 26.8 Linear Slope An 1.4 Cath 0.7		Galvanostatic
Bockris (69) & Kita	0.5 mol l^{-1} H_2SO_4	0.05	42-58	Tafel Slope An 2.2-6.0 Cath 3.4-10.0 Linear Slope An 2.9-4.2 Cath 1.9-3.5	4.7 - 19 x 10^{-9}	Galvanostatic
Bockris (70) & Enyo	0.5 mol l^{-1} H_2SO_4	0.1	55	Tafel Slope An 3.7 Cath 3.3 Linear Slope 2.8	5 x 10^{-9}	Galvanostatic
Hurlen (73)	0.5 mol l^{-1} H_2SO_4	0.5		1.0		Galvanostatic

* Based on total electrode area.

CHAPTER 5

THE DIFFERENTIAL CAPACITANCE OF POLYCRYSTALLINE COPPER IN AQUEOUS SOLUTION

5.1. ACID AND NEUTRAL ELECTROLYTES

5.1. (a) Experimental

The preparation of electrolytes and electrodes has been described in Section 3.1. The test electrode was (3.14×10^{-2} cm^2) was prepared from spectroscopically pure wire supplied by Johnson Matthey Company Limited. The electrolytic cell is shown in Figure 11. The electrode interphase was matched as a series combination of resistance and capacitance using the Schering bridge circuit described in Section 3.2.

The electrode was mechanically polished on roughened glass using conductivity water as a lubricant, and then chemically etched (HNO_3, 35% v/v) as suggested by HILLSON (57). This technique was found to give reproducible results.

5.1. (b) Results

Figure 12 shows typical faradaic current vs. potential curves for $NaClO_4$, KNO_3, K_2SO_4 and H_2SO_4 electrolytes. The experimentally polarizable region for the $NaClO_4$, KNO_3 and K_2SO_4 electrolytes at pH ~ 4.8 extended from 0.25 to -0.9 V and for H_2SO_4 from 0.2 to -0.4 V.

For $NaClO_4$ and KNO_3 electrolytes, stable values of the electrode impedance were obtained after about 30 min. electrode/electrolyte contact.

FIG.11 Electrolytic cell used for double layer and faradaic impedance studies.

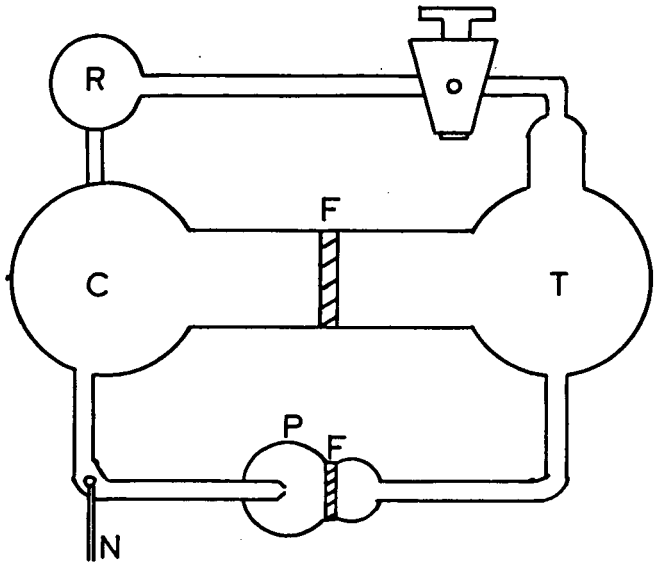

N, Nitrogen inlet
F, Frit
P, Purification limb
R, Reference limb
C, Counter electrode
T, Test electrode

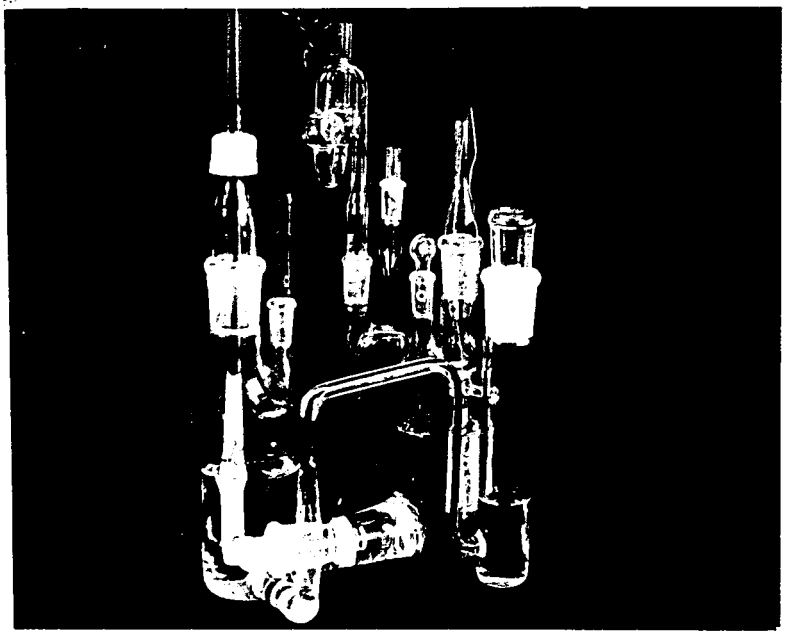

FIG.12 Polycrystalline Cu.
Faradaic current - potential curves.

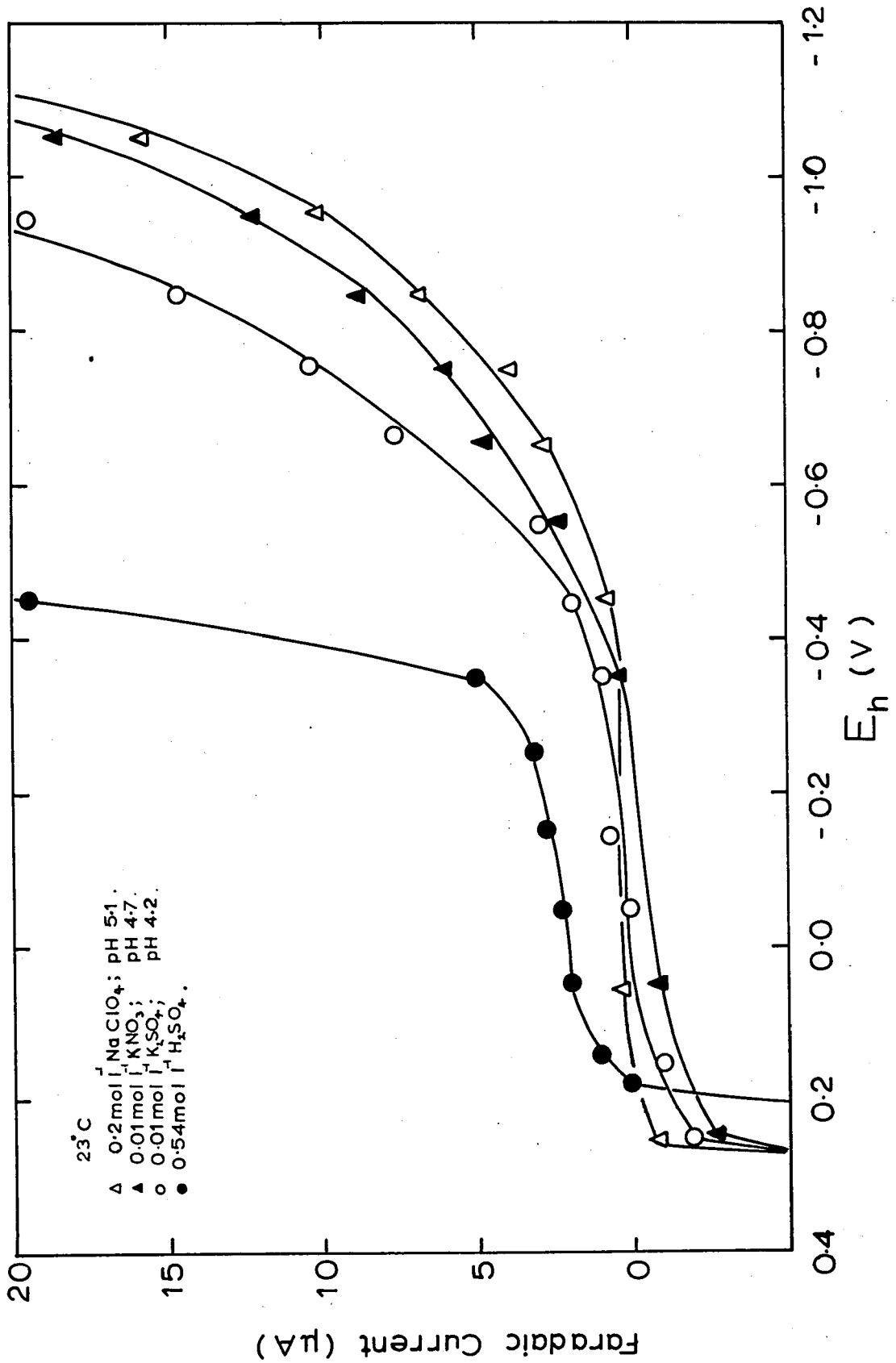

The electrodes remained stable for at least 10 h. For H_2SO_4 and K_2SO_4 at least 3 h of electrode/electrolyte contact was necessary for electrode stability, the ensuing stable period was somewhat shorter than for either $NaClO_4$ or KNO_3. Replicate electrode impedances indicated a variation of less than 12% about a mean. Impedances were less reproducible in K_2SO_4 than H_2SO_4 and considerably less than in $NaClO_4$ and KNO_3 electrolytes.

Hysteresis was observed at both the positive and negative extremes of the polarizable region ($NaClO_4$, KNO_3, K_2SO_4 > 0.2 V and < -0.5 V; H_2SO_4 > 0.15 V and < -0.25 V). Electrodes forced to potentials outside these regions, and then returned to the "stable" region, required some time to revert to equilibrium. Anodic hysteresis (equilibration time 15 min) was less pronounced than cathodic (60 min); electrolytic systems containing SO_4^{2-} ion were generally more subject to hysteresis than those based on either KNO_3 or $NaClO_4$ electrolytes.

Figure 13 shows typical differential capacitance curves for polycrystalline copper in $NaClO_4$ at different concentrations. Figure 14 shows typical differential capacitance curves in KNO_3, K_2SO_4 and H_2SO_4 electrolytes. Figure 15 shows the variation of R_E with potential for each electrolyte. The curves for KNO_3 and $NaClO_4$ are similar in shape, but considerably different from those of the two sulphate electrolytes. Figure 16 shows the extent of frequency dispersion observed in the present experiments. On the same diagram are presented the data of BOCKRIS and CONWAY (56) and PEARSON and SCHRADER (57).

5.1. (c) Discussion

Figure 12 indicates that the polarizable region is not ideal. R_E

FIG.13 Polycrystalline Cu in $NaClO_4$.
Differential capacitance curves.

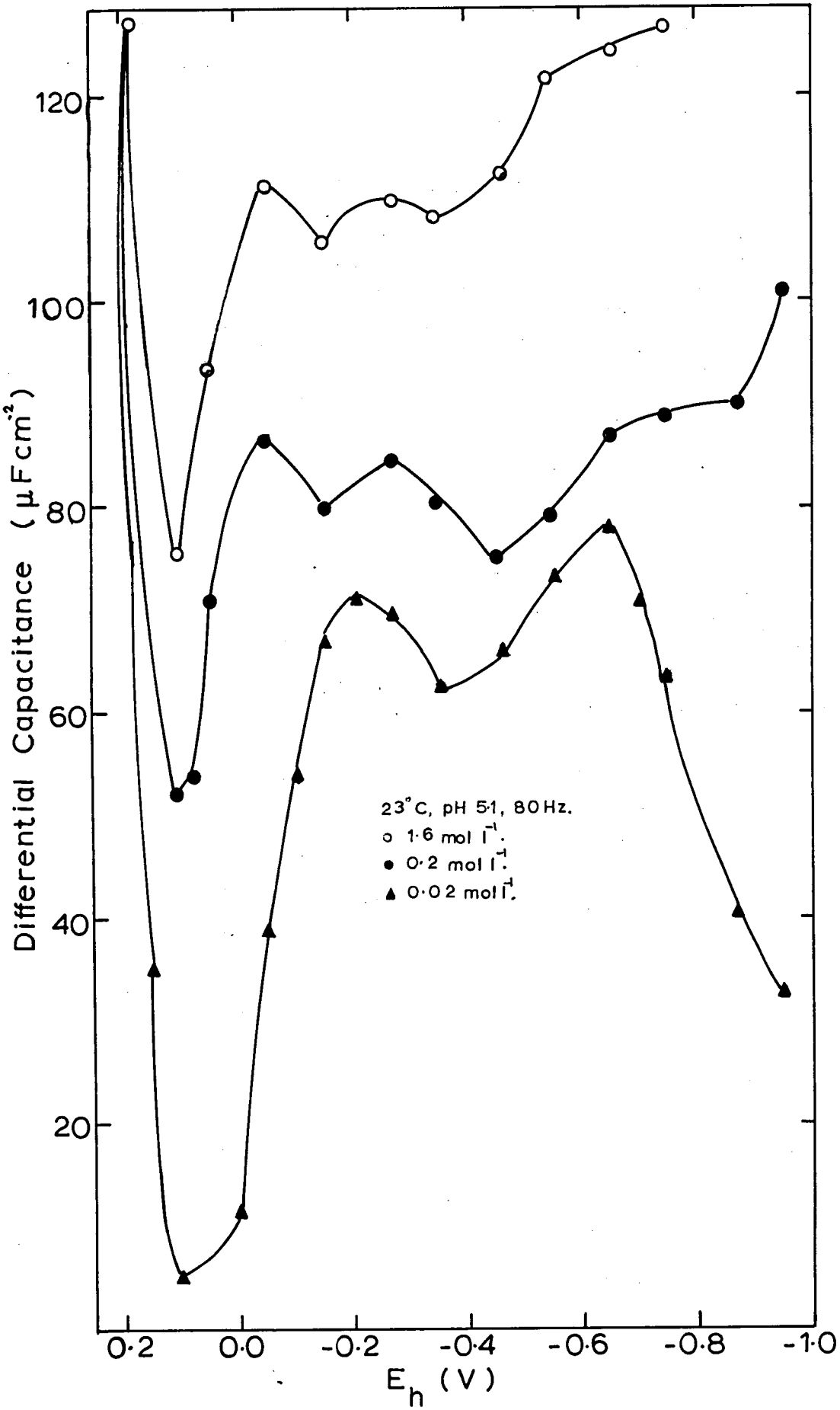

FIG.14 Polycrystalline Cu.

Differential capacitance curves.

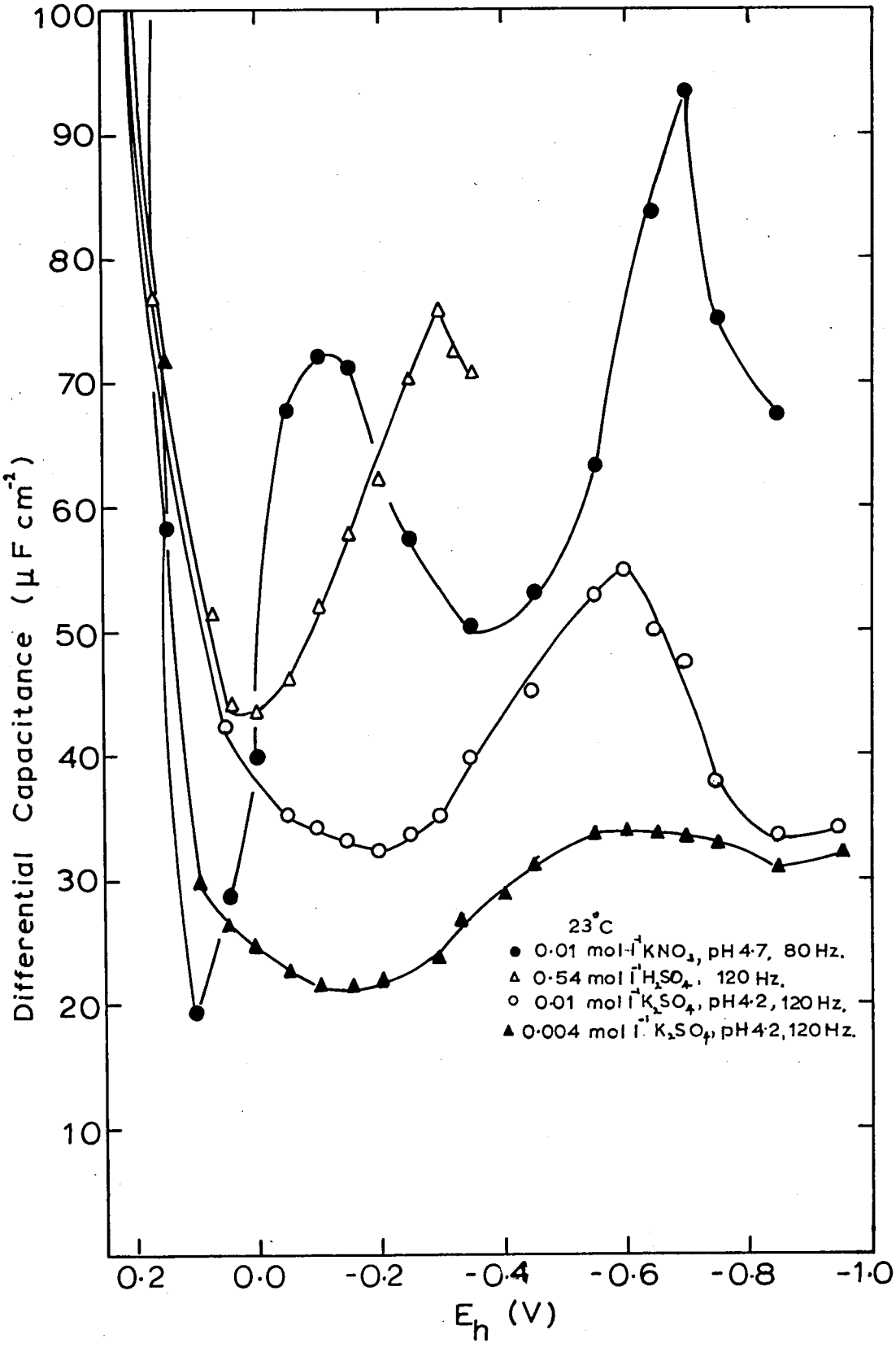

FIG. 15 Polycrystalline Cu.
R_ϵ - Potential curves.

23°C, Electrode area 3.14×10^{-4} cm^2.

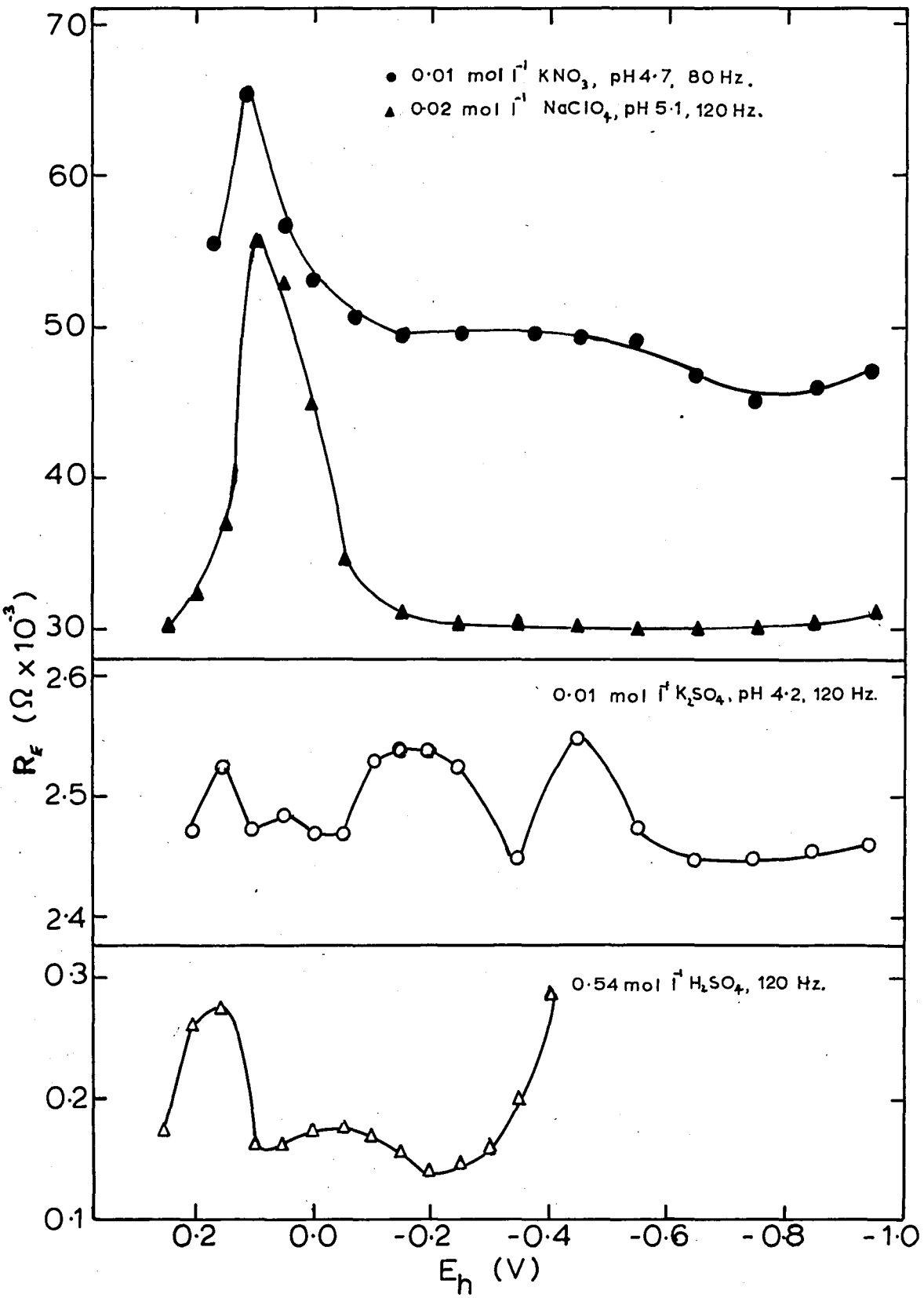

(Figure 15) is potential dependent, indicating some interaction between the electrode and the electrolyte. In the case of KNO_3 and $NaCLO_4$, a pronounced maximum in R_E occurs at ~ 0.1 V and thereafter R_E is constant; for K_2SO_4 and H_2SO_4, the peak at ~ 0.1 V is much less pronounced but is followed by further variations in the potential range below 0.0 V. Thus, it is clear that in the case of SO_4^{2-} electrolytes particularly, and the other electrolytes, at potentials greater than 0.1 V impedance measurements do not represent the true metal/aqueous solution interphase.

Identification of the p.z.c. from capacitance minima in dilute solutions of SO_4^{2-} electrolytes is not likely to be successful. On the other hand, in the case of NO_3^- and CLO_4^- electrolytes at potentials more negative than 0.1 V, the situation is apparently more tractable.

The capacitance curves for similar concentrations of KNO_3 and $NaCLO_4$ are very similar. A deep minimum occurs at 0.1 V, a minor peak at between 0.0 and -0.2 V, followed by a further peak at -0.6 V. These details, particularly the minimum at 0.1 V, become more clearly defined at low concentration.

Copper and hydrogen form a compound, possibly CuH, which can be produced in aqueous solution (83, 84). It is therefore possible that the capacitance peak at -0.6 V immediately before hydrogen evolution represents a pseudo-capacitance peak connected with the formation of this compound. The peak at -0.1 V, preceeding the reactions of compound formation and hydrogen evolution, is therefore likely to be due to hydrogen ion adsorption.

The identity of the process corresponding to the deep minimum at 0.1 V is not completely settled. Work function E_z data (3) predicts that E_z for copper is to be expected in the range 0.1 to -0.4 V. The sharp increase

FIG.16 Polycrystalline Cu in H_2SO_4. Dispersion of capacitance.

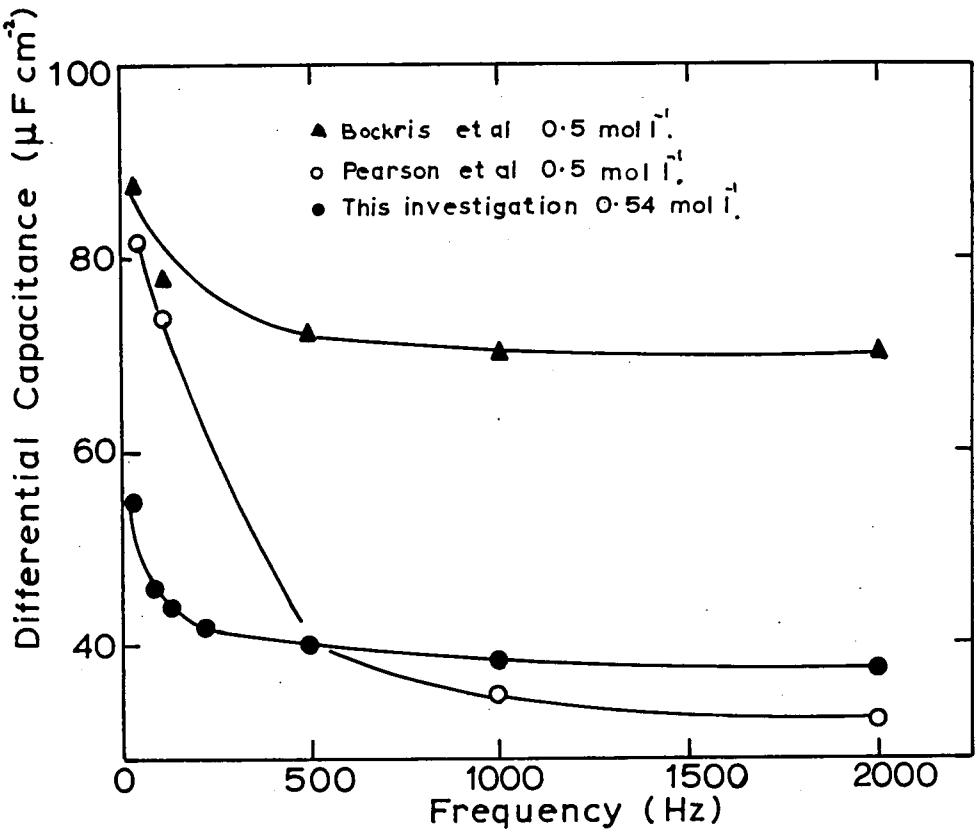

FIG.17 Polycrystalline Cu in H_2SO_4. Differential capacitance curves.

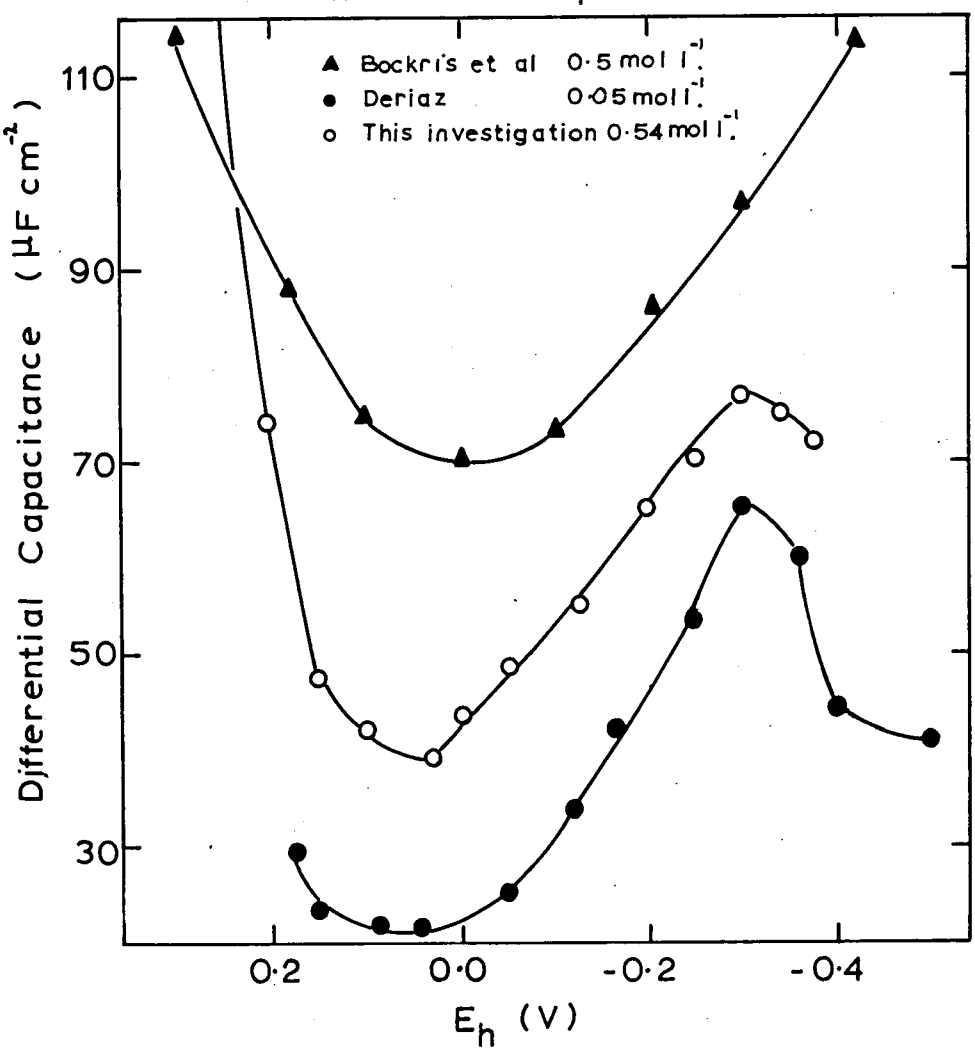

in R_E in the region of 0.1 V indicates some interaction between the electrode and the electrolyte. It seems likely that at this potential two effects are "overlapping" to some extent: the development of the capacitance minimum characteristic of the diffuse part of the double layer and the pseudo-capacitance peak due to hydrogen ion adsorption. In this case it is clear that the value of the p.z.c. cannot be estimated to any degree of accuracy.

The impedance data in SO_4^{2-} electrolytes are more complicated than in NO_3^- or CLO_4^-. It is suggested that a further complicating factor here is the adsorption of the sulphate anion, which to some extent interferes with the adsorption of hydrogen ion at -0.2 V and suppresses pseudo-capacitance peaks due to this adsorption and the resultant compound formation.

Figure 17 shows differential capacitance curves in H_2SO_4 obtained by other workers. Absolute comparison of these results is difficult because of different electrode preparation techniques and methods of obtaining values of C_L. However, the present work indicates a similar curve to that obtained by DERIAZ (62) with a peak at -0.3 V; BOCKRIS and CONWAY (58) obtained a broader curve with no peak at -0.3 V. The frequency dispersion obtained at 0.0 V in H_2SO_4 (0.54 mol l^{-1}) electrolyte was similar to that obtained by BOCKRIS and CONWAY (58) in H_2SO_4 (0.5 mol l^{-1}), and less than that obtained by PEARSON and SCHRADER (59) in the same electrolyte. Some dispersion of frequency must inevitably be due to a certain degree of surface roughness as discussed by de LEVIE (60). In concentrated electrolytes (1 mol l^{-1}) the extent of dispersion due to this is likely to be small. It seems likely, therefore, that the dispersion observed in 0.5 mol l^{-1} H_2SO_4 is due to a frequency-dependent capacitance corresponding to the adsorption-desorption process as already discussed.

5.2. ALKALINE ELECTROLYTE

5.2. (a) Experimental

The experimental procedures have been described in Section 5.1.

5.2. (b) Results

A plot of faradaic current vs. potential is shown in Figure 18. An experimentally accessible region extends from -0.10 to -0.80 V. At the negative limit of the polarizable region hydrogen evolution occurred and at the positive limit a solid phase was formed at the electrode. Within the experimentally polarizable region the resistive component of the electrode impedance was observed to remain constant. However, at the positive limit it increased markedly.

Figures 19 and 20 show typical differential capacitance curves in the concentration range 0.925 to 0.007 mol l^{-1} NaOH. The shape of the curves was similar for all concentrations and showed two maxima at ~ -0.30 V and ~ -0.65 V. The relative magnitudes of these peaks increased with electrolyte concentration. The associated minima at ~ -0.5 V and ~ -0.8 V decreased with decreasing concentration. The potentials at which the maxima and minima occurred were concentration dependent and became more negative with increasing concentration. At potentials more positive than about -0.2 V the capacitance decreased very markedly, becoming time dependent, and after sufficient time very small.

The electrode capacitance showed considerable frequency dispersion and resulted in a two-fold increase in capacitance due to a reduction in frequency from 1,000 Hz to 100 Hz.

FIG.18 Polycrystalline Cu in NaOH.
Faradaic current potential curve.
0·925 mol l^{-1} NaOH.

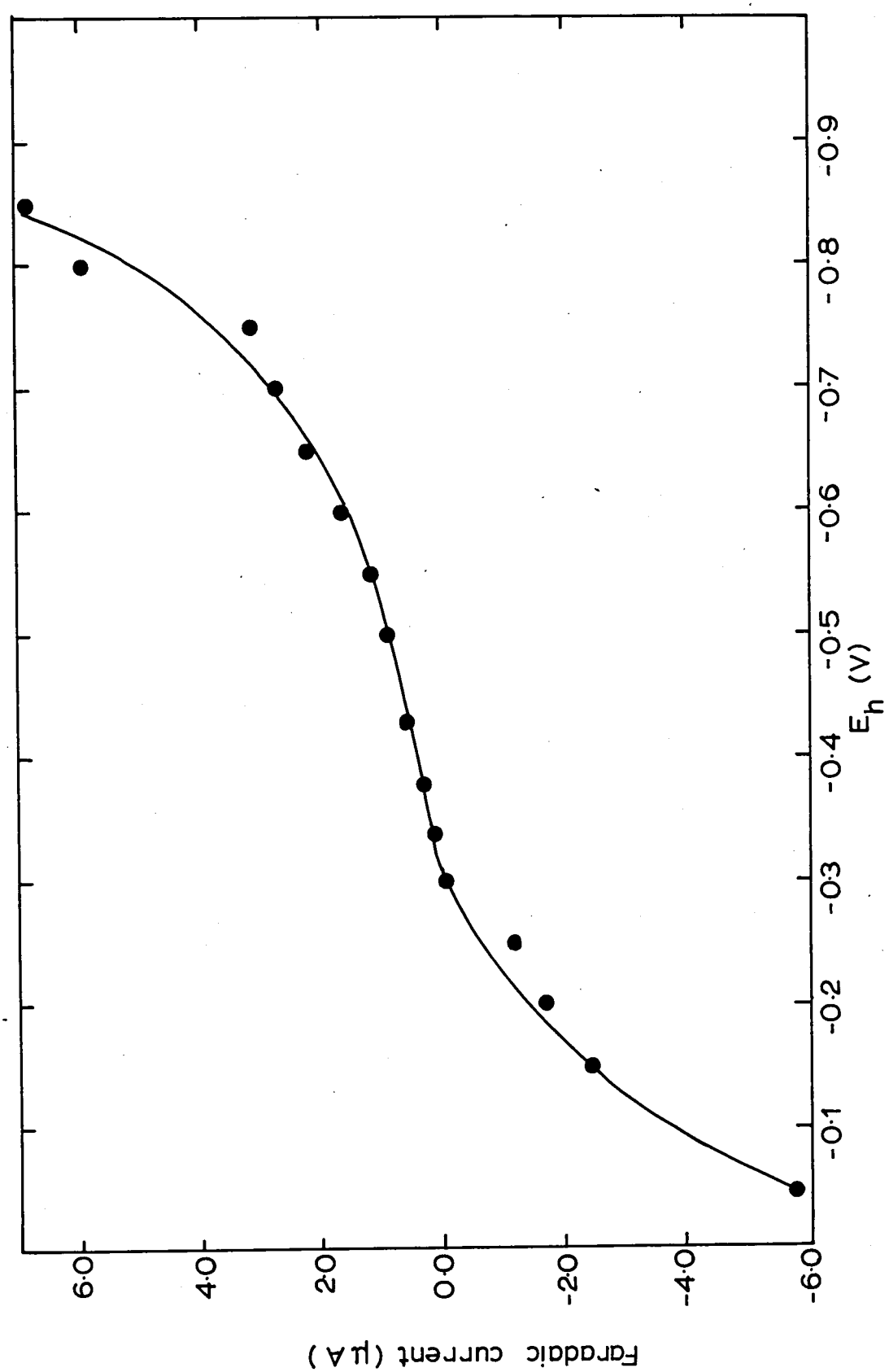

FIG.19 Polycrystalline Cu in NaOH.

Differential capacitance curves.

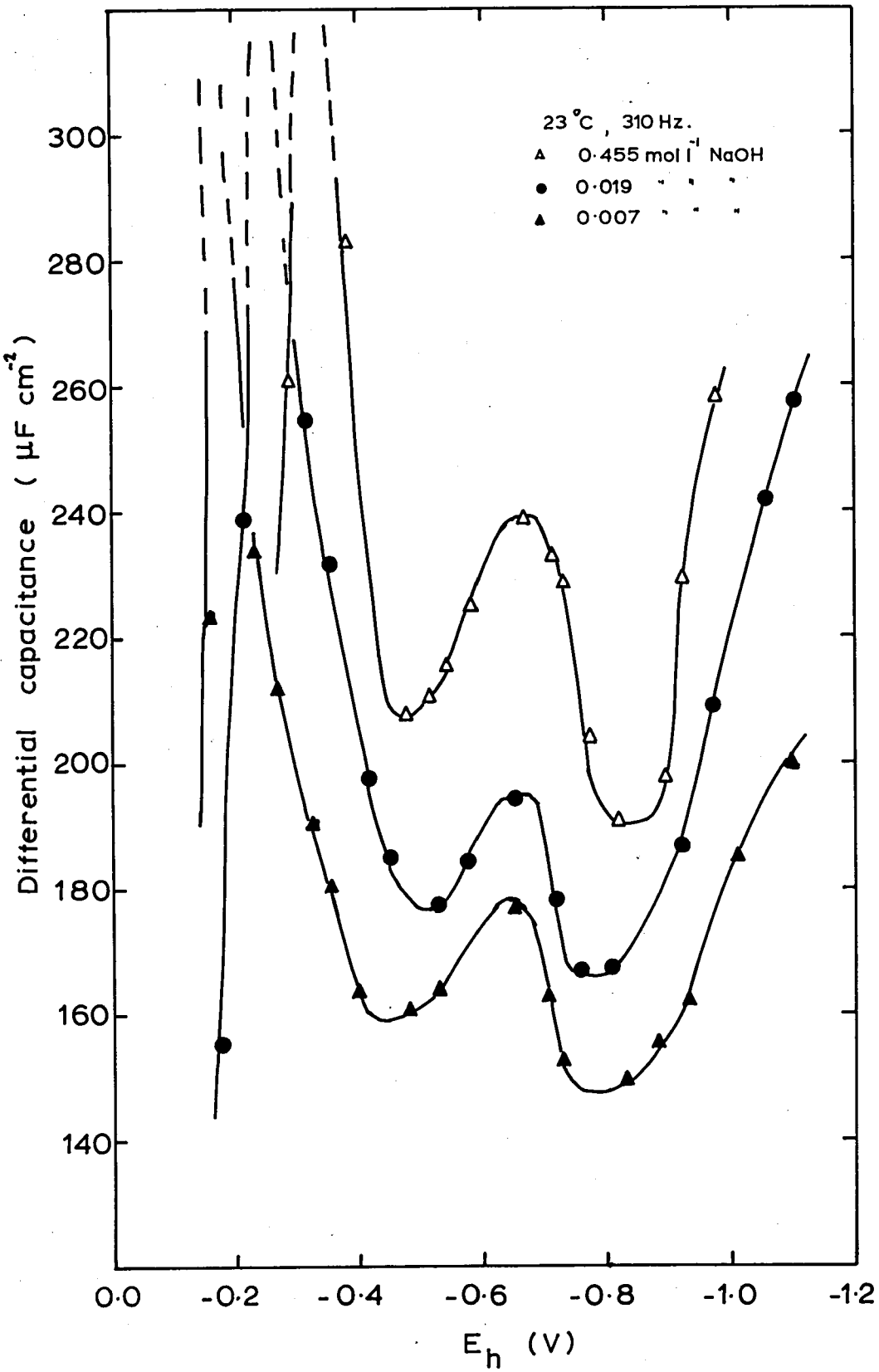

FIG, 20 Polycrystalline Cu in NaOH.

Frequency dependence of capacitance.

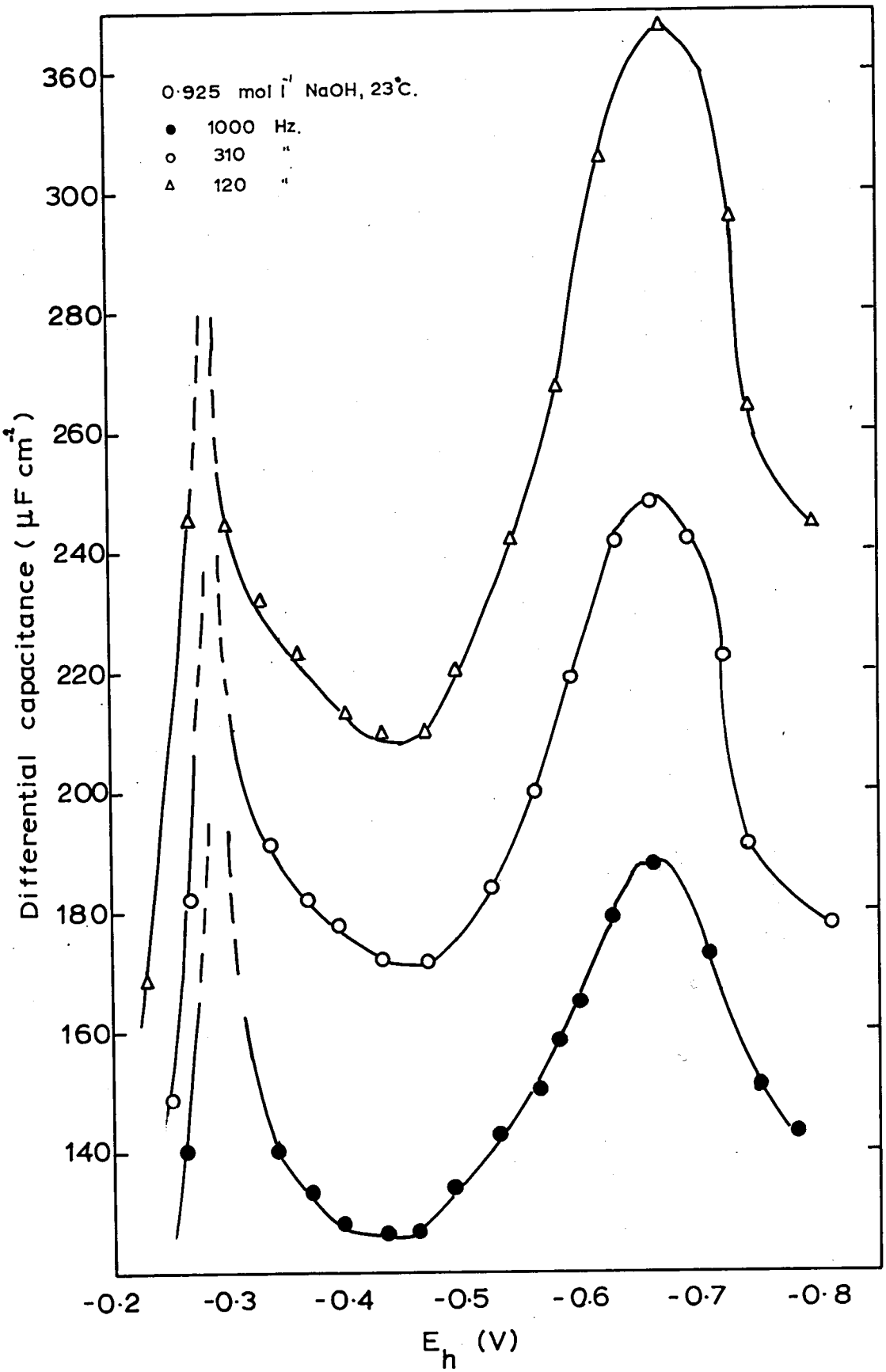

5.2. (c) Discussion

The potential (~ -0.3 V) at which the first capacitance peak occurs corresponds to the equilibrium potential for the formation of cuprous oxide. The formation of this compound on copper has been confirmed by potential sweep measurements (85). It can therefore be concluded that this peak represents the formation of Cu(I) oxide or hydrated oxide at the surface. The thickness of this film depends on the experimental conditions of the electrode. The maximum in the pseudo-capacitance corresponds to half-monolayer formation (86). This maximum should be of the order of 10^3 μF cm^{-2}; however, such high values were never obtained as stable readings due to the non-polarizability of the electrode, resulting in rapid changes of capacitance with potential. Once the film completely covers the electrode surface the observed decrease in capacitance is due to thickening of the oxide film, so that values decrease with film thickness in accordance with the flat plate capacitor theory.

The second peak at ~ -0.65 V lies between the potential of lattice disruption and the potential of hydrogen evolution, and therefore represents a reaction at the electrode surface which occurs at a potential negative with respect to the standard electrode potential of both H^+/H_2 and $Cu_2O/Cu,OH^-$. The only possible process involving available species which can occur within these limits is that between hydrogen ion and the copper electrode. This can be considered as the formation of an adsorbed layer of hydrogen ion at the electrode or the formation of a layer of copper hydride. If the latter is considered then it must be emphasised that this layer does not thicken since the capacitance remains high, (cf. the fall in capacitance at the positive limit). This is confirmed by the fact that the occurrence of the capacitance

peak at ~ -0.65 V is not accompanied by any significant change in the electrode resistance. It is likely therefore that the peak represents monolayer coverage of the electrode; however, it is not possible to confirm this point by electrometric methods due to the limited polarizability of the system. The fall in capacitance to a minimum at ~ -0.8 V indicates that no further interaction occurs at the electrode until the capacitance begins to rise at the potential corresponding to hydrogen evolution. Whether or not hydrogen evolution occurs from the base copper surface or from a hydride layer cannot be deduced from these measurements; such a question is of considerable interest.

The extent of the frequency dispersion (Figure 20) is considerably greater than that observed for acid and neutral electrolytes. An analysis of the frequency dispersion was made according to de LEVIE (60). The relationship of measured capacitance was linear with $\omega^{-\frac{1}{2}}$. The dispersion of frequency may therefore be considered as arising from inhomogeneity of the surface rather than faradaic effects. Had the latter been present the simple $\omega^{-\frac{1}{2}}$ dependency would not have been observed; faradaic effects are also unlikely in view of the constancy of the magnitude of the frequency dispersion throughout the experimentally polarizable region. (This latter observation does not apply to the small potential region around -0.3 V.) It is interesting to note that the magnitudes of the capacitances observed in this investigation (generally greater than 160 μF cm^{-2}) are higher than those observed for acid and neutral electrolytes (generally less than 100 μF cm^{-2}). This further supports the presence of extra electrode capacitance components due to adsorption.

The differential capacitance curves in the concentration range up

to 0.45 mol l^{-1} form a family in which the capacitance increases steadily with concentration (Figure 19). At 0.925 mol l^{-1} (Figure 20) the magnitude of the capacitances around the minimum at ~ -0.5 V fell below those observed at some of the lower concentrations although elsewhere in the potential range the capacitances were higher for the more concentrated solution. A number of replicate experiments showed that this effect was not an artefact. No reason can be advanced to account for this effect.

No potential was observed at which could be seen the development of a diffuse layer minimum. This is not surprising since in the expected potential region of E_z either strong OH^- adsorption or lattice disruption effects are occurring.

CHAPTER 6

THE Cu(II)/Cu EXCHANGE IN NITRATE ELECTROLYTE

The measurements described in Chapter 5 show that it is likely that adsorption of the sulphate ion occurs at the interphase at potentials corresponding to that of the Cu(II)/Cu exchange. In contrast there was no evidence for the adsorption of the anion from acidified nitrate electrolytes over the same potential range. It was therefore considered worthwhile to investigate the exchange reaction at a polycrystalline copper electrode under conditions free from adsorption.

6.1. EXPERIMENTAL

The preparation of electrolytes and electrodes has been described in Section 3.1. The electrical circuits have been described in Section 3.2. and 3.3. The electrolytic cell used for impedance measurements has been described in Section 5.1. (a). The electrolytic cell used for the galvanostatic measurements is shown in Figure 21.

6.2. RESULTS

6.2. (a) Impedance Measurements

The method of treatment of faradaic impedance results has been discussed in Section 2.3. The circuit transformations used to transform the measured electrode impedance into faradaic components are given in Appendix 2.

FIG. 21 Polycrystalline Cu.

Electolytic cell used for galvanostatic measurements.

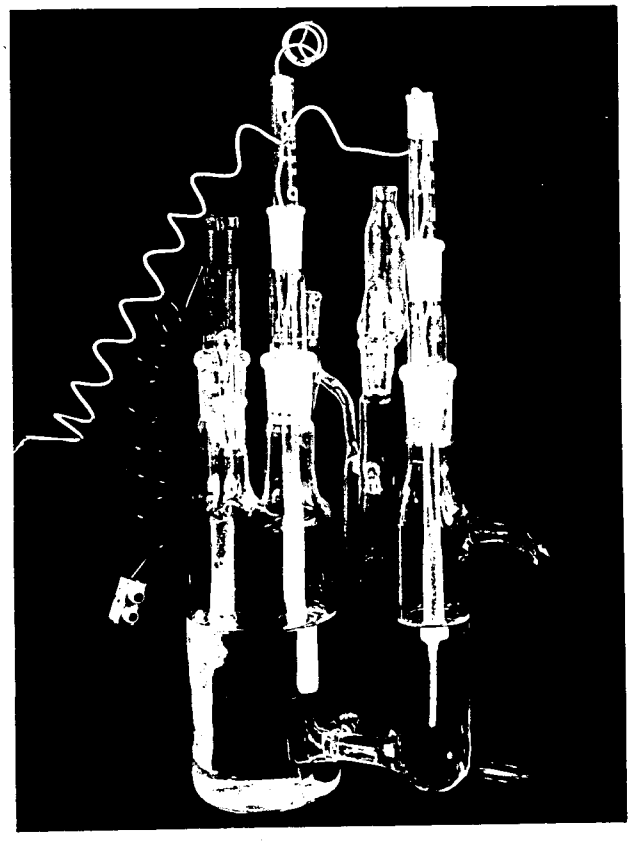

Electrode stability: A chemical etch in HNO_3 was found to give reproducible results. No detectable change was observed in the electrode impedance from the time of the first available measurement (~ 10 min after electrode/electrolyte contact). This stability persisted for at least 72 h.

Figure 22 shows typical faradaic impedance curves. Well defined values of Δ, the difference between the in-phase and out-of-phase components of the electrode impedance, were obtained at the two limits $\omega \rightarrow o$ and $\omega \rightarrow \infty$. These values were characteristic of the systems investigated and Table 3 shows mean values of Δ and the computor selected values of the double layer capacitance, at various $[Cu^{2+}]$. These values are in agreement with the magnitude expected from the capacitance studies in the absence of the exchanging ion.

TABLE 3.

$[Cu^{2+}]$/mol l^{-1}	$C_L/\mu F\ cm^{-2}$	$\Delta_{\omega \rightarrow \infty}/\Omega$	$\Delta_{\omega \rightarrow o} - \Delta_{\omega \rightarrow \infty}/\Omega$
	23°C	23°C	23°C
0.0356	53	12.0	37.5
0.0185	40	22.0	20.0
0.0102	50	20.0	29.0
0.0081	45	35.2	39.0
0.0042	48	40.0	36.0
0.0040	38	37.5	32.0

Figure 23 shows the behaviour of the impedance curves at various temperatures in the range 0 - 50°C. At higher temperatures the impedance curves approximate to classical behaviour over the frequency range employed. Table 4 shows the variation of the exchange current, adatom flux and adatom

FIG. 22 Polycrystalline Cu in KNO_3.
Typical impedance curves.

Electrode/electrolyte contact time 9 h.
0·0356 mol l^{-1} Cu^{2+}, total $[NO_3^-]$ 1 mol l^{-1}
with KNO_3, pH 3, 23 °C.
area $3{\cdot}14 \times 10^{-2}$ cm^2.

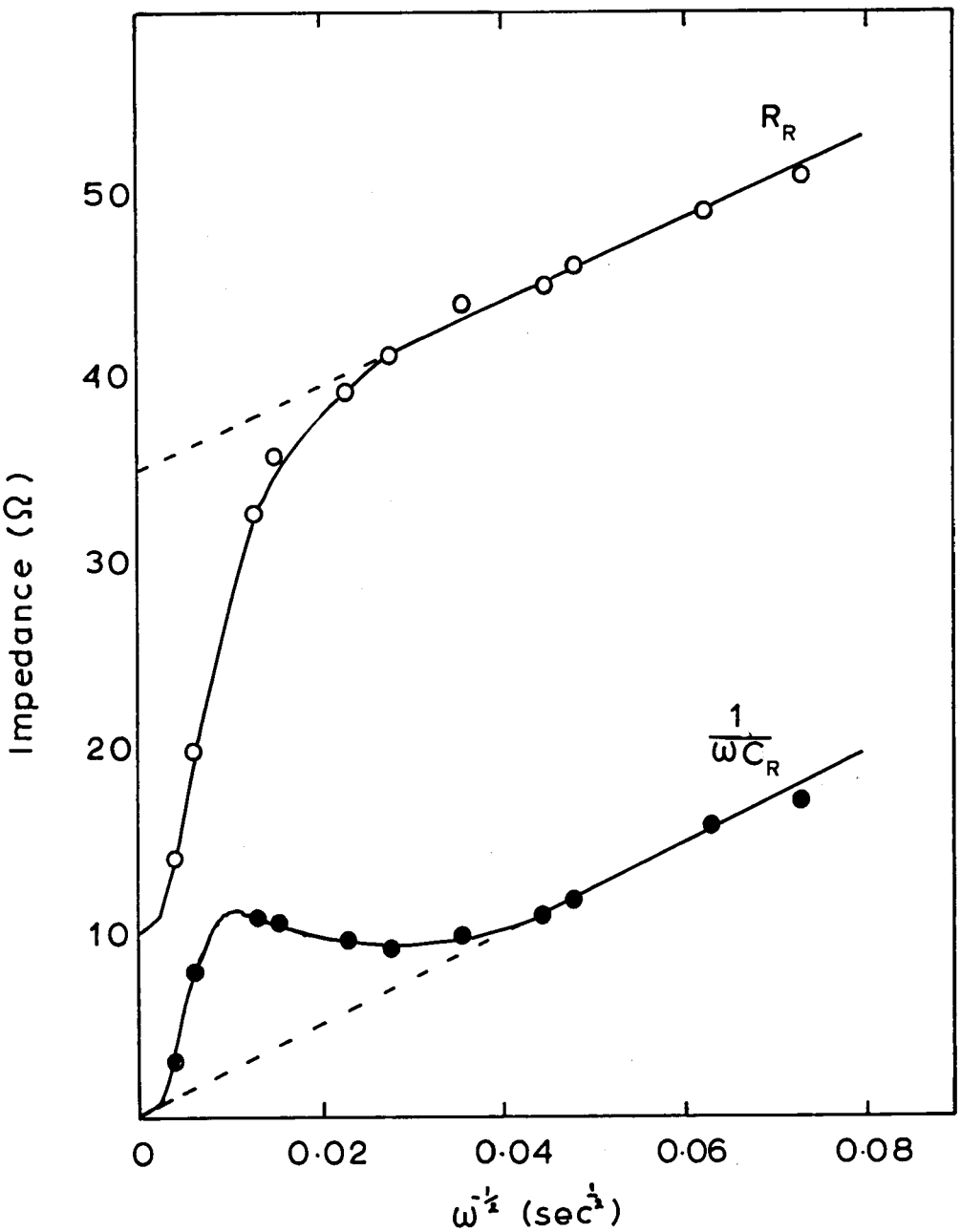

FIG.23 Polycrystalline Cu in KNO_3.

The temperature dependence of impedance curves.

0·0365 mol l^{-1} Cu^{2+}, total $[NO_3^-]$ 1 mol l^{-1} with KNO_3, pH3, electrode area $3{\cdot}14 \times 10^{-2}$ cm^2.

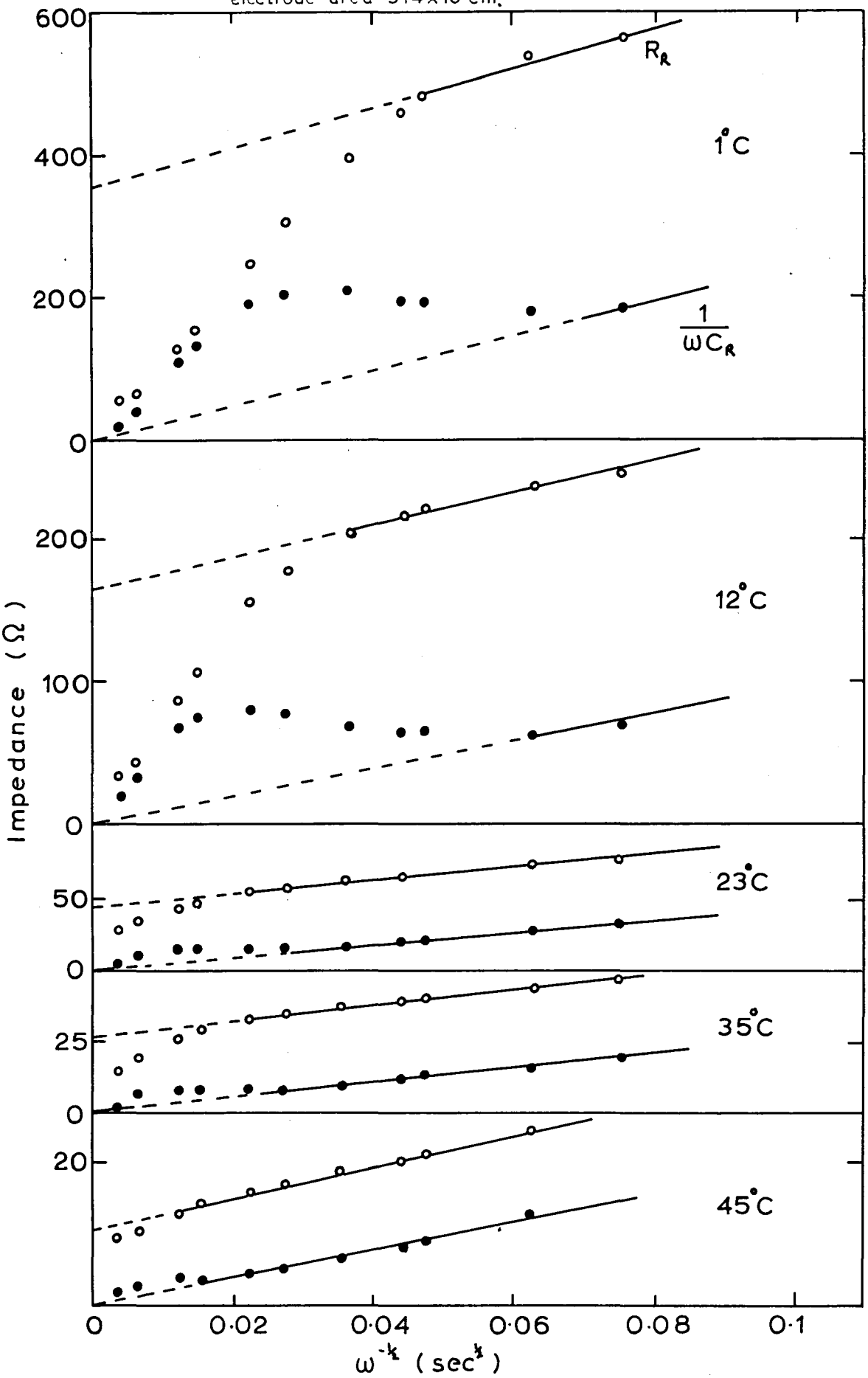

population with temperature for a typical set of results.

TABLE 4.

T/°C	i_o/mA cm^{-2}	zFV^o_g/mA cm^{-2}	Γ_o /mol cm^{-2}
1	5.4	1.9	9.0×10^{-12}
14	15.9	3.6	7.5×10^{-12}
23	15.7	20.4	1.3×10^{-11}
35	23.6	47.2	2.0×10^{-10}
45	36.5	109.5	-

6.2. (b) Galvanostatic Measurements

The value of η_D, the charge transfer overpotential, was obtained by extrapolation of the η_D-t curves to zero time (equivalent to $\omega \longrightarrow \infty$), after subtraction of the ohmic overpotential. The results of replicate experiments were identical, showing no time dependence from the first instance (~ 1 min after electrode/electrolyte contact) up to 72 h. Figure 24 shows typical η_D-i plots at various $[Cu^{2+}]$. Table 5 gives values of R_D which were calculated assuming linearity of the η_D-i plots at low overpotential.

TABLE 5.

$[Cu^{2+}]$/mol l^{-1}	R_D/Ω cm^2
	23°C
0.0356	0.7
0.0139	1.0
0.0059	1.25
0.004	1.4

FIG. 24 Polycrystalline Cu in KNO_3.

Typical overpotential - faradaic current data.

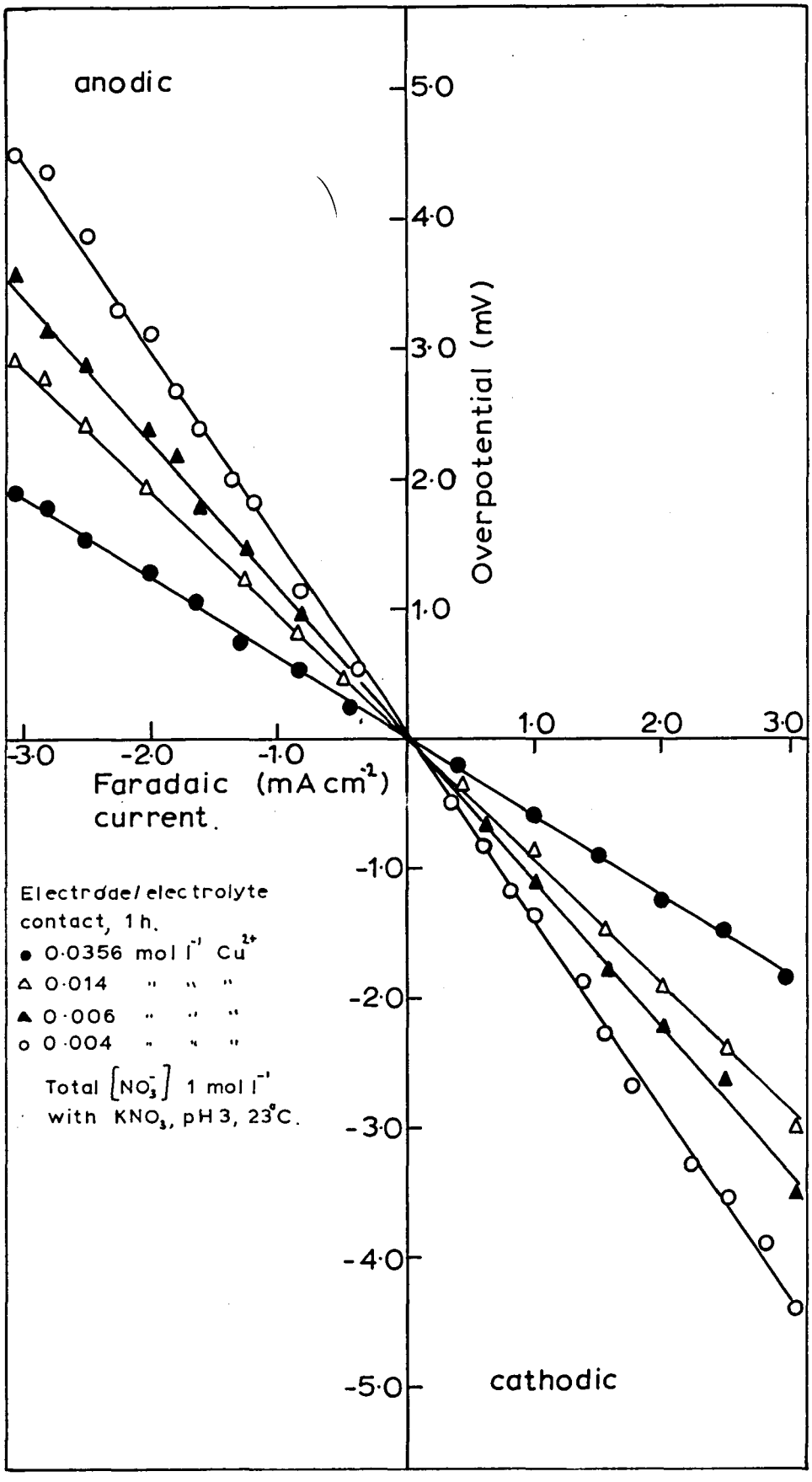

6.3. DISCUSSION

6.3. (a) Adatom Populations

The surface adatom populations were calculated from the resonant frequencies of the impedance curves using equation [20]. Due to broadness of these maxima the determinations were subject to some error. However, Table 6 shows that within the limits imposed by the experimental procedure the surface adatom population is not dependent on $[Cu^{2+}]$.

TABLE 6.

$[Cu^{2+}]$/mol l^{-1}	Γ_o/mol cm^{-2}
	23°C
0.0356	1.24×10^{-11}
0.0185	1.28×10^{-11}
0.0102	1.42×10^{-11}
0.0081	8.35×10^{-12}
0.0042	9.25×10^{-12}
0.0040	1.01×10^{-11}

The hypothetical number of atoms in a surface may be calculated but a roughness factor must also be assumed (2 - 3). The ratio of the adatom population (in atom cm^{-2}) and the total number of atoms in that surface gives the proportion of sites on the surface that are active. Thus, for copper, the fraction of sites which are active in the present series of experiments is $1.3 \times 10^{-3} - 10^{-4}$.

6.3. (b) Warburg Impedance

Examination of the slope of the impedance curves in the linear region indicates that the concentration dependence of the Warburg coefficient

varies in the expected manner but values are 4 - 5 times higher than expected from calculations, assuming that the area of the electrode corresponds to the superficial area. Such a difference is in agreement with the observations of other workers. Thus, BOCKRIS and CONWAY (58) found values ~ 1.3 times higher and HILLSON (57) ~ 30 times higher than the theoretical value.

A comparison of the theoretical and experimental values of the Warburg coefficient cannot be used to indicate the number of active sites on the electrode surface since the theory strictly applies only to the diffusion of species in solution and not on the electrode surface. However, it is clear that not all of the electrode surface is active.

6.3. (c) Exchange Current and Charge Transfer Coefficient

For sulphate electrolytes cathodic and anodic Tafel slopes of 120 and 40 mV per decade obtained by BOCKRIS et al. (70-72) were interpreted (assuming symmetry factors of 0.5) as indicating a slow Cu(II)/Cu(I) exchange followed by a faster Cu(I)/Cu step. Similar data have also been obtained by others (65, 72, 73). Confirmatory evidence by BOCKRIS and CONWAY (58) has been reported from faradaic impedance measurements, for which d log i_o/d log $[Cu^{2+}]$ is 0.75. Support for this value from other work is not particularly convincing and experimental values range from 0.3 to 0.6 (59, 67, 70, 72, 75).

In the present study d log i_o/d log $[Cu^{2+}]$ from faradaic impedance and low overpotential galvanostatic measurements (Figure 25) is 0.55 $\pm$ 0.10 and 0.36 $\pm$ 0.05 respectively. No equivocal reason can be advanced for this difference in the values which arises from the divergence of the values of

FIG. 25 Polycrystalline Cu in KNO_3.
The dependence of exchange current on concentration.

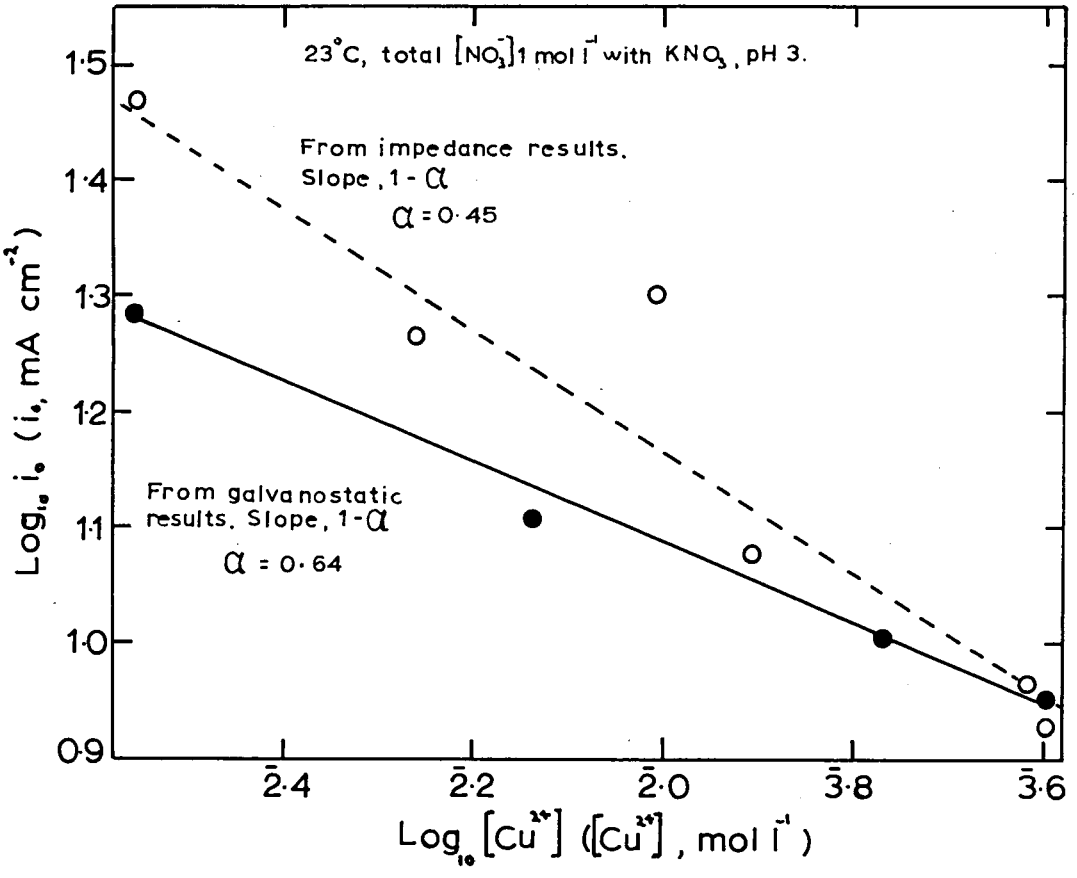

i_o obtained by the two methods. This difference in i_o is significant at the higher values of $[Cu^{2+}]$, (> 0.015 mol l^{-1}). A possible explanation may be connected with the inherent difference in the two methods for, whereas in the faradaic impedance experiments the electrode is always poised at equilibrium, in the galvanostatic experiments the electrode potential is uncontrolled during the immediate pre-polarisation periods. The data in Table 6 shows that the concentration of adsorbed atoms at the electrode is independent of $[Cu^{2+}]$ and the slope of the lines in Figure 25 must therefore represent the dependence of the exchange current on $[Cu^{2+}]$ only.

Figure 26 shows a typical Tafel plot corresponding to anodic and cathodic galvanostatic experiments; also plotted are the value of the exchange current obtained from the low overpotential measurements and the slopes of the lines representing the reaction as a single two-electron transfer. The results from low overpotential measurements are not consistent with those from high overpotential measurements. Thus, the "equilibrium" value of i_o is not obtained by extrapolation of either cathodic or anodic Tafel lines for < 100 mV. The anodic branch of Figure 26 in the region 20 - 100 mV conforms reasonably well to a value of i_o with α corresponding to that obtained from d log i_o/d $[Cu^{2+}]$. The cathodic branch may well contain a limiting region which conforms to these parameters but it is obscured to a large extent by experimental scatter of results. It appears therefore that about the equilibrium the reaction is a two-electron transfer and at higher overpotentials the mechanism becomes more complicated. The slopes of anodic and cathodic branches of the Tafel plots at high overpotential and the differing anodic and cathodic intercepts at $\eta_D = 0$ confirm that under the

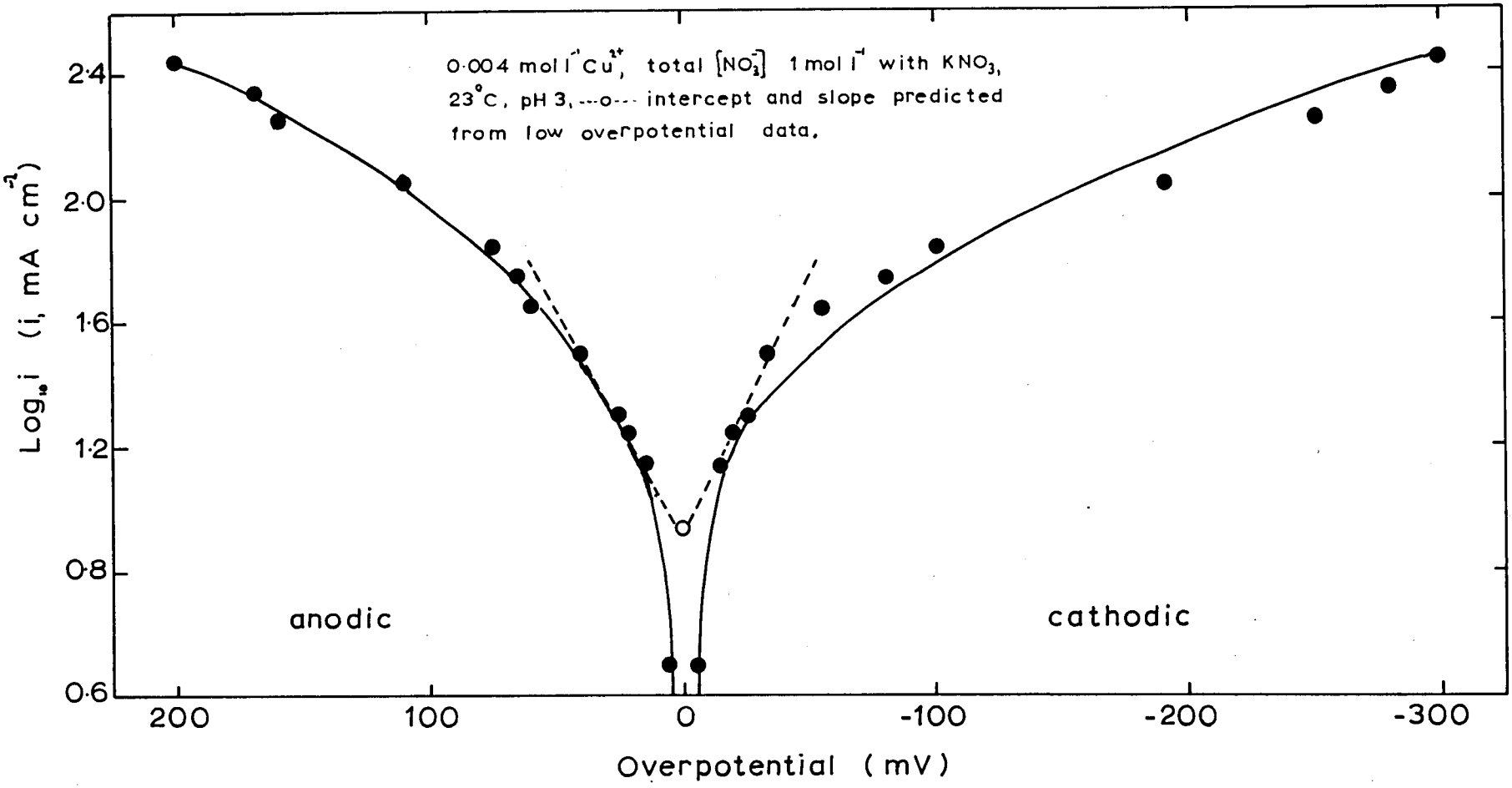

FIG.26 Polycrystalline Cu in KNO_3. Tafel curves.

condition of high overpotential the reaction involves the participation of Cu(I) species as observed by others for the reaction in sulphate electrolytes (70-72, 75).

6.3. (d) Activation Enthalpies

Figure 27 shows a plot of log i_o against 1/T. An enthalpy of activation, ΔH_D, determined from the slope of this plot, can be attributed to the charge transfer process. ΔH_D is calculated to be 34.0 $\pm$ 4.0 k J mol^{-1}.

The process of adatom diffusion and adatom incorporation into the lattice has been measured as $zF\ V_g^o$. The temperature dependence of this quantity is shown in Figure 28. The slope of Figure 28 gives the activation enthalpy, ΔH_k, of this lattice building (crystallisation) process. ΔH_k is calculated to be 67.0 $\pm$ 4.0 k J mol^{-1}.

Values of Γ_o are difficult to measure accurately because of the broadness of the "local maxima", particularly at low temperatures. The enthalpy of adsorption, ΔH_d, (i.e. the heat required to remove an ion from the lattice and place it in an adsorbed state on the surface) is calculated from the temperature dependence of Γ_o (Figure 29) and is best assessed as 42.0 $\pm$ 10.0 k J mol^{-1} (mean calculated from five systems).

6.3. (e) Rate-determining Process

Comparison of the relative magnitudes of charge transfer (i_o) and crystallisation ($zF\ V_g^o$) processes in the temperature range investigated (Figures 27 and 28) indicates that a change in the rate controlling process is occurring. Under the conditions in which experiments are carried out,

FIG. 27 Polycrystalline Cu in KNO_3.
Temperature dependence of exchange current.

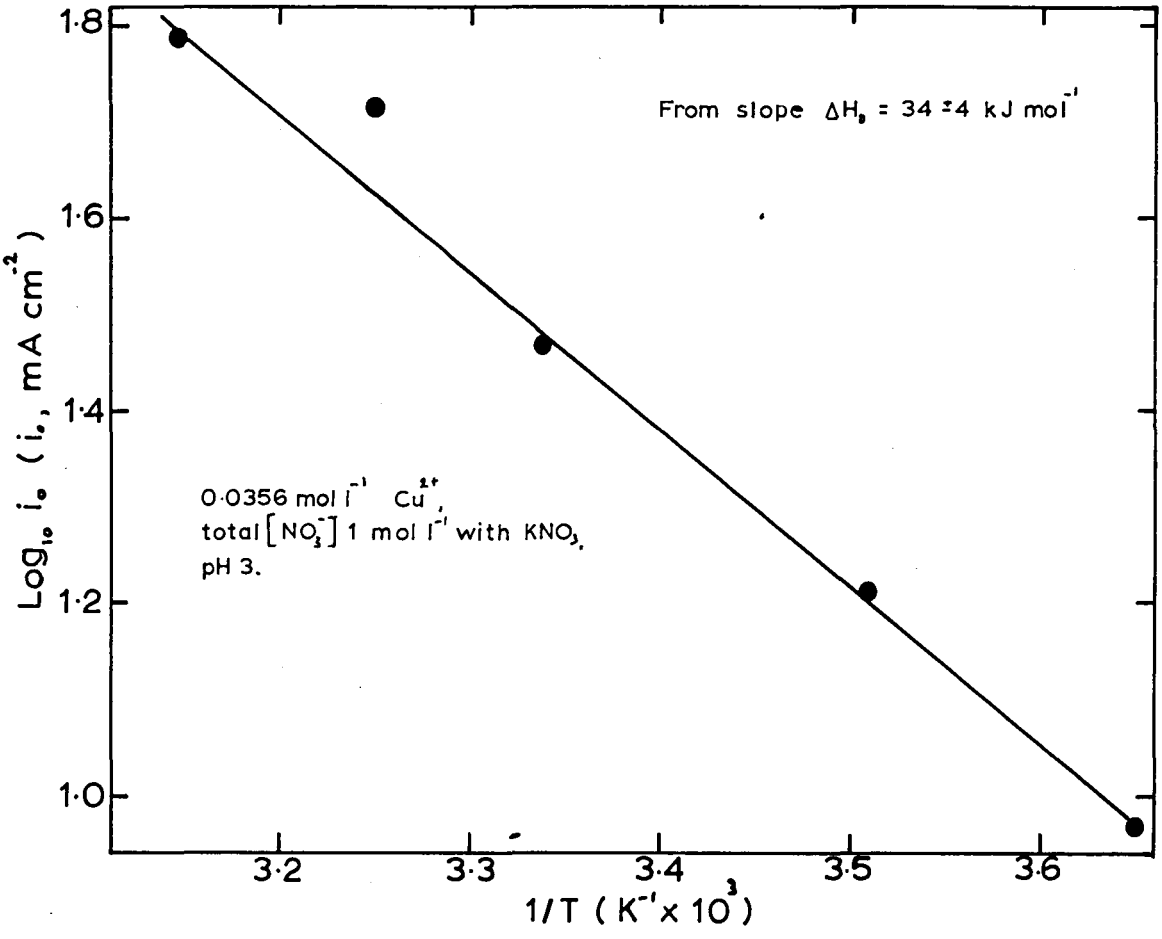

FIG. 28 Polycrystalline Cu in KNO_3.
Temperature dependence of adatom flux.

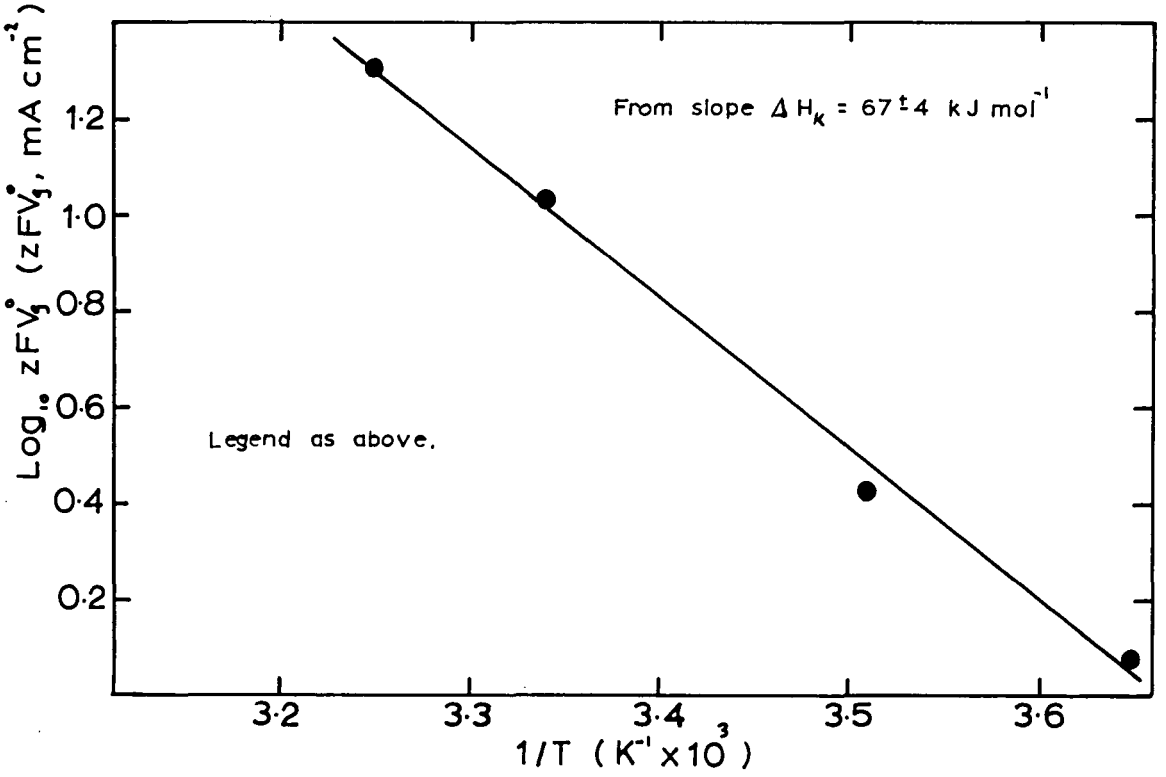

FIG. 29 Polycrystalline Cu in KNO_3.
The dependence of adatom concentration on temperature.

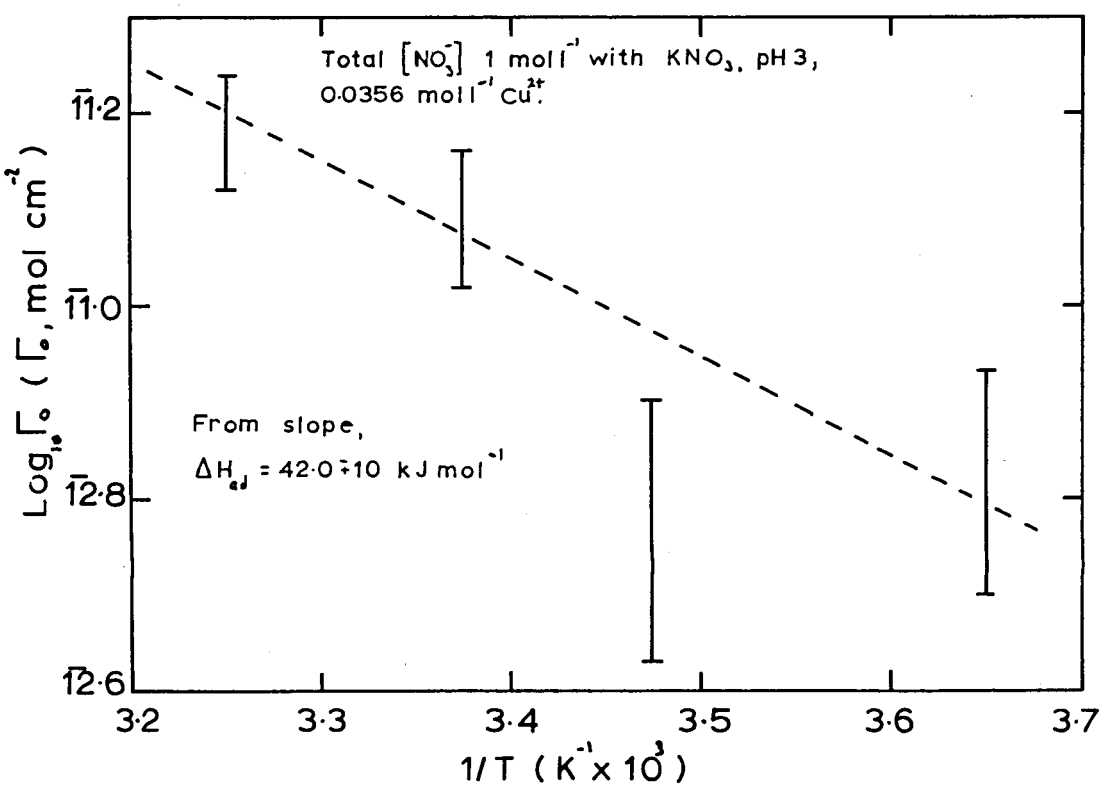

the rate controlling process is that for which the greatest free energy of activation is required. Free energies were calculated according to the equation given in Section 2.4.

Thus at 23 C, we take $i_o \sim 30$ mA cm (for ~ 0.04 mol l^{-1} Cu(II) for an "electrode concentration" of 0.14 mol cm^{-3} (compared with the hypothetical unit amalgam concentration of 1 mol cm^{-3}. Hence the hypothetical electrode concentration is density/atomic weight). Comparison of Γ_o, the adatom population, with that expected for a surface completely covered by adatoms indicates that $\sim 10^{-3}$ of the surface is active. This gives I_o at $23^oC \sim 450$ mA cm^{-2}. Thus using equations [29] and [31] ΔS_D is calculated as -7.8 J k^{-1} mol^{-1}. For the adatom process the standard flux, F_o, is calculated to be ~ 70 mA cm^{-2}. Thus by similar calculations, ΔS_k is obtained as $\sim +88$ J k^{-1} mol^{-1}.

Calculations repeated for different temperatures demonstrate that at 40 - 50°C, the processes of charge transfer and adatom crystallisation contribute equally to the overall electrode reaction. The change in rate controlling process is also exhibited in the impedance curves where at higher temperatures the relaxation effects are greatly diminished. The enthalpies of activation, entropies and free energies of activation for the two processes are given in Table 7.

TABLE 7.

	0°C	23°C	45°C
ΔH_D/k J mol^{-1}	34.0	34.0	34.0
ΔS_D/J k^{-1} mol^{-1}	-8.35	-7.8	-9.7
ΔG_D/k J mol^{-1}	36.3	36.3	37.1
ΔH_k/k J mol^{-1}	67.0	67.0	67.0
ΔS_k/J k^{-1} mol^{-1}	+88.0	+88.0	+91.5
ΔG_k/k J mol^{-1}	43.0	41.0	37.9

6.3. (f) The Crystallisation Process

The separation of the crystallisation process into two separate steps was discussed in Section 2.2. The present results show that for this system the crystallisation process may be regarded as having only one rate determining component. Table 3 shows that R_k is not a function of $[Cu^{2+}]$ (and hence i_o). The form of the impedance curves is in all cases similar to those predicted by GERISCHER (23, 24). The enthalpy of activation for the process of adatom diffusion results from the difference between the activation enthalpies for crystallisation and that required to remove an atom from the lattice to the surface, $(\Delta H_k - \Delta H_{ad})$. This difference, about 20 - 25 k J mol^{-1}, is large for surface self diffusion but is nevertheless sufficiently small to indicate that this process is not rate controlling.

CHAPTER 7

THE Cu(II)/Cu EXCHANGE IN SULPHATE ELECTROLYTE

It was decided to investigate the kinetics of the Cu(II)/Cu exchange in sulphate electrolyte in order to compare the results both with previously reported measurements for sulphate electrolyte and also with the adsorption free nitrate system (Chapter 6).

7.1. EXPERIMENTAL

The preparation of electrolytes and electrodes has been described in Sections 3.2. and 3.3. The electrolytic cell used for impedance measurements has been described in Section 5.1. (a). The electrolytic cell used for the galvanostatic measurements has been described in Section 6.1. (Figure 21).

7.2. RESULTS

7.2. (a) Impedance Measurements

Various methods of electrode pretreatment were investigated. The results are shown in Table 8.

Maximum period of stability was achieved when the electrode was etched chemically (2 sec) with HNO_3 (30%) after mechanically polishing on roughened glass using bidistilled water as a lubricant.

Following previous work (58, 59, 64) in which it was reported that the electrolyte system behaved as a simple Randles model, attempts were made to present the experimental impedance data using complex plane diagrams (30) -

TABLE 8.

0.0377 mol l^{-1} $[Cu^{2+}]$, electrode area 3.14×10^{-2} cm^{-2}

Electrode pretreatment	$C_L/\mu F\ cm^{-2}$	R_D/Ω	R_K/Ω
HNO_3 etch	32	45	170
-ve polarise for few secs o/c for $1\frac{1}{2}$ h	41.5	50	140
H_2O_2/HOAc etch o/c for 3 h	41.5	65	225
Mech. polish only o/c for 3 h	48	10	55
H_2 gassed off o/c for 1 h	160	5	25
-ve polarise for 10 min Readings immediately	35	60	170
$FeCl_3$ etch	50	50	140

Figure 30. This representation indicates that the process is more complex than simple charge transfer and diffusion in solution. Russian work (64) indicated that displacement of the electrode potential from its equilibrium value resulted in complex plane diagrams resembling transformation of impedance data corresponding to systems without diffusion polarisation, i.e. completely semi-circular plots. This was not found to apply in the present experimental study (Figure 30); no explanation can be advanced for the Russian workers' results. A similar treatment of results was used in this series of experiments to that employed for nitrate electrolyte (Figure 31). Values of Δ, the difference between the in-phase and out-of-phase components, were obtained at the limits $\omega \rightarrow 0$ and $\omega \rightarrow \infty$. Table 9 shows mean values of Δ and also computor selected values of C_L at various $[Cu^{2+}]$.

FIG. 30 Polycrystalline Cu in H_2SO_4.
Typical complex plane diagrams.

(a) measurements made at potential 20 mV -ve. of equilibrium.

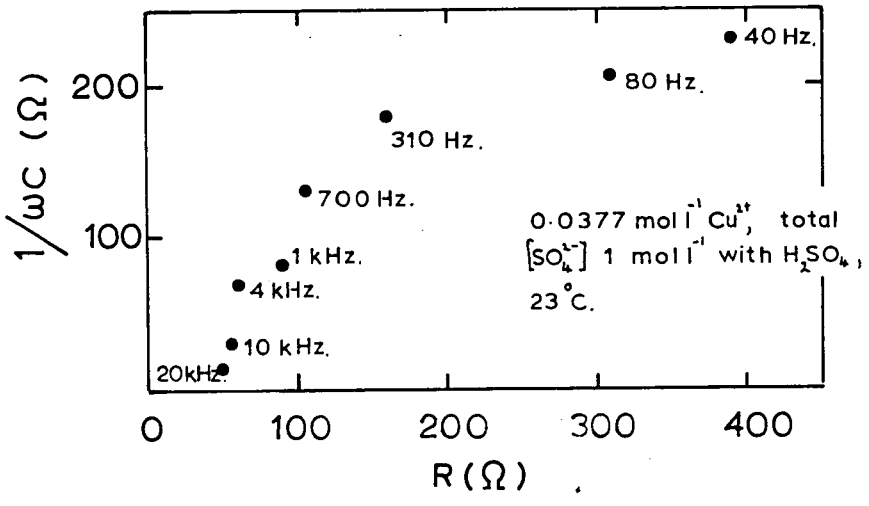

(b) measurements made at equilibrium potential.

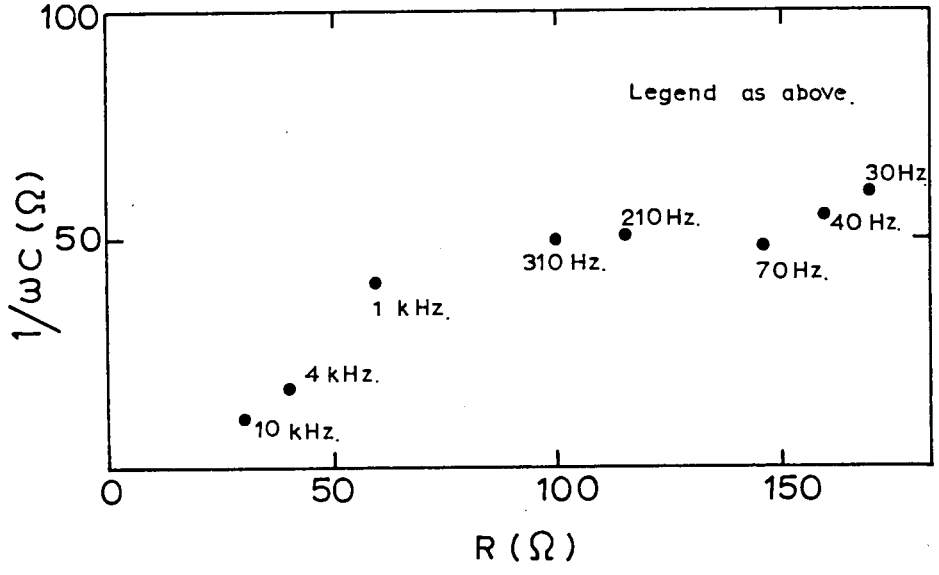

FIG. 31 Polycrystalline Cu in H_2SO_4.

Typical impedance curves.

Electrode/electrolyte contact time 48 h.
0·0478 mol l^{-1} Cu^{2+}, total $[SO_4^{2-}]$ 1 mol l^{-1} with H_2SO_4, 23 °C, electrode area $3{\cdot}14 \times 10^{-2}$ cm^2.

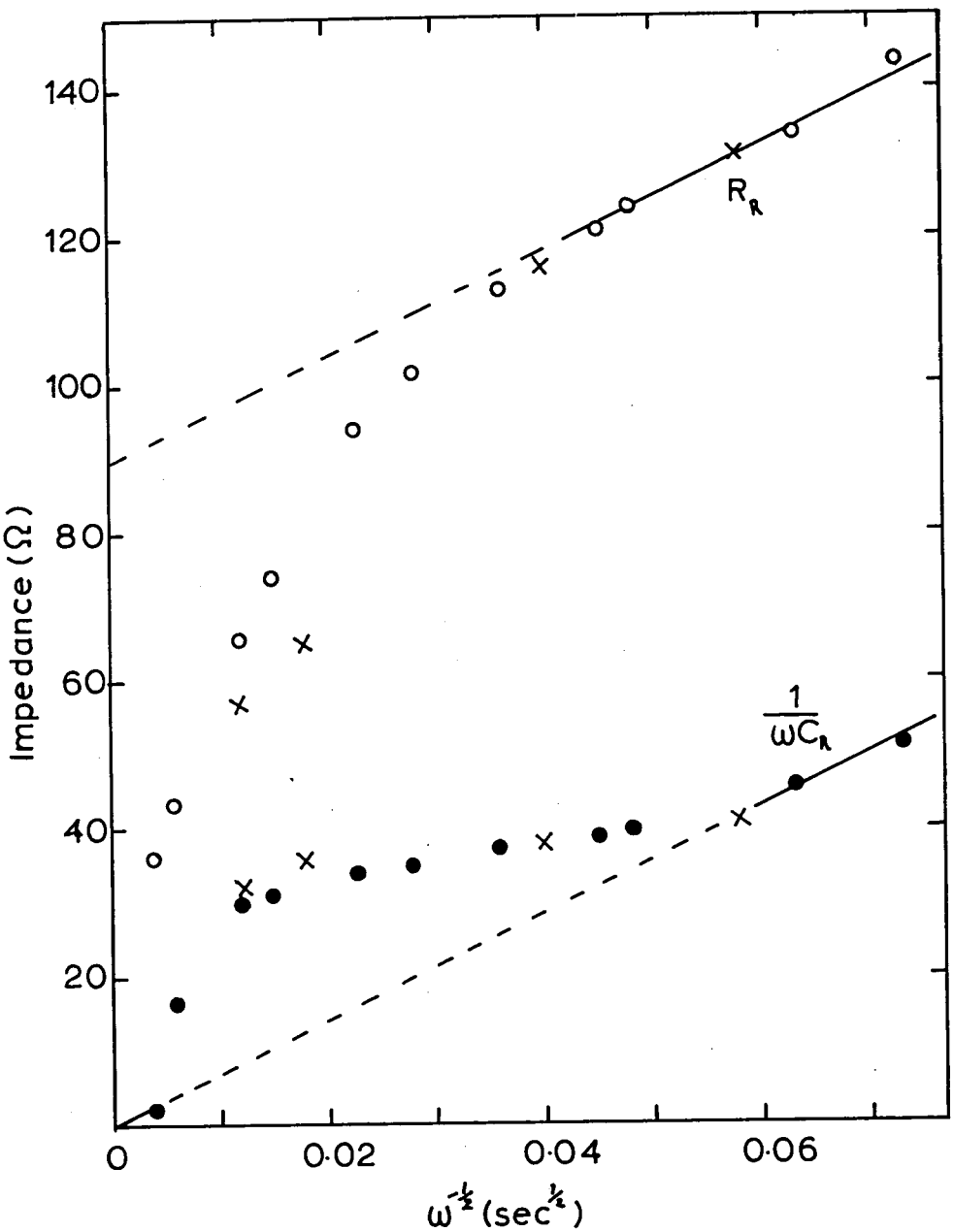

x - Data from Pearson and Schrader (59), 0·0562 mol l^{-1} Cu^{2+}.

TABLE 9.

23°C, electrode area 3.14 x 10 cm^{-2}.

$[Cu^{2+}]$/mol l^{-1}	$C_L/\mu F\ cm^{-2}$	$\Delta_{\omega \to \infty}/\Omega$	$\Delta_{\omega \to 0} - \Delta_{\omega \to \infty}/\Omega$
0.0974	74	13.3	45
0.0478	55	14.5	76
0.0377	32	25	150
0.0123	42	35	130
0.0092	49	38	177

The values of the double layer capacitance are in good agreement with those expected from the differential capacitance data (Chapter 5) and are slightly greater than the values obtained for the exchange in nitrate electrolyte (Chapter 6). It was more difficult to decide the value of C_L from the computor match because of the larger range of frequency over which relaxation occurred. The fact that the best value corresponds to the differential capacitance data to a large extent confirms that the correct choice has been made.

Figure 32 shows the variation of the impedance spectra over a range of temperatures, 0 - 50°C. The linear extrapolation at lower frequencies occurs over a much smaller range of frequencies than observed for the case of nitrate electrolyte. However, it should be noted that the investigation of the structure of the interphase showed complications for the case of sulphate electrolyte. Although the return to the low frequency slope in the case of the resistive component is not particularly well defined at higher frequencies, there is clear indication for the out-of-phase component that this is so. Clearly, results at higher frequencies are desirable. However, the present apparatus was limited to an upper frequency of 20 kHz.

FIG. 32 Polycrystalline Cu in H_2SO_4.
The temperature dependence of impedance curves.
0·0377 mol l^{-1} Cu^{2+}, total $[SO_4^{2-}]$ 1 mol l^{-1} with H_2SO_4, electrode area $3{\cdot}14 \times 10^{-2}$ cm^2.

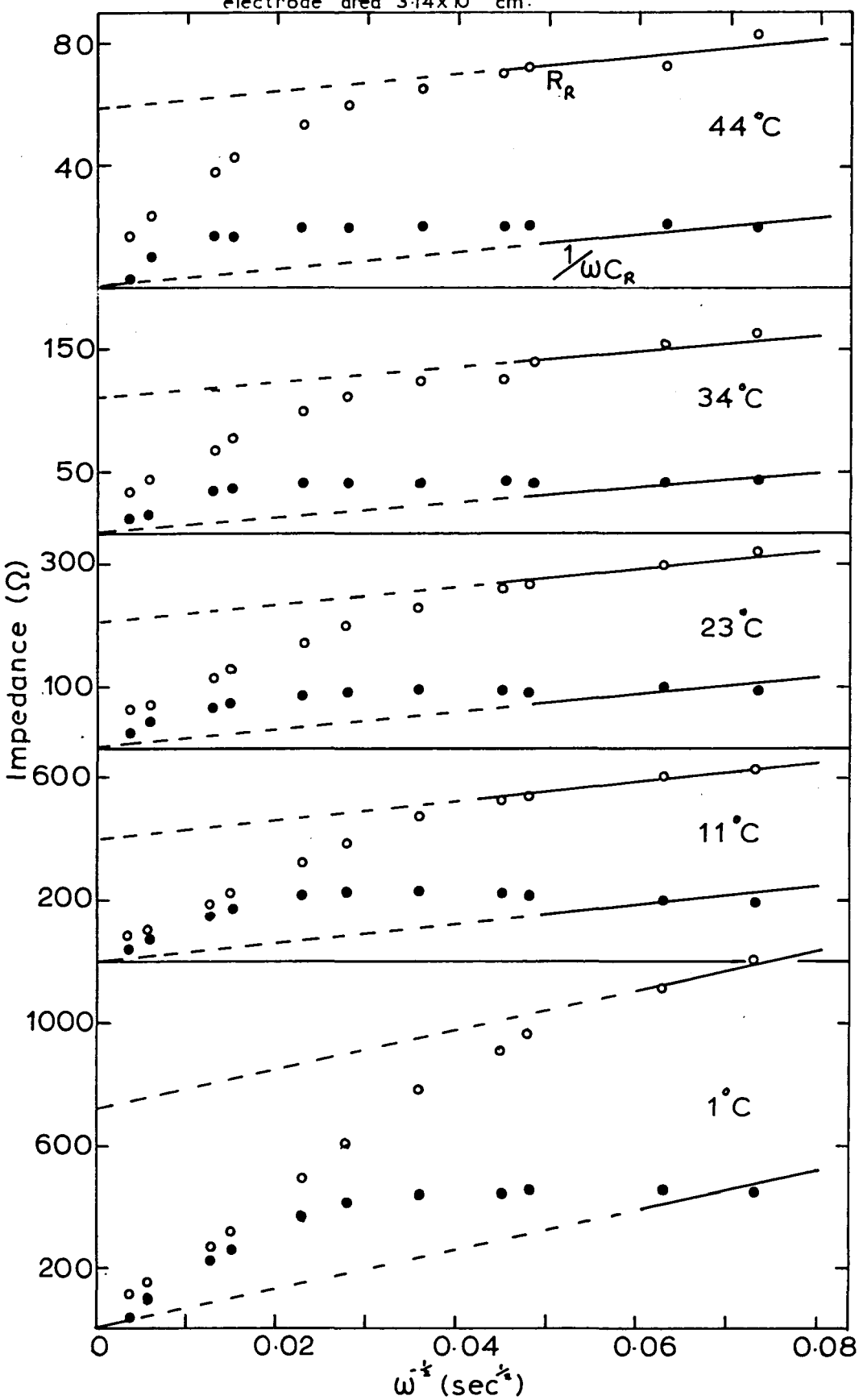

7.2. (b) Galvanostatic Measurements

η_D - i plots and also Tafel plots were obtained using current pulses of 100μ sec (corresponding to $\omega \longrightarrow \infty$) and 6 m sec (corresponding to $\omega \longrightarrow 0$) length. Typical η_D - i plots from low overpotential data are shown in Figures 33 and 34. Typical Tafel plots are shown in Figure 35.

7.3. DISCUSSION

7.3. (a) Relaxation in Impedance Spectra

Relaxation in impedance spectra has been observed in a previous investigation by LORENZ (25). A recent paper by PEARSON and SCHRADER (59) can be interpreted equally well in terms of relaxation and Figure 31 shows results from these workers plotted on curves obtained in the present experiments (some normalisation was necessary to allow for the difference in electrode areas). The early papers of HILLSON (57) and BOCKRIS and CONWAY (58) show no relaxation, although HILLSON (57) shows departure from linearity at low frequencies. In comparison with the present and other literature values of i_o, the high value of i_o obtained by BOCKRIS and CONWAY (58) can be possibly explained by their use of encapsulated, "initially dry" electrodes and the measurement of the impedance immediately after contact with the electrolyte. There is a large amount of data to show that at the instance of forming an interphase i_o may be very high indeed and stable electrodes are only produced after a period of o/c. This may also account for the relaxation free impedance plots observed by BOCKRIS and CONWAY (58).

7.3. (b) Participation of Adatoms

Comparison of the differences between the in-phase and out-of-phase components of the electrode impedance as frequency is increased indi-

FIG. 33 Polycrystalline Cu in H_2SO_4.

Overpotential - faradaic current data for 100 μs. pulse length.

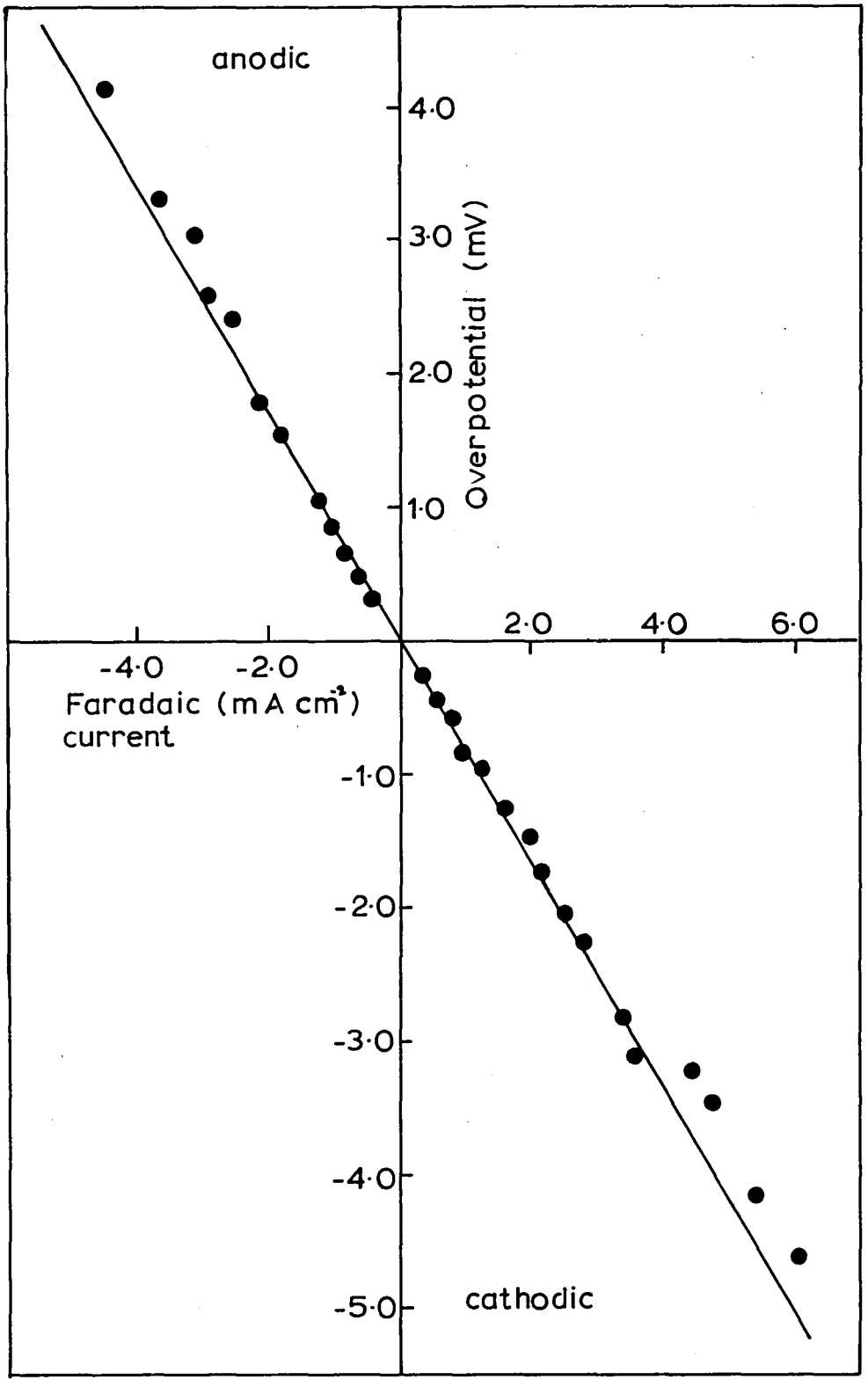

FIG.34 Polycrystalline Cu in H_2SO_4.
Overpotential - faradaic current data
for 6 ms. pulse length.

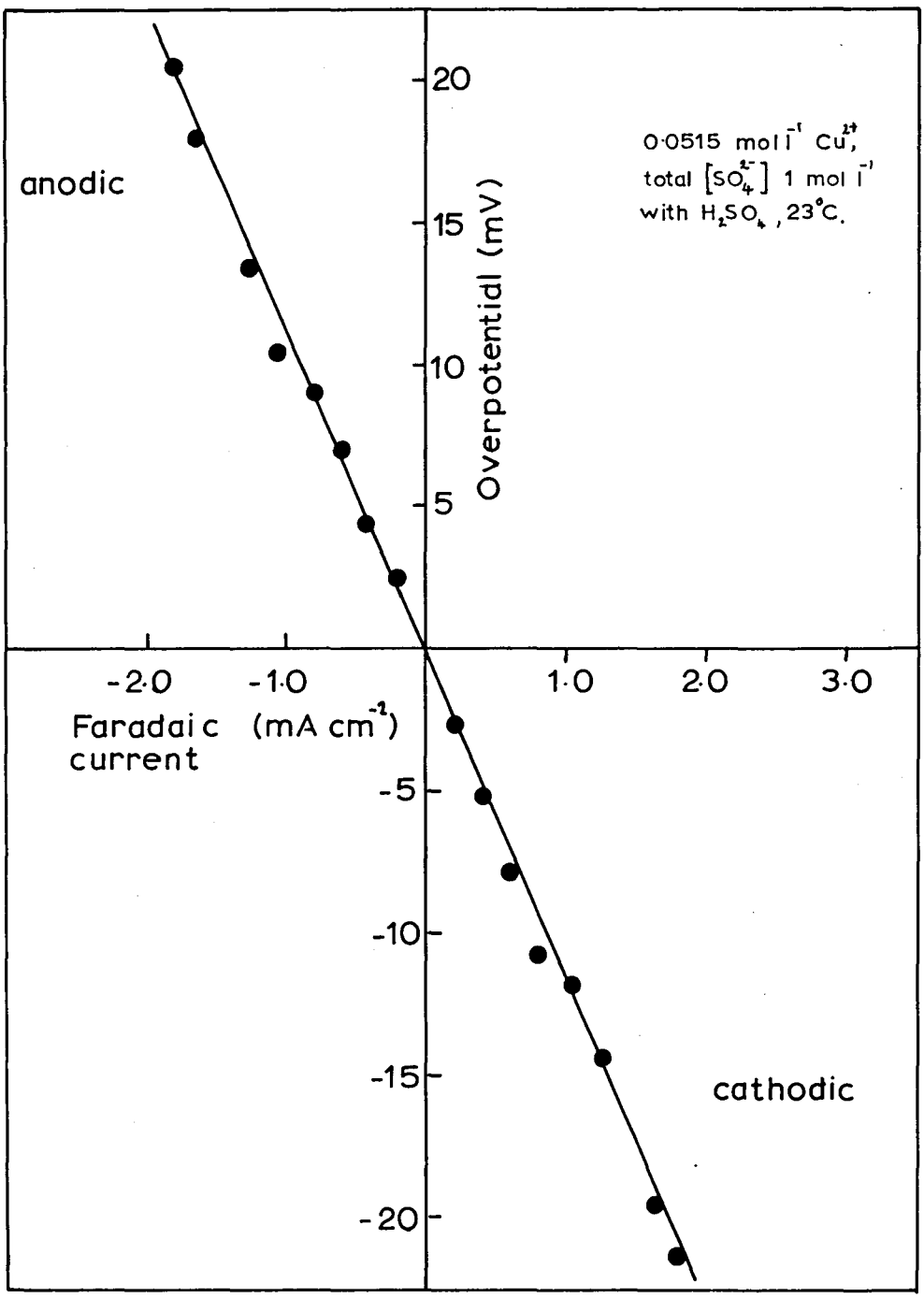

FIG. 35 Polycrystalline Cu in H_2SO_4.

Tafel plots.

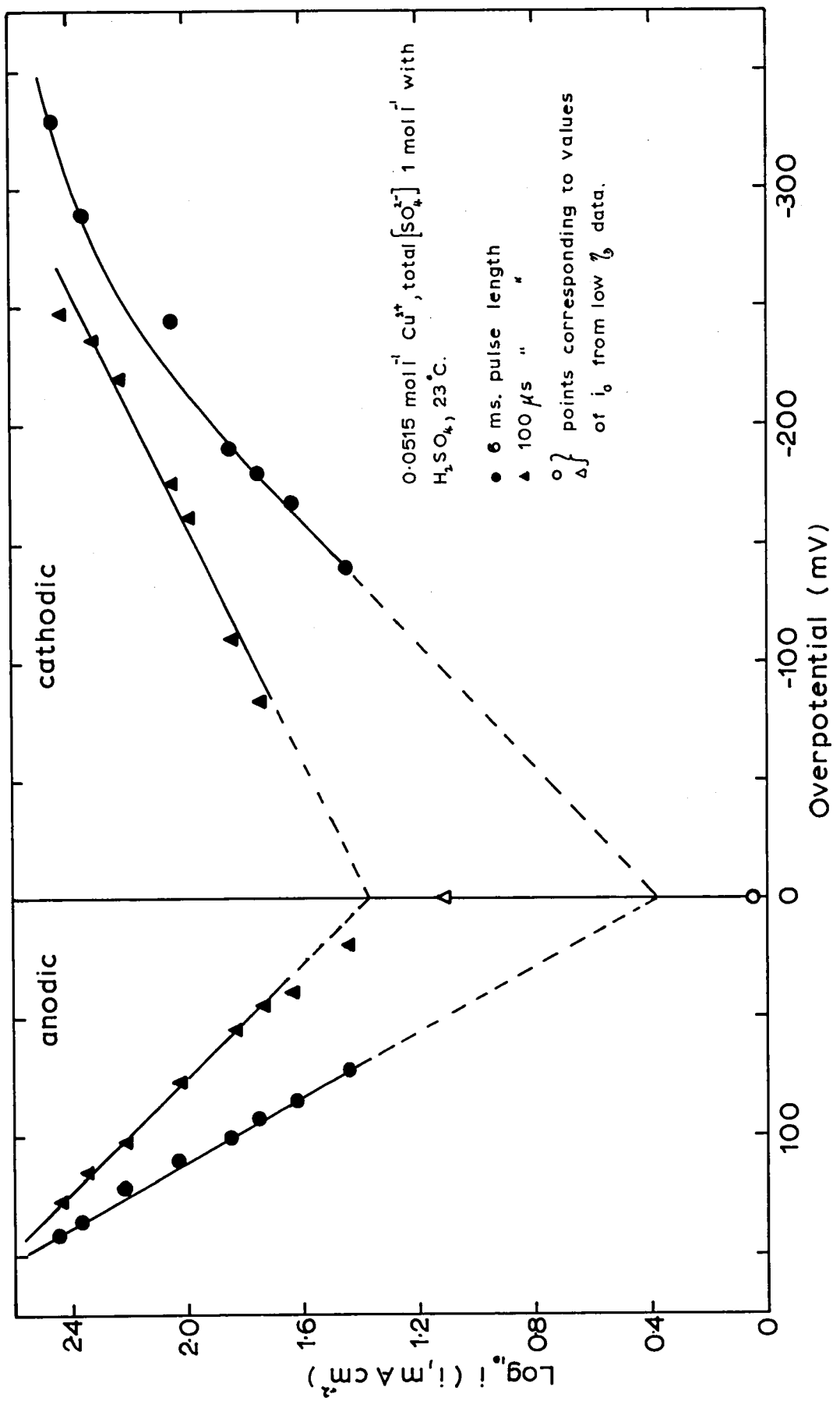

cates that relaxation occurs over a wider range of frequencies than observed for the case of nitrate electrolyte. Similar to observations in nitrate electrolyte, since R_k is greater in magnitude than R_D it can be concluded that the process of incorporation (or release) of atoms into the lattice is the rate determining step in the exchange process. The relaxation broadening, observed in the case of sulphate electrolyte, can be interpreted in terms of adsorption of the anion, which engenders a more heterogeneous surface on the electrode. In the case of nitrate electrolyte the relaxation effects were eliminated at higher temperature whereas in the present case the effects are still apparent over the whole of the temperature range investigated, in agreement with the intrusion of the adsorbed sulphate on the crystallisation process.

7.3. (c) Activation Enthalpies

Figure 36 shows a plot of log i_o against 1/T. ΔH_D determined from the slope is calculated to be 31.0 ± 4.0 k J mol^{-1} (cf. 34.0 ± 4.0 k J mol^{-1} for nitrate case). ΔH_k for the adatom incorporation process, from a plot of log zFV_g^o against 1/T (Figure 37), is calculated to be 51.0 ± 4.0 k J mol^{-1} (cf. 67.0 ± 4.0 k J mol^{-1} for the nitrate case). An approximate value for the enthalpy of adsorption of adatoms, ΔH_{ad}, is obtained from a plot of log Γ_o against 1/T (Figure 38). This is assessed as 27.0 ± 10.0 k J mol^{-1} (cf. 42.0 ± 10.0 k J mol^{-1} for the nitrate case).

The enthalpy of activation for the process of adatom diffusion on the electrode surface, $\Delta H_k - \Delta H_{ad}$, is therefore 20 - 25 k J mol^{-1} (cf. 20 - 25 k J mol^{-1} for the nitrate case).

Comparison of the enthalpies of activation for the various components of the electrode process in the two different supporting electrolytes

FIG.36 Polycrystalline Cu in H_2SO_4. Temperature dependence of exchange current.

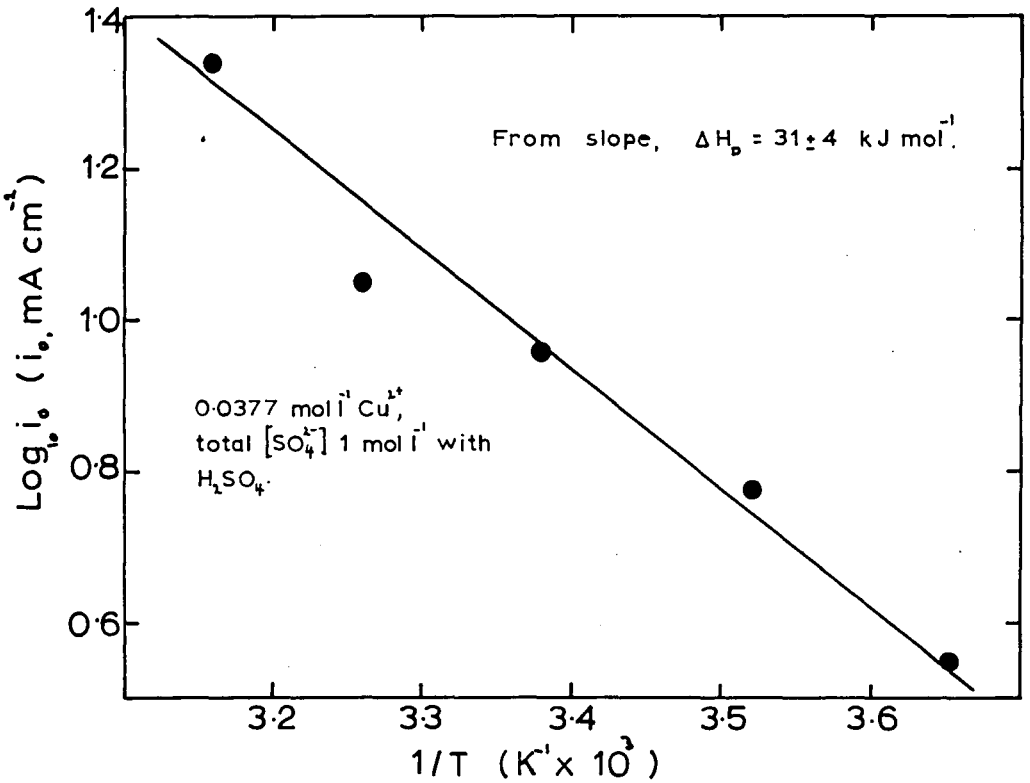

FIG.37 Polycrystalline Cu in H_2SO_4. Temperature dependence of adatom flux.

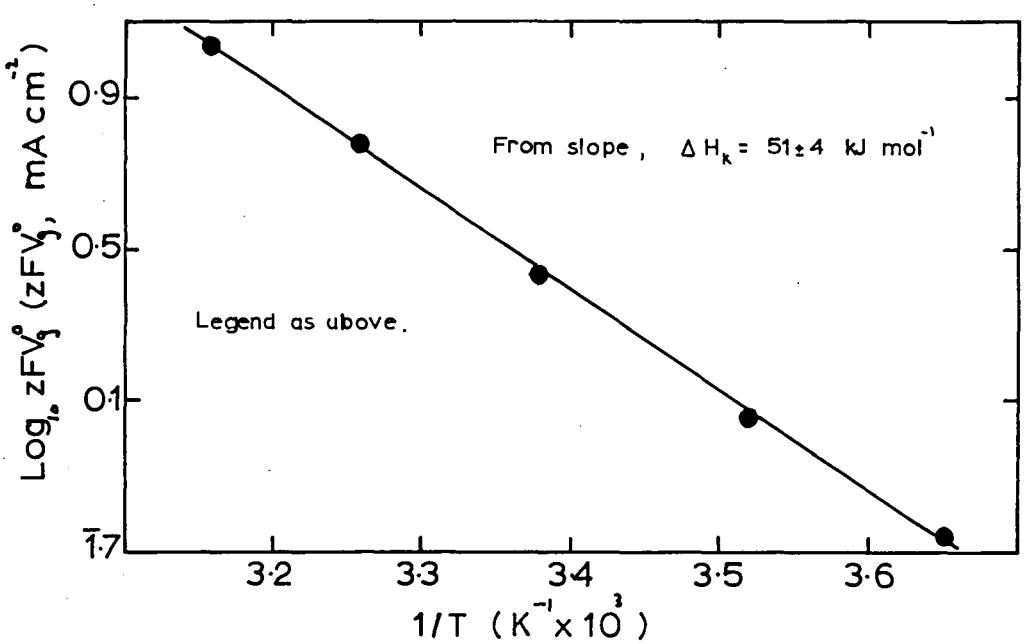

FIG.38 Polycrystalline Cu in H_2SO_4.
The temperature dependence of adatom concentration.

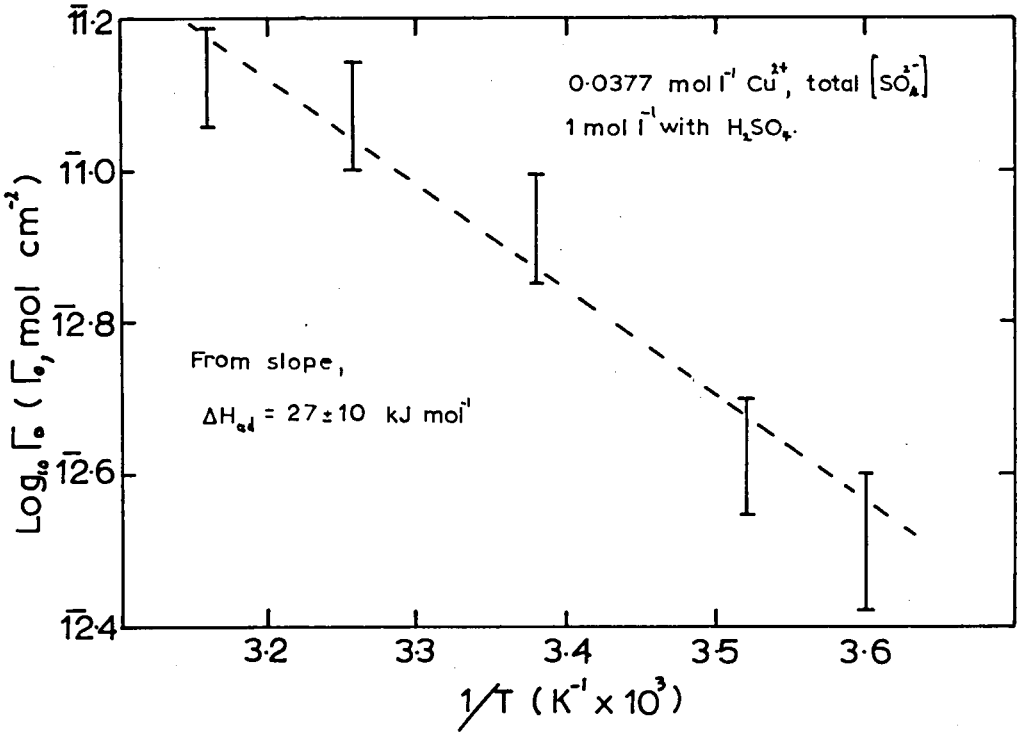

FIG.39 Polycrystalline Cu in H_2SO_4.
The dependence of exchange current on concentration.

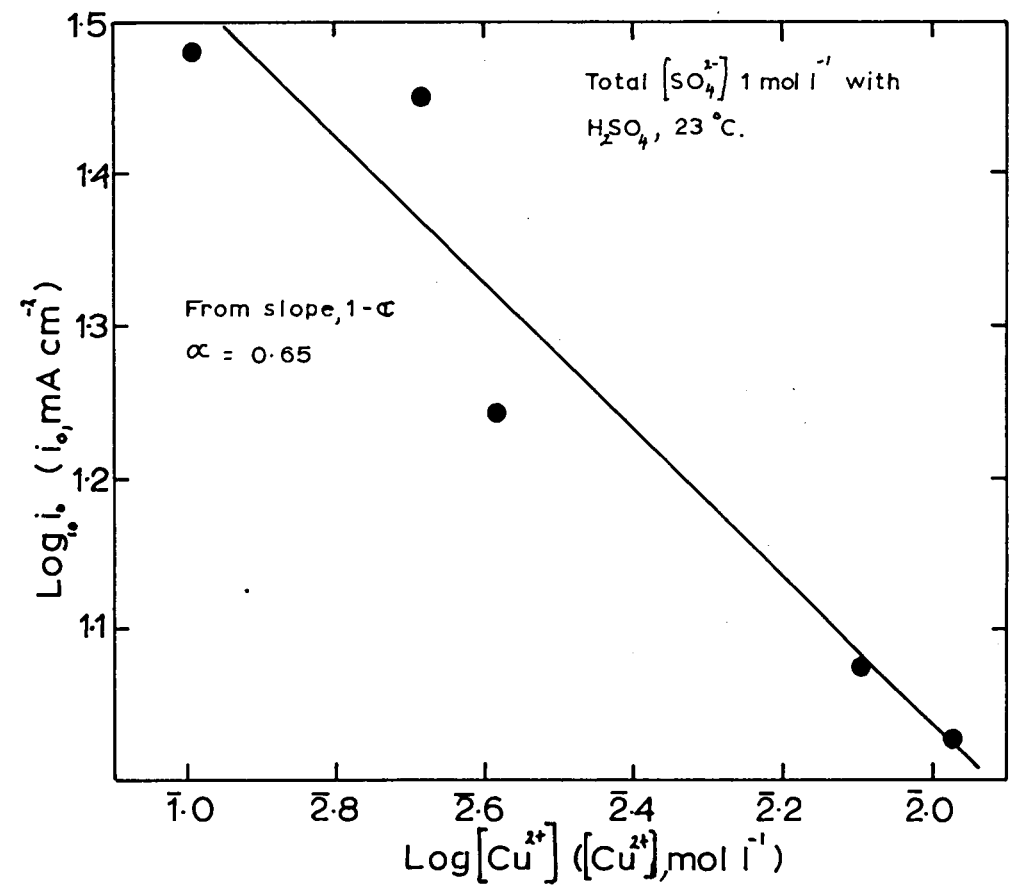

indicates that, while the adsorption of the sulphate anion does not inhibit the diffusion of adatoms on the surface, the process of incorporation into the lattice must involve the displacement of adsorbed anions. A lower enthalpy of activation for the adsorption of adatoms is obtained in the case of sulphate electrolyte; the adsorption of sulphate possibly stabilises these atoms of very low co-ordination number. The expected effect of the adsorption of anions at kink sites (also low co-ordination number) would be to increase the enthalpy of activation of the crystallisation process since the adsorbed anion must be displaced. However, the adsorption of the anion may stabilise atoms of low co-ordination number at the electrode surface which tend to be unstable in the presence of non-interacting electrolytes. A lower enthalpy of activation for the crystallisation process would therefore be expected. It should also be noted that in the case of sulphate electrolyte, stable results were only obtained after a significantly longer period of contact with the electrolyte than in the case of the nitrate electrolyte. This conforms with the possibility of increased interaction of sulphate anion with the electrode, which ultimately prolongs the life of the unstable adspecies at the surface.

7.3. (d) The Charge Transfer Process

i_o is about 30 mA cm^{-2} for 0.0478 mol l^{-1} $[Cu^{2+}]$ and compares very well with the majority of the values obtained from impedance measurements. The present investigation shows that at the equilibrium there is no direct evidence for the participation of Cu(I) species. The apparent charge transfer coefficient obtained from the dependence of exchange current on concentration of electroactive species (Figure 39) is given by $d \log i_o / d \log [Cu^{2+}]$ and a value of 0.65 is obtained.

7.3. (e) The Use of Galvanostatic Experiments

It should be noted that a range of values for i_o can be obtained which are to some extent dependent on the length of the applied pulse. This may well account for the range of values reported in the literature. In both the cases of low overpotential data and also Tafel plots, there is a marked difference in the magnitudes of the values obtained for the exchange current density when using 100μ sec and 6 m sec pulses.

Results obtained using the 100μ sec pulses are comparable to the values of exchange current calculated from the impedance data using the intercept $\Delta = \infty$ (equivalent to R_D). Exchange current densities obtained from experiments using 6 m sec pulses are much lower in magnitude and may be compared to the "apparent value" calculated using the impedance intercept $\Delta \longrightarrow 0$ (equivalent to $R_D + R_k$). These results are compared in Table 10.

TABLE 10.

Method	$[Cu^{2+}]$ mol l^{-1}	$\frac{RT}{zF} \times \frac{1^*}{Rp}$ mA cm^{-2}
Low overpotential galv. Pulse 100μ sec	0.0515	12.8
Low overpotential galv. Pulse 6 m sec	0.0515	1.13
Tafel region galv. Pulse 100μ sec	0.0515	24.0
Tafel region galv. Pulse 6 m sec	0.0515	2.3
Impedance using intercept $\Delta \longrightarrow \infty$	0.0478	28.2
Impedance using intercept $\Delta \longrightarrow 0$	0.0478	4.5

* where $Rp = (R_R - \frac{1}{\omega C_R})$ or $d\eta/di$.

It is likely therefore that the total electrode process is observed when using the longer time current pulses. It should be noted however that even with the short time pulses, assymmetrical Tafel plots are obtained (Figure 35). As was observed in the case of nitrate electrolyte, the results for cathodic overpotential are considerably more scattered than on the anodic side. This may be interpreted in terms of the charge transfer process becoming a two-stage process at higher overpotentials.

CHAPTER 8

POLYCRYSTALLINE CADMIUM IN AQUEOUS SOLUTION - A LITERATURE REVIEW

DOUBLE LAYER STUDIES

BORISOVA and ERSHLER (87, 88) have reported the results of differential capacitance studies on solid cadmium in KCl electrolyte. A value of -0.9 V was reported for the p.z.c. HAMPSON and LARKIN (89) confirmed these measurements and extended the investigation to $NaClO_4$ electrolytes. Generally the shapes of the curves obtained were similar to those of BORISOVA and ERSHLER (87, 88) and the electrode behaved in an identical manner. A value of -0.91 $\pm$ 0.025 V was reported for the p.z.c. BARTENEV, SEVAST'YANOV and LEIKIS (90) have studied the structure of the double layer at a polycrystalline cadmium electrode in an extensive range of electrolytes:-

NaF,	Na_2SO_4,	NaCl,
NaBr	NaI.	

A value of -0.72 $\pm$ 0.02 V was reported for the p.z.c. It was also reported that measurements in Na_2SO_4 in the pH range 2 - 10 showed that the p.z.c. was independent of pH. Except in the case of NaI electrolyte, where adsorption was shown to be present, in all cases the shapes of the differential capacitance curves were considerably different from those reported by previous workers (87-89). More recently reported investigations by BARTENEV et al. (91, 92) have suggested that the results obtained by other workers were obtained using an insufficiently reduced cadmium surface. Results for a range of Na_2SO_4 electrolytes show a minimum at -0.76 V.

THE EXCHANGE REACTION IN NEUTRAL OR ACID ELECTROLYTES

The kinetics of the exchange reaction at polycrystalline cadmium in neutral or acid electrolytes has been studied very little. In sulphate supported electrolytes LORENZ (35) found i_o, at 0.05 mol l^{-1} Cd^{2+} for example, as ~ 1 mA cm^{-2}. Using an impedance method, in 0.7 mol l^{-1} $CdSO_4$, BRODD (93) found the exchange current density to be ~ 14 mA cm^{-2}. A more recent paper by HEUSLER and GAISER (94), who used galvanostatic techniques, has discussed the charge transfer process as two one-electron transfers. These kinetics were explained by assuming that the transfer coefficient for each step is 0.5 and that the intermediate is a well defined monovalent species.

It is noteworthy that none of these investigations discusses the effects of pH and the possibility of intrusion of the OH^- ion at the interphase. A previous investigation in this laboratory by LARKIN (5) showed that in perchlorate electrolytes at pH ~ 7.0, time stability of the electrode impedance could be attributed to the development of a film on the electrode surface.

THE EXCHANGE REACTION IN ALKALINE ELECTROLYTES

There has been considerably more interest in the behaviour of solid cadmium in alkaline electrolytes (95-114), particularly in connection with its application in the nickel-cadmium alkaline cell. The mechanism of the anodic reaction has been the subject of considerable discussion: the dissolution-precipitation mechanism (97-99, 112) and the solid state mechanism involving ionic transport through the film (101, 111). The chemical nature of the surface film has also been discussed. HUBER (98), BREITER and

WEININGER (106) and BREITER and VEDDER (109) have reported results indicating the formation of CdO. On the other hand CROFT (111), FALK (112) and ARMSTRONG et al. (110) found no evidence for the participation of CdO. It has been suggested by LAKE and CASEY (99) that CdO is formed initially, before conversion to $Cd(OH)_2$. DEVANATHAN and LAKSHMANAN (112) proposed a mechanism in which CdO formation occurs in parallel with the formation of $Cd(OH)_2$. A more recent study by OKINAKA (113) using the ring-disc electrode showed results which favoured the participation of a CdO film. In the passive range of potential $Cd(OH)_2$ was shown to grow on the film by a solid state ionic transport mechanism. The formation of CdO by initial adsorption of OH^{-1} from solution is also favoured by L'VOVA, GRACHEV and PANIN (114), although the results show no direct evidence to support this mechanism.

CHAPTER 9

THE DIFFERENTIAL CAPACITANCE OF POLYCRYSTALLINE CADMIUM IN AQUEOUS SOLUTION

As a consequence of the uncertainties surrounding the structure of the double layer at polycrystalline cadmium in aqueous solution (87 - 92) it was decided to investigate the structure of the interphase at polycrystalline cadmium in aqueous NaF and Na_2SO_4 electrolytes.

9.1. EXPERIMENTAL

The preparation of electrolytes and electrodes has been described in Section 3.1. The electrical circuit for the Schering bridge has been described in Section 3.2. The electrolytic cell has been described in Section 5.1. (a).

Electrode Pretreatment: Electrode surfaces were prepared by mechanically polishing on roughened glass using bidistilled water as lubricant. The electrodes were then electropolished in $HClO_4$ (10%) or H_3PO_4 (50%). Some electrodes were allowed to stand in $HClO_4$ (10%) after electropolishing.

9.2. RESULTS

Figure 40 shows typical faradaic current vs potential curves for polycrystalline cadmium in NaF (at pH ~ 4) and Na_2SO_4 (pH 5.5) electrolytes. In both cases the experimental polarisable region extends from ~ -0.6 V to ~ -1.3 V (NHE).

FIG. 40 Polycrystalline Cd.

Faradaic current-potential curves.

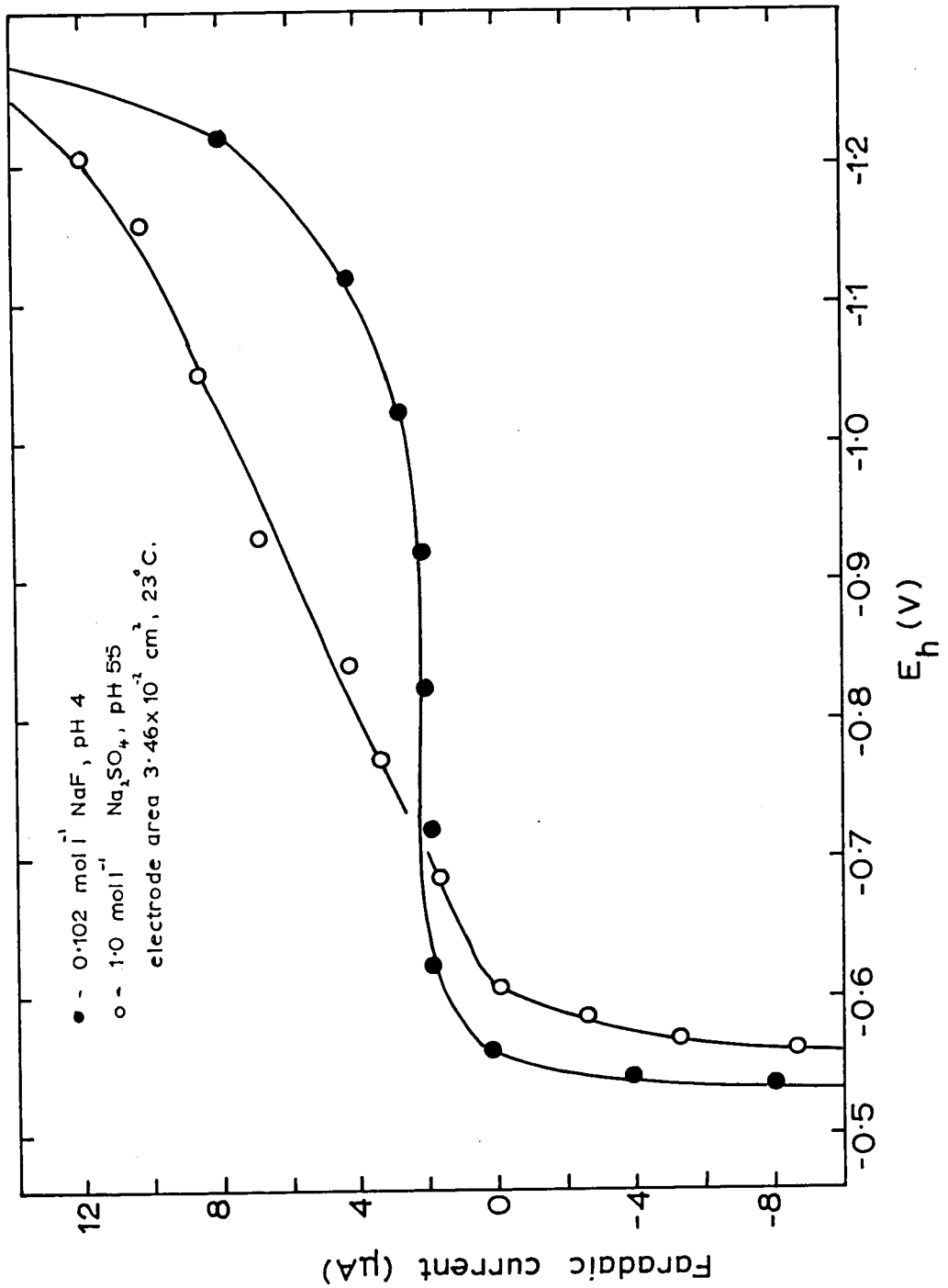

In order to compare the results with those of LEIKIS et al (90 - 92), the measurements were taken after the electrode had been polarised at ~ -1.2 V for 2 - 3h. Figure 41 shows typical differential capacitance curves for polycrystalline cadmium in NaF (pH ~ 4), at various frequencies in the range 100 - 1000 Hz. At the positive extreme of the potential range the capacitance values rose rapidly and the measurements became unstable.

Figure 42 shows typical differential capacitance curves for polycrystalline cadmium in Na_2SO_4 electrolytes at various pH values in the range 1 - 11.

9.3. DISCUSSION

Figure 41 shows that in NaF electrolyte the general shape and position of the curves shown by LEIKIS et al (90) were observed. Although the values of capacitance were somewhat higher in the present case, a minimum was observed at -0.8 ± 0.05 V; this may be identified as the p.z.c.

A disturbing feature of the Russian work for Na_2SO_4 electrolytes was a reported insensitivity of the system to changes in pH in the range 2 - 10. This was not observed in the present investigation. Figure 42 shows that the differential capacitance curves of LEIKIS et al (90 - 91) could not be repeated and that there was a marked change of the curves with pH in the range 1 - 11. For such a significant change in pH it might have been expected that there should be a shift in the potential of the onset of the h.e.r., as observed in the present case. It was suggested in the Russian work that curves of the type obtained by HAMPSON and LARKIN (89),

were caused by an insufficiently reduced surface. Electropolishing in $HClO_4$ or H_3PO_4 may produce a film on the electrode surface which is then removed by the negative polarisation. The possibility of the present curves being obtained on insufficiently reduced electrodes has been precluded since, in addition to the observed agreement with curves in the NaF system, identical results (to those obtained from electropolished electrodes only) were obtained both from electrodes which were chemically etched ($HClO_4$, 10%) only and also from electropolished electrodes followed by further etching in $HClO_4$. It is suggested that the sulphate ion is adsorbed at the interphase. No equivocal reason can be advanced for the difference between the present and the Russian investigations. It should be noted that adsorption of sulphate ion has been observed at copper (Chapter 5), gold (115) and lead (116) electrodes, as would be expected for the case of a double negatively charged ion.

Also a further disturbing feature of the Russian investigation was that the reported change of capacity (for both NaF and Na_2SO_4) with frequency in the range 110 - 5000 Hz was less than 3%. This indicates that the electrode has a mercury smooth surface (the observed frequency dispersion on a mercury drop electrode is ~ 1%).

Although the use of micro-electrodes, careful electrode preparation and electropolishing will reduce dispersion effects due to surface roughness to a minimum, it is unlikely that a polycrystalline cadmium metal surface can behave in the manner of a smooth liquid surface as reported by the Russian workers.

FIG. 41 Polycrystalline Cd in NaF.
Differential capacitance curves.

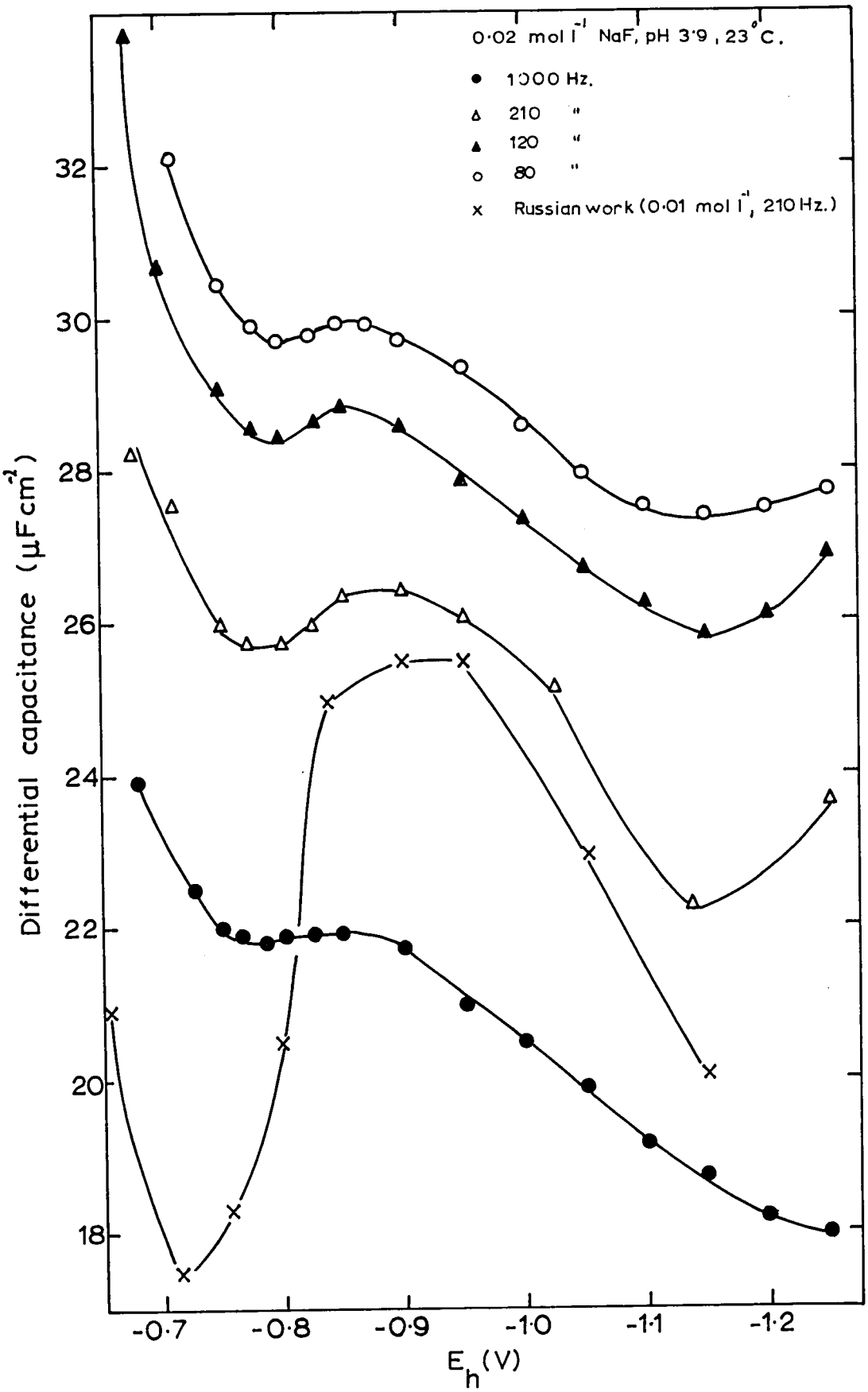

FIG. 42 Polycrystalline Cd in Na_2SO_4.
Differential capacitance curves.

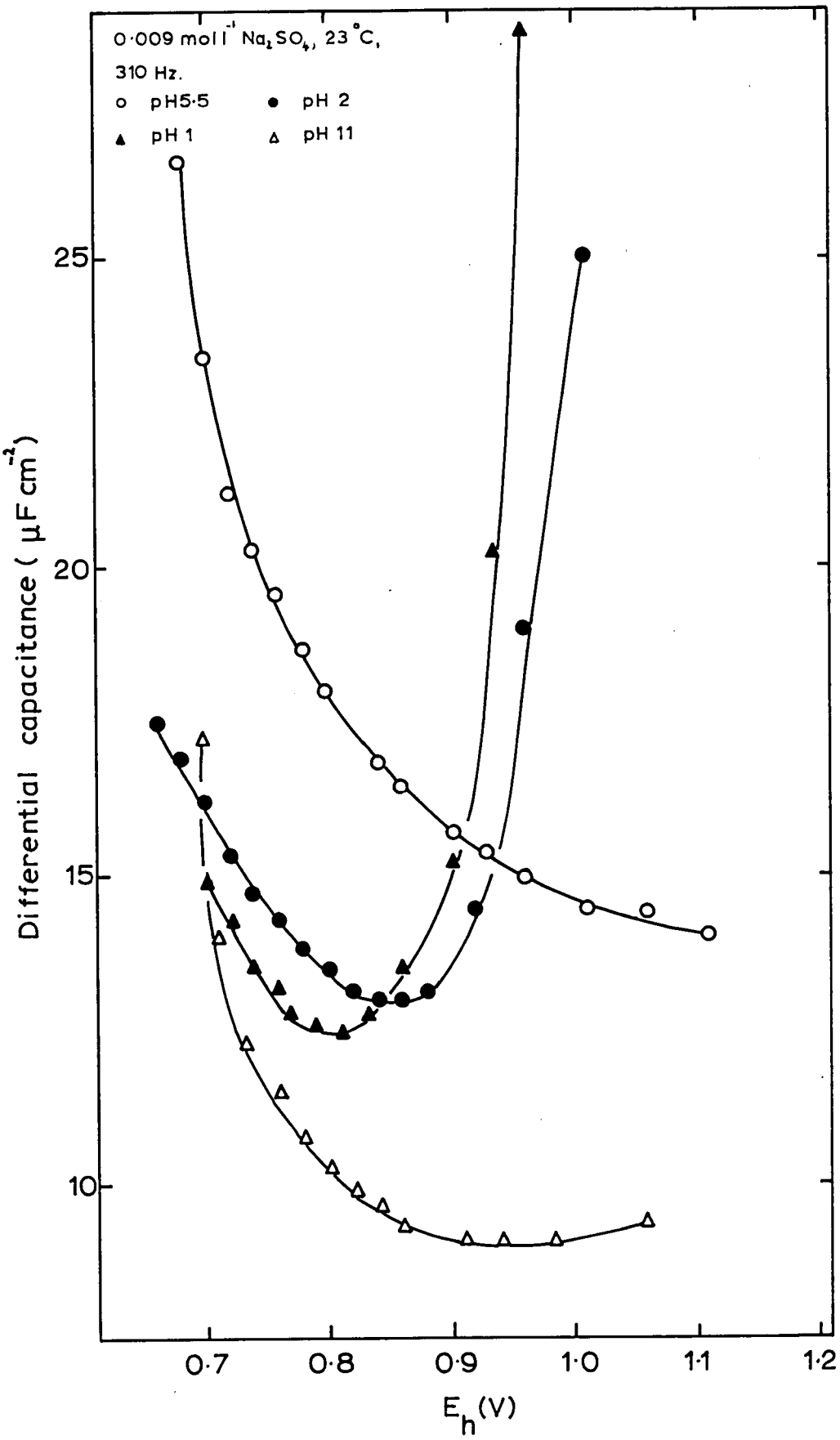

CHAPTER 10

THE Cd(II)/Cd EXCHANGE IN PERCHLORATE ELECTROLYTE

Studies of the interphase using the potential dependence of the electrode differential capacitance may be expected to provide information on electrolyte conditions for which the electrode interphase would be free of adsorption and the development of films. It is clear from a study of these that adsorption of the OH^- ion on the cadmium electrode is unimportant at potentials around the potential of zero charge, E_z, and at more cathodic potentials. Adsorption of anions is however most marked on the anodic side of E_z. E^o_{Cd} is $\sim$ 0.4 V more positive than E_z. Exchange measurements are therefore made with the electrode positively charged with respect to the electrolyte. It is likely that at these potentials the adsorption of OH^- is important and may lead to the development of films unless both potential and electrolyte conditions are carefully chosen. Thus, for example, if electrodes are electropolished at very anodic potentials, even in perchloric acid (10%), films may be produced.

Preliminary experiments have shown that for conditions of moderate anodic polarisation (within 150 mV of E^o_{Cd}), the development of films may be avoided if the pH of the electrolyte is sufficiently low (5). It was decided to investigate the exchange reaction at a solid cadmium elec-

trode in perchlorate* electrolyte under conditions of low pH.

10.1. EXPERIMENTAL

The preparation of electrolytes and electrodes has been described in Section 3.1. The electrical circuits have been described in Sections 3.2. and 3.3. The electrolyte cell used for impedance studies has been described in Section 5.1. (a). The electrolytic cell used for the galvanostatic measurements is shown in Figure 43.

Electrode Pretreatment: Electrode surfaces were prepared by mechanically polishing on roughened glass under water followed by electrochemically etching in perchloric acid (10%). Some electrodes were further "normalised" by chemically etching in perchloric acid (10%) for about 15 min. Electrodes were washed in bidistilled water before fitting into the electrolytic cell and were inserted without drying or contact with the air.

10.2. RESULTS

10.2. (a) Impedance Measurements

Treatment of Data: The method of analysing and presenting the impedance data as impedance spectra has been discussed in Section 2.3. Mathematical analyses of the data were also made using the complex plane transformations (30).

Footnote* At the time of commencement of this work the results of LEIKIS et al (90 - 92) had not been published. Consequently the choice of electrolyte to be used was made on consideration of the ability of the anion to form complexes with cadmium ion. It was considered, that in this respect, perchlorate would be a suitable anion since $HClO_4$ was the strongest (common) acid and in general perchlorate complexes are unknown.

FIG.43 Polycrytalline Cd in $NaClO_4$.

Galvanostatic technique - the electrolytic cell.

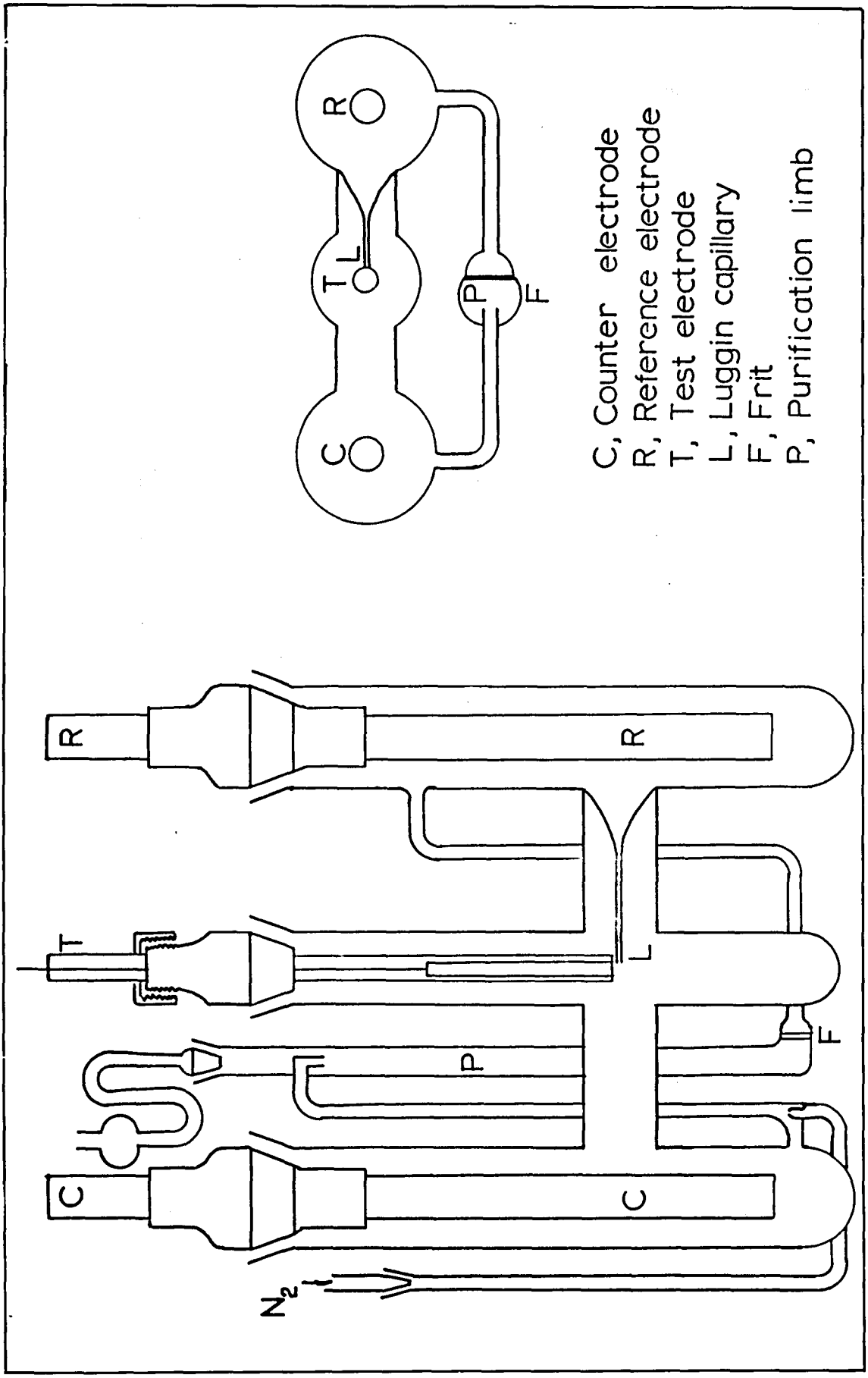

Time dependence: Figure 44 shows the time-dependence of the difference between the in-phase, R_R, and out-of-phase, $1/\omega\ C_R$, components of the electrode faradaic impedance (after correction for C_L and electrolytic resistance, R_E), $\Delta_{\omega \to \infty}$ and $\Delta_{\omega \to 0} - \Delta_{\omega \to \infty}$. Stable values were obtained after ~ 4 h. and consistent results were obtained up to ~ 24 h. after initial electrode/electrolyte contact.

Variation of exchange current with $[Cd^{2+}]$: Figure 45 shows a typical faradaic impedance frequency spectrum. Figure 46 shows the variation of exchange current with $[Cd^{2+}]$. From the slope d log i_o/d log. $[Cd^{2+}]$, a value of 0.35 is obtained for the apparent charge transfer coefficient.

Variation of exchange current with temperature: Figure 47 shows the variation of exchange current with temperature in the range 0 - 23°C. Satisfactory measurements could not be obtained at higher temperatures.

The variation of the adatom flux ZFV_g^o, with 1/T did not give a good linear plot. The results were very scattered and the spread of data was too great to allow a reliable value of the enthalpy of activation for this process to be abstracted.

10.2. (b) Galvanostatic Measurements

Time dependence: Figure 48 shows the time-dependence of overpotential for typical electrodes at a fixed current density, i using a pulse length ~ 700μ sec. It is clear that the electrode pre-treatment influences the overpotential during the initial stages of the electrode/electrolyte contact

FIG. 44 Polycrystalline Cd in $NaClO_4$.

The time dependence of the electrode impedance.

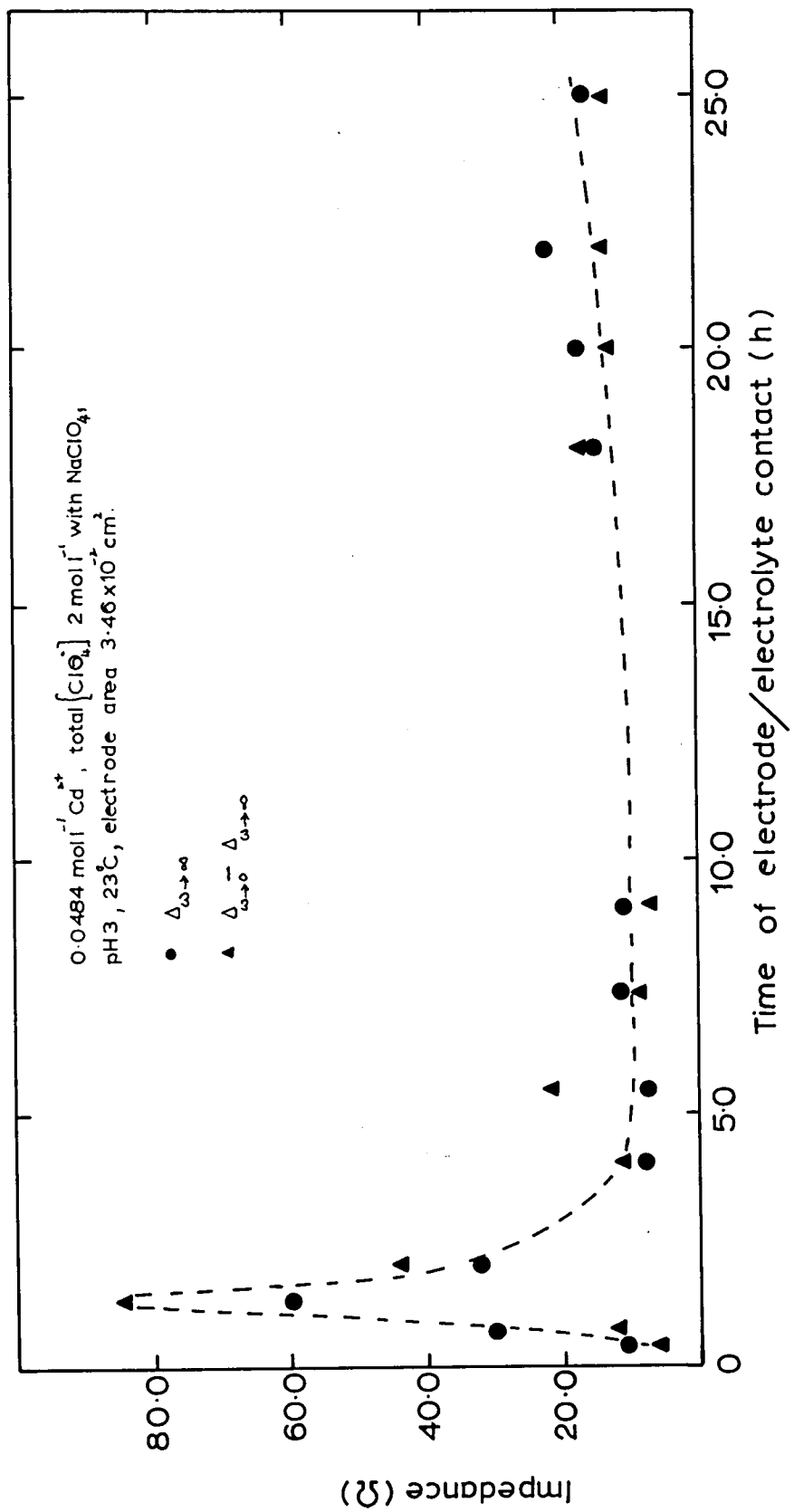

FIG. 45 Polycrystalline Cd in $NaClO_4$.
Typical impedance curves.

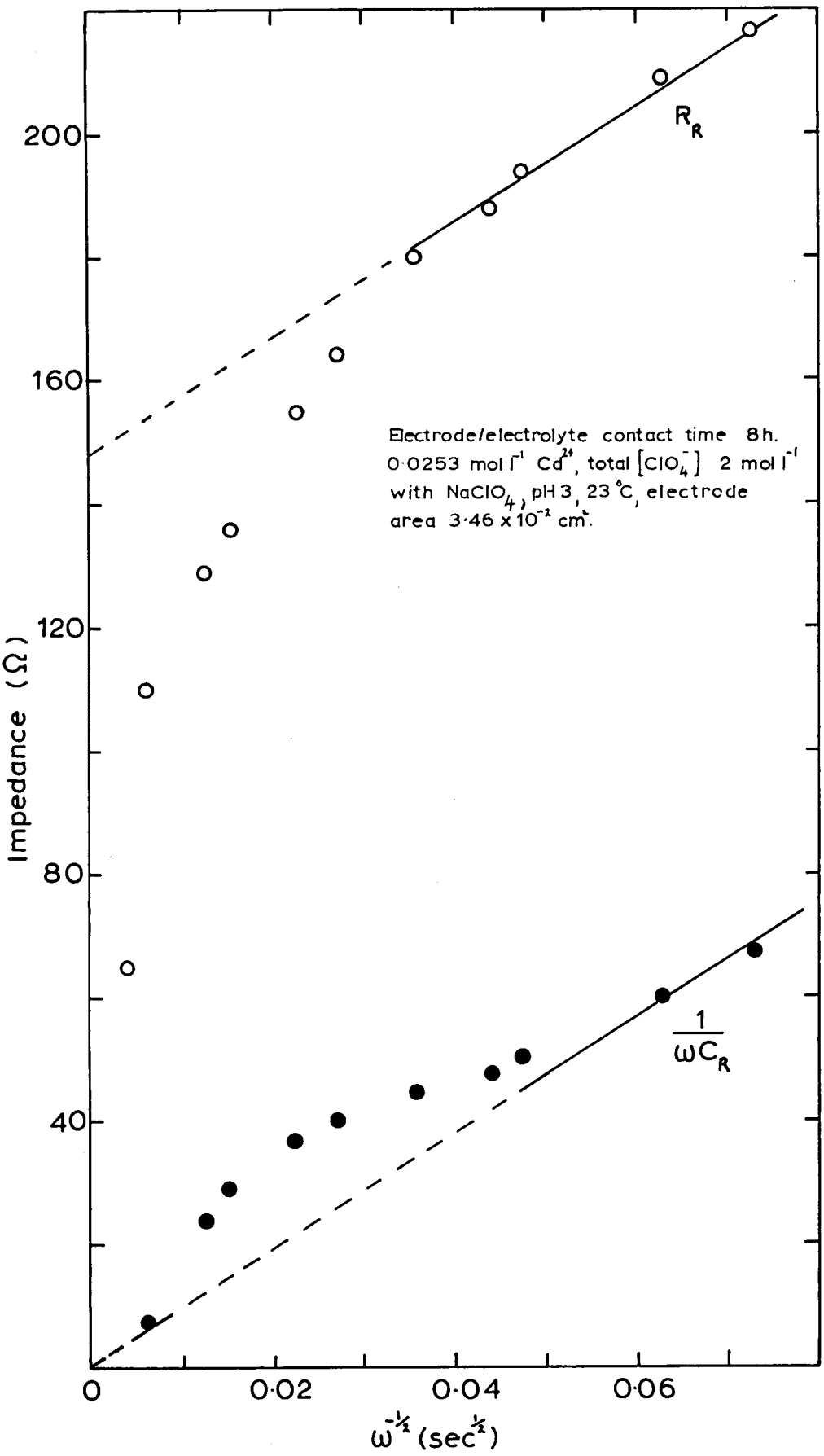

FIG. 46 Polycrystalline Cd in $NaClO_4$.

The dependence of exchange current on concentration. (impedance)

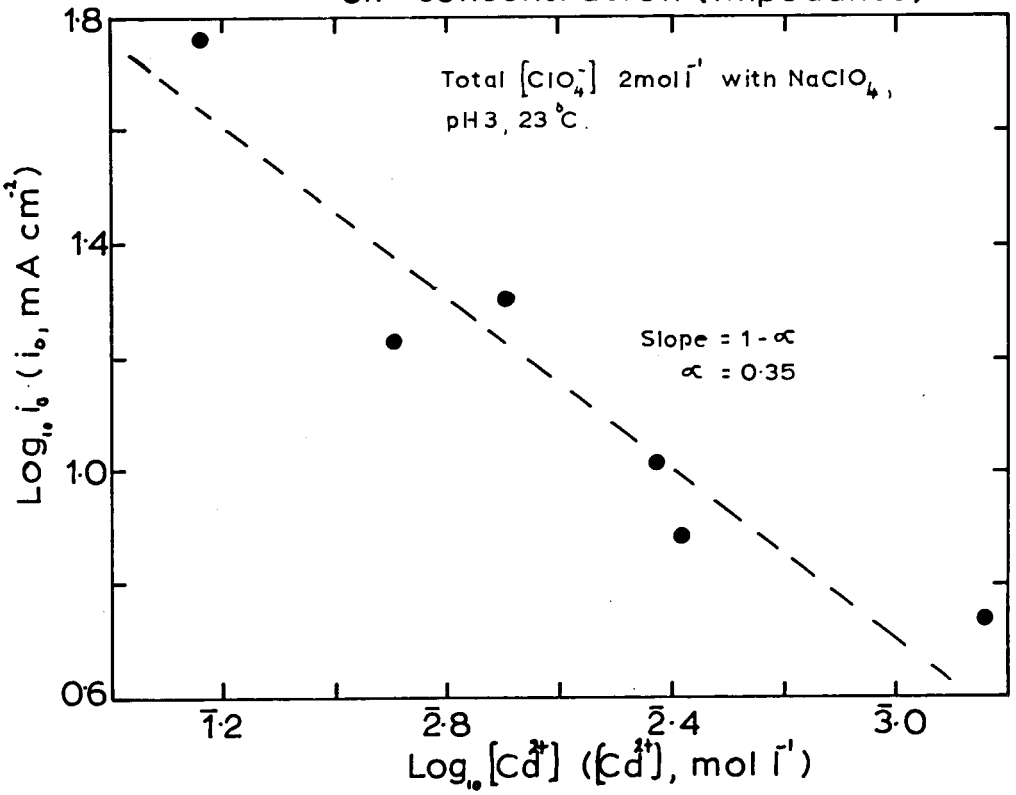

FIG. 47 Polycrystalline Cd in $NaClO_4$.

The dependence of exchange current on temperature. (impedance)

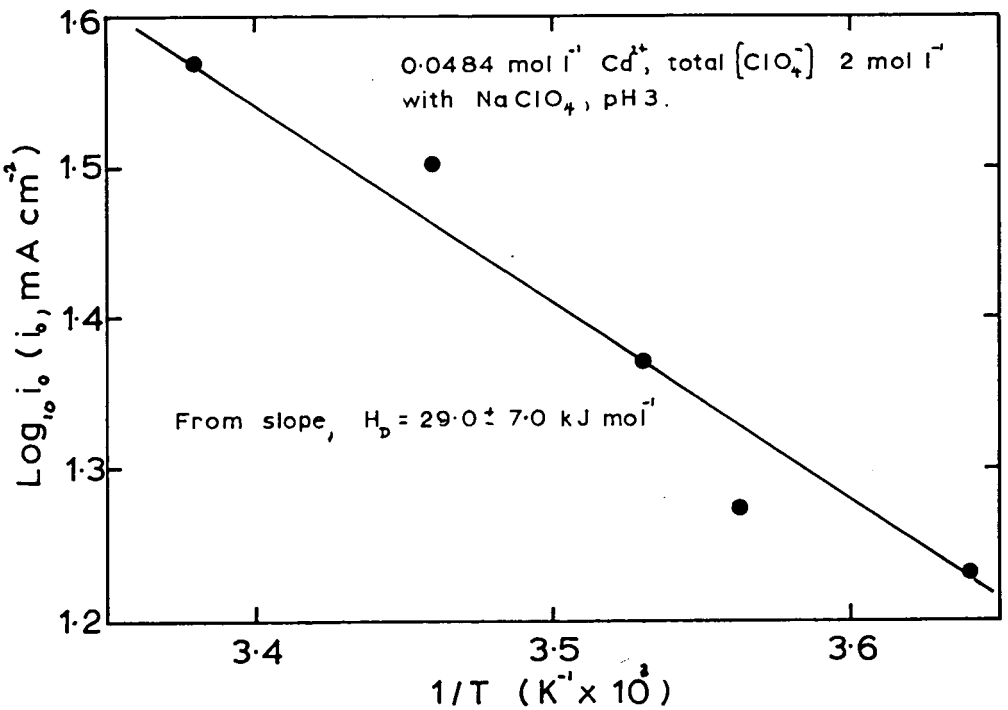

FIG. 48 Polycrystalline Cd In $NaClO_4$.
The time dependence of overpotential.

0·452 mol l^{-1} Cd^{2+}, total $[ClO_4^-]$ 2 mol l^{-1} with $NaClO_4$, 23°C, faradaic current 3·08 mA cm^{-2}.

○ - electrochemically etched
● - 'normalised' (see text)

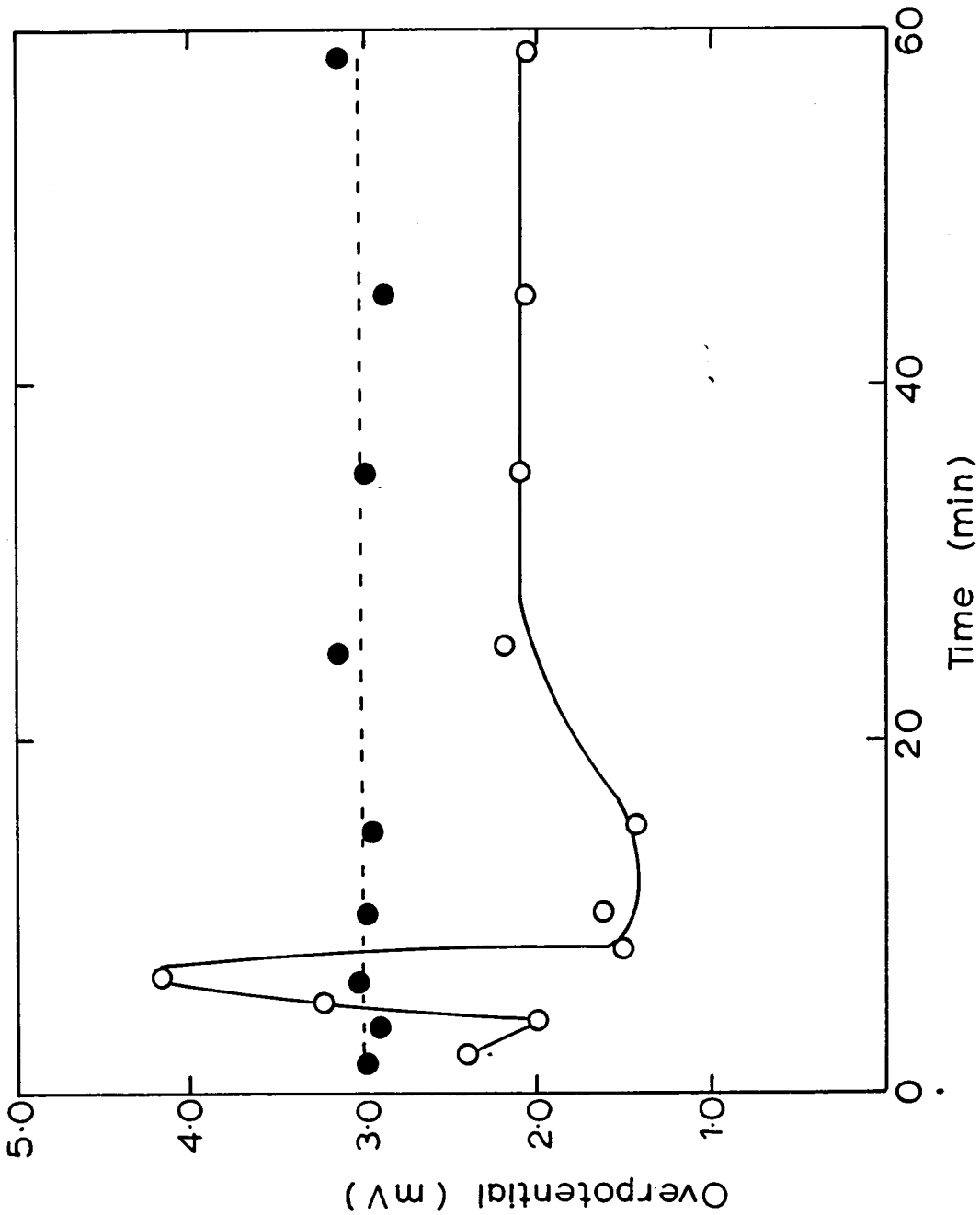

but provided that sufficient time (1 h) is allowed for the electrode to stabilise, overpotential is time-independent.

Variation of exchange current with $[Cd^{2+}]$: Typical η_D -i data are shown plotted in Figure 49. Deviations from the linear η_D -i relationships were observed, as expected at η_D > 10 mV. The apparent exchange current was calculated geometrically and iteratively following the procedure of FARR and HAMPSON (117). Both methods gave the same value of i_o.

The exchange current for the anodic reaction is frequently not identical with that for the cathodic reaction in the same electrolyte as shown by the non-symmetry of some η_D -i curves, (Figure 49, open circles). Table 11 shows that the extent of this difference rarely exceeds 10% at high $[Cd^{2+}]$ and is well below the experimental limit of significance at low $[Cd^{2+}]$. Table 12 shows values of exchange currents calculated from the mean slope at the origin of the anodic and cathodic curves.

TABLE 11

$[Cd^{2+}]$/M	i_o/mA cm^{-2} (anodic) 23°C	i_o/mA cm^{-2} (cathodic) 23°C	C_L/μF cm^{-2} (mean value) 23°C
0.452	28.4	21.3	36
0.235	13.9	13.1	26
0.095	4.0	4.7	34
0.0617	2.5	2.1	34

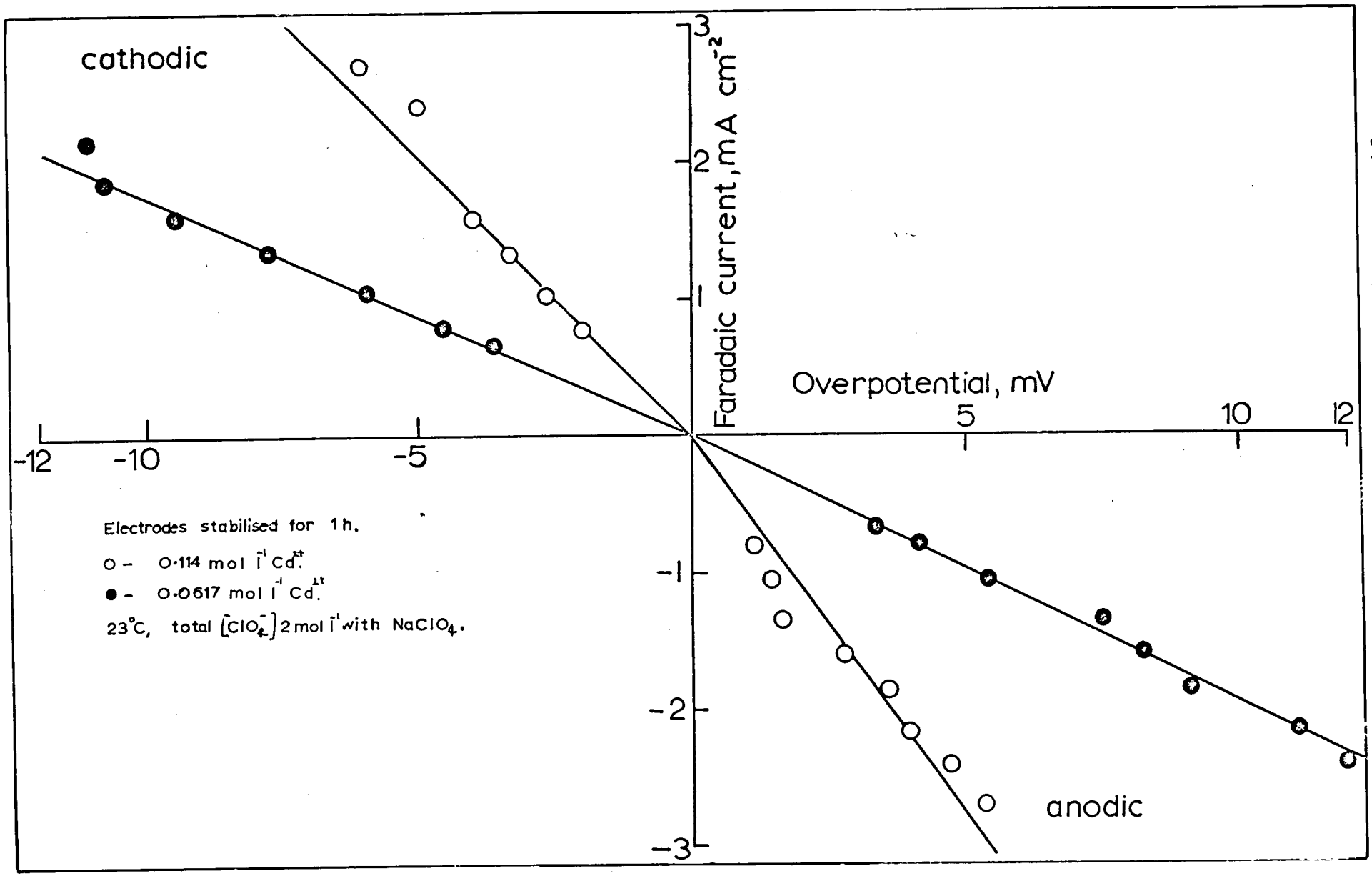

FIG.49 Polycrystalline Cd in $NaClO_4$.
Typical overpotential - faradaic current data.

TABLE 12.

$[Cd^{2+}]$/M	i_o/mA cm^{-2} 23°C	$[Cd^{2+}]$/M	i_o/mA cm^{-2} 23°C
0.452	24.84	0.114	5.28
0.452	11.4	0.103	3.4
0.32	10.8	0.095	4.35
0.235	13.53	0.0617	3.74
0.196	6.69	0.0617	2.28
0.196	5.4	0.049	2.3
0.114	5.83	0.028	2.0

Figure 50 shows the variation of mean exchange current with $[Cd^{2+}]$. From the slope of the log i_o vs log $[Cd^{2+}]$ curve the apparent charge transfer coefficient follows. α is calculated to be 0.23 $\pm$ 0.03 from a least-squares fit of all the available anodic and cathodic results. This value is not significantly different from the values obtained by considering exclusively anodic values (α_a = 0.21 $\pm$ 0.02) or cathodic values (α_c = 0.24 $\pm$ 0.02).

Whilst at low temperatures both anodic and cathodic branches of the η -i curves were symmetrical, at high temperatures the anodic overpotentials became time-dependent and increased steadily with time. There was apparently no pronounced change in C_L or in the physical appearance of the electrode. Figure 51 shows the variation of exchange current with temperature in the range 0° - 50°C. For temperatures exceeding 40°C, only the stable cathodic value was used for the correlation. The spread of results was rather greater than expected; this appeared to be a feature of the cadmium exchange.

FIG.50 Polycrystalline Cd in $NaClO_4$.
The dependence of exchange current on concentration.(galvanostatic)

23°C, total $[ClO_4^-]$ 2 mol l^{-1} with $NaClO_4$.

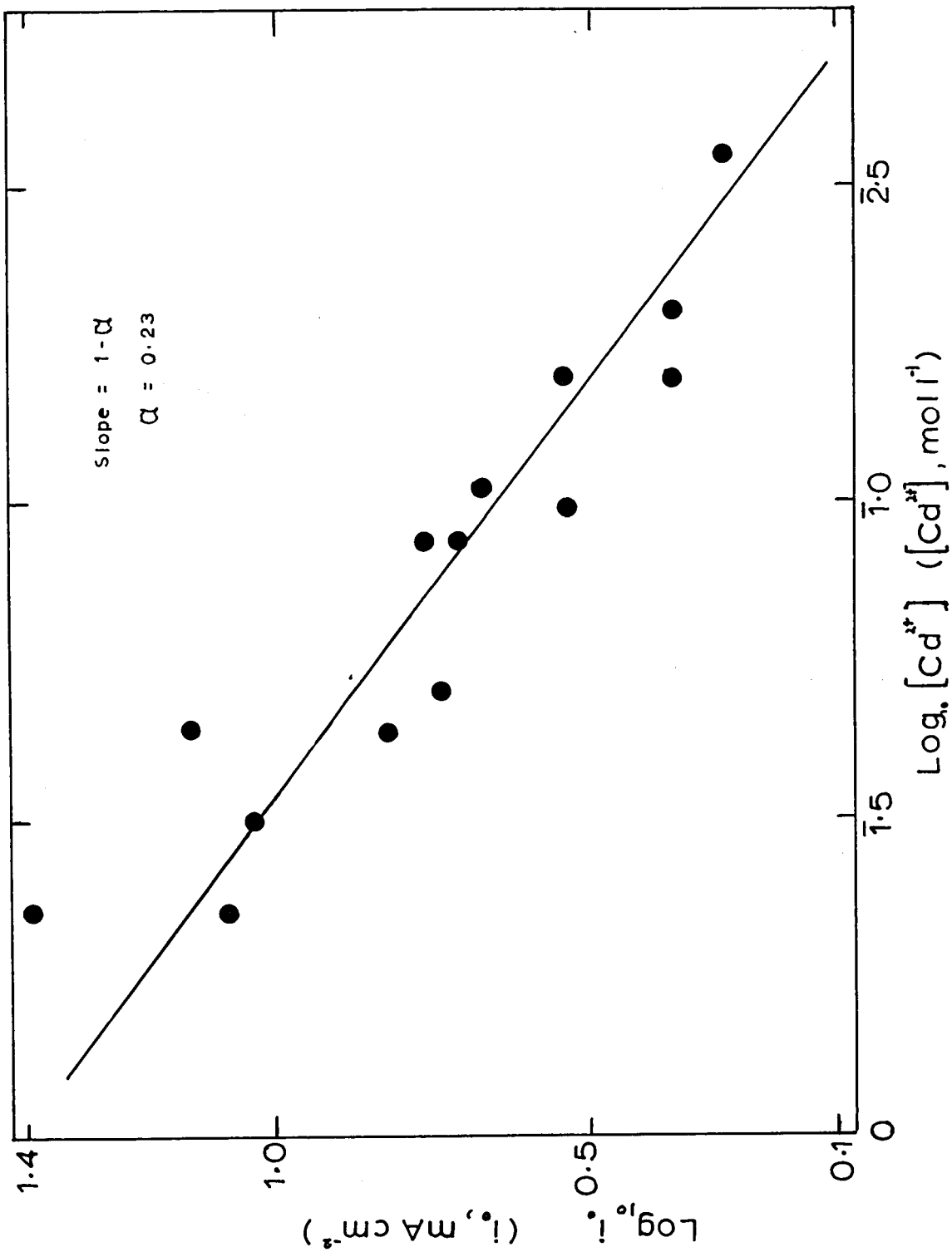

FIG.51 Polycrystalline Cd in $NaClO_4$.
The temperature dependence of exchange current. (galvanostatic)

0.0617 mol l^{-1} Cd^{2+}, total $[ClO_4^-]$ 2 mol l^{-1} with $NaClO_4$.

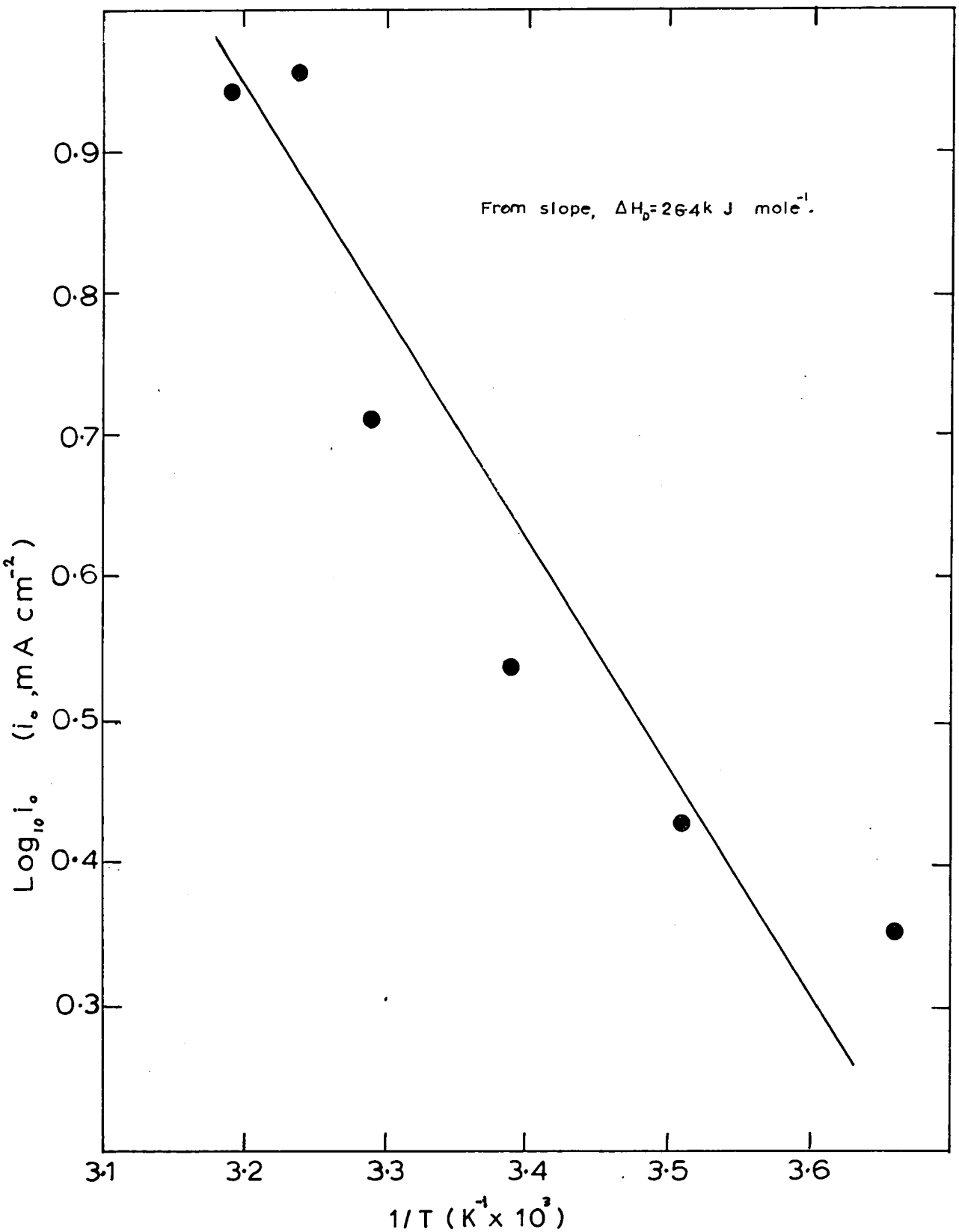

10.3. DISCUSSION

10.3. (a) Use of Complex Plane Analysis

Figure 52 shows a typical complex plane impedance plot. The semi-circular type of plot, becoming linear at lower frequencies, expected for a single rate determining process in addition to diffusion in solution is not obtained. The semi-circle is distorted and appears elongated in the direction of the real axis, and the transition to a straight line is much too gradual at low frequencies. Theoretically, if two rate determining processes are present and separable in time, then we should observe two semi-circles overlapping and finally degenerating into a straight line. The complex plane method shows clearly that more than one rate determining process in addition to charge transfer is present. However, the two processes are not resolvable in time. This is seen from the frequency spectrum (Figure 45) where although relaxation is clearly observable, parallel R_R and $1/\omega\ C_R$ lines are never really obtainable at the higher frequencies. An estimation of the radii corresponding to the circular complex plane transformation made from the frequency spectrum was satisfactory only in the case of the total polarization resistance (R_K and R_D).

10.3. (b) Relative Rates of Crystallisation and Charge Transfer Processes

As a consequence of the uncertainty of R_D from frequency spectra the magnitude of i_o can only be taken as approximate and it is estimated that an error of $\pm$ 25% attaches to the values reported in Table 13. The

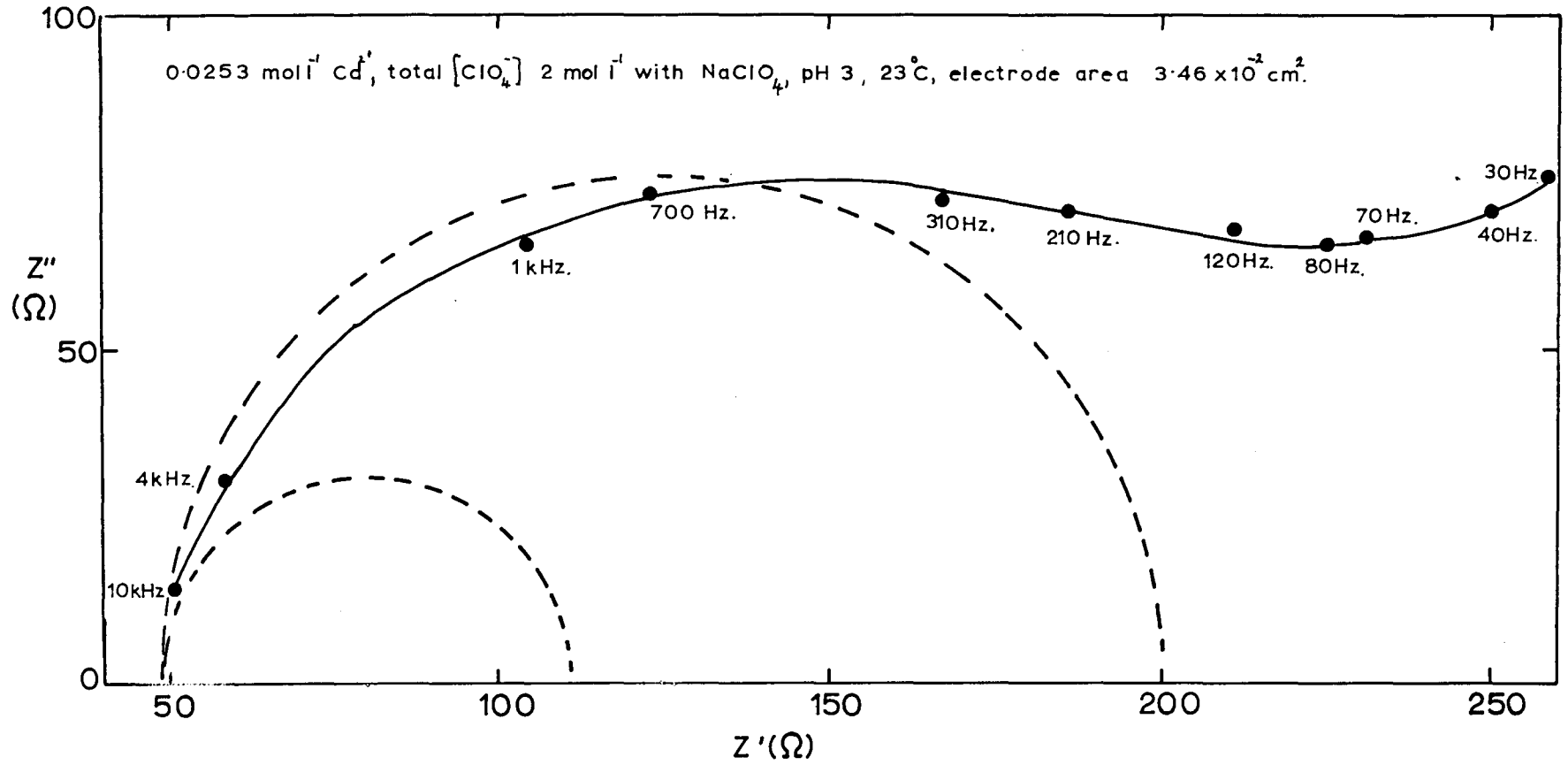

FIG.52 Polycrystalline Cd in $NaClO_4$. Complex plane transformation.

Dotted lines represent semi-circular transformations with diameters equivalent to the intercepts $\Delta_{\omega \to \infty}$ and $\Delta_{\omega \to 0}$ from frequency spectra (Fig. 45).

values obtained are somewhat higher than those obtained from galvanostatic measurements.* In the range of $[Cd^{2+}]$ investigated, the relative magnitudes of the exchange current density and adatom flux indicate that the processes of charge transfer and crystallisation have rates of the same magnitude. A comparison of the two parameters is given in Table 13.

TABLE 13.

$[Cd^{2+}]$/mol l^{-1}	i_o/mA cm^{-2}	ZFV_g^o/mA cm^{-2}
0.175	58.0	48.0
0.0755	18.6	7.45
0.0484	20.5	28.4
0.0253	10.2	5.1
0.024	7.6	6.5
0.007	5.5	1.9

The results presented in Table 14 show that Γ_o, the surface adatom concentration, is independent of $[Cd^{2+}]$. The relationship between exchange current and concentration of electroactive species:

$$i_o = ZFKC_o^{1-\alpha} \qquad [30]$$

is therefore justified and no adjustment of α is necessary to allow for changes in Γ_o.

---

*Footnote: A number of investigations of exchange reactions at solid metal electrodes in this laboratory have yielded higher i_o values from the a.c. method than from the galvanostatic method.

TABLE 14.

$[Cd^{2+}]$/mol l^{-1}	$10^{12}\ \Gamma_o$/mol cm^{-2}
0.175	5
0.0755	2
0.0484	30
0.0253	16
0.024	21
0.007	22

It can be seen from Table 13 that the adatom flux is related to $[Cd^{2+}]$ in the same manner as the exchange current density. This may be compared to other systems where ZFV_g^o is not related to the concentration of electrolactive species. This, according to the mathematical treatments of FLEISCHMANN et al (26, 27) indicates that the process of diffusion of adsorbed species at the surface exerts some control over the rate of crystallisation. This significant additional controlling process has the effect of introducing an extra component in the electrode analogue and whilst it is clear that the incorporation of a further term in the electrode analogue would complicate the frequency response, it has not been found possible to decompose the experimental data so that the component processes are resolvable. Nevertheless it is clear that the extra controlling process would further complicate the frequency response of the electrode interphase expected from a GERISCHER type model (23, 24).

Charge transfer process: The apparent value of α, obtained from the slope $d \log i_o / d \log [Cd^{2+}]$ is 0.34 (f.i.) and 0.23 (galvanostatic). The charge transfer reaction has been discussed as a two-step process by HEUSLER and

GAISER (94). From high overpotential measurements it was deduced that the mechanism of charge transfer involved a Cd(I) intermediate:

$$Cd^{2+} + e \rightarrow Cd^{+}_{ad} \qquad [31]$$

$$Cd^{+}_{ad} + e \rightarrow Cd_{ad} \qquad [32]$$

It was assumed that both steps [31] and [32] have a transfer coefficient of 0.5 and that the intermediate must be a well-defined monovalent species.

These conclusions have been based upon work in the Tafel region where transitions between two and one electron transfer steps are clearly possible. Clearly measurements made within $\pm$ 3 mV of the equilibrium do not completely rule out two 1-e transfer steps since if α is truly 0.5 for two 1-e transfers then the observed values of α = 0.35 and 0.23 are in good agreement with expectations.

The value of α, is significantly less than that (0.68) observed for amalgam electrodes under similar electrolyte conditions (118). The difference is not surprising since the double layer characteristics at an amalgam electrode are very different from those at a solid metal electrode. The principal reason for this is that the potential of the $Cd^{2+}/Cd(Hg)$ electrode is negative to E_z for mercury, whereas the potential of the Cd^{2+}/Cd electrode is positive to E_z for cadmium metal.

It is difficult to compare the work reported here with that of BRODD (93) and LORENZ (35). The electrolytes used by these workers were different from those presently employed. Electrode purities and pre-treatments are unspecified and no account was taken of time stability. However,

the values of i_o reported are within an order of magnitude of the values reported here and this agreement is not unsatisfactory.

Enthalpy of activation: A value for the enthalpy of activation for the charge transfer process, ΔH_D, was obtained from impedance measurements as ~ 29 kJ mol^{-1}. This value is slightly greater than that obtained for the galvanostatic measurements, 26.3 kJ mol^{-1}, but is consistent with values for the charge transfer process in other solid metal exchanges. An inability to obtain results at higher temperatures was observed; the significant decrease in the high frequency impedance values was consistent with the formation of a film at the electrode surface.

The inability to obtain a value for ΔH_K from the variation of adatom flux with temperature is difficult to explain. The metallurgical feature of the metal may account for this behaviour. Cadmium has the h.c.p. structure and may be compared to zinc which also has the h.c.p. structure and also demonstrated this type of erratic behaviour (119). It is possible that the metal surface may be undergoing continual modification such than an equilibrium state is never attained. Examples of this may be the more stable face of a crystal developing in preference to less stable faces, atoms of lower co-ordination number being progressively removed to sites of higher co-ordination, and pits developing with subsequent growth of other areas of the electrode. Consequently consistent measurements of the crystallisation process can never really be obtained. A further possible explanation is in terms of the temperature dependence of the component processes of the crystallisation step. It may be that a

changeover in the "surface diffusion"/"lattice formation" as the major rate-controlling reaction would account for the observed behaviour.

Purity Requirement: It is noteworthy that this system required a greater degree of purification than any so far investigated in these laboratories. In this respect it resembled the exchange at an amalgam electrode (118). In the case of these latter experiments it was suggested that the borosilicate glass was the complicating factor. In the present experiment attempts to completely eliminate the borosilicate glass from the system were not possible. However, prolonged cleaning did enable stable results to be obtained. It should be noted that an initial cleaning period (using purified, activated charcoal) of 4 months was required before the system became stable.

CHAPTER 11

THE Cd(II)/Cd EXCHANGE IN ALKALINE SOLUTION

The majority of reported investigations of the Cd electrode in alkali have been concerned with the morphological aspects of the surface film which is nucleated and grown as the anodic reaction proceeds. Published data on the charge transfer reaction is scarce in spite of the rapidly growing interest in the nickel-cadmium alkaline battery. The exchange reaction in alkaline solution has been shown to be a fast process (120) possibly as the result of the stabilising effect of adsorption on the species involved in the charge transfer process. It is unlikely that the process is accelerated due to the formation of an oxide film as this type of catalysis is extremely unusual. It was decided to investigate the exchange process in ultra-pure alkaline electrolytes using the a.c. impedance method and the double impulse galvanostatic technique of GERISCHER and KRAUSE (43). For a fast reaction the latter technique was in this case preferred rather than the single impulse technique.

11.1. EXPERIMENTAL

The preparation of electrolytes and electrodes has been described in Section 3.1. The electrical circuits for impedance measurements and galvanostatic measurements have been described in Section 3.2. and 3.4. respectively. The electrolytic cell used for impedance measurements has been described in Section 5.1. The electrolytic cell used for

the galvanostatic measurements has been described in Section 6.1.

11.2. RESULTS

11.1. (a) Impedance Results

The results could be represented as relaxation free Randles plots in the frequency range down to ~ 70 Hz. At frequencies below this level, the out-of-phase component tended to depart from linearity. No divergence was found in the in-phase line.

It was found that the computor selected values of capacitance required to evaluate the analogue decreased with time of electrode/ electrolyte contact (Table 15).

The variation of R_R with time is shown in Figure 53.

TABLE 15.

Time	$Co/\mu F\ cm^{-2}$
0 min	120
15 "	84
20 "	87
45 "	93
60 "	81
135 "	64
220 "	58
450 "	43
22 h	34

The best Randles type impedance plots were obtained after ~ 20 - 30 min electrode/electrolyte contact. Figure 54 shows a typical impedance plot.

In the range of $[Cd^{2+}]$ investigated there was no significant

FIG. 53 Polycrystalline Cd in NaOH.

Variation of R_R with time.

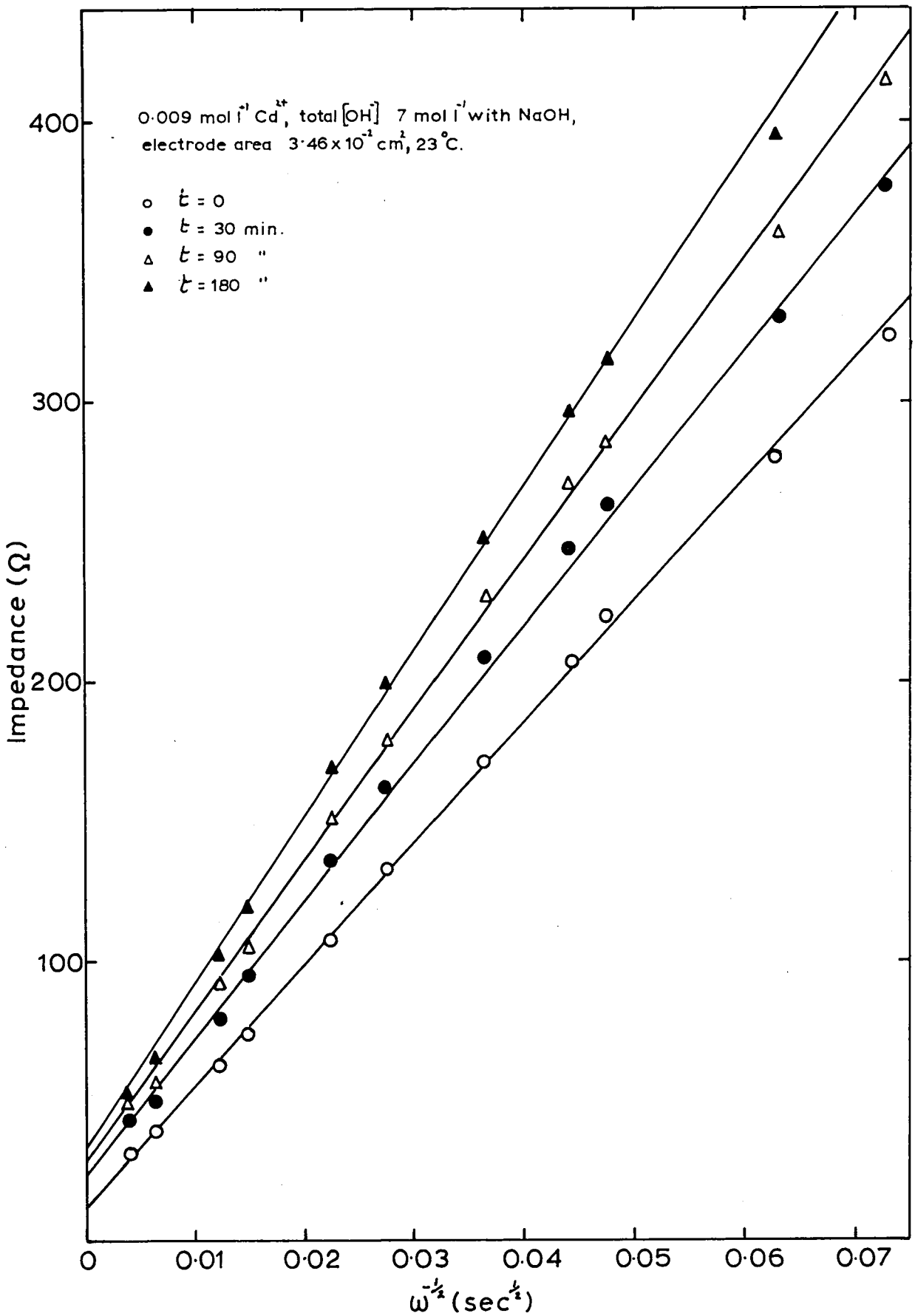

FIG. 54 Polycrystalline Cd in NaOH.

Typical impedance plot.

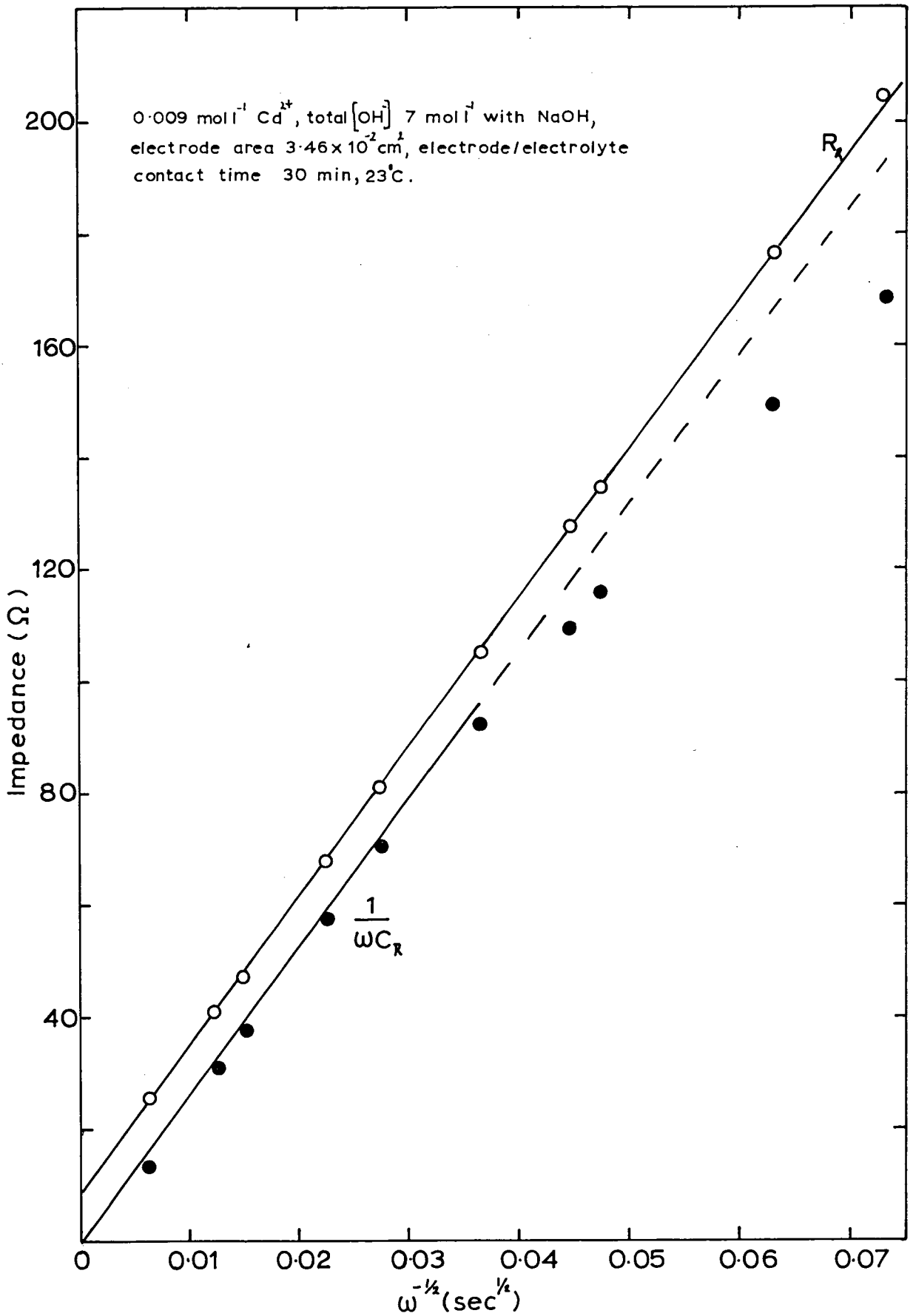

change in the intercept, Δ, and the slope of the impedance plots (Table 16).

TABLE 16.

$[Cd^{2+}]$/mol l^{-1}	Δ/Ω	i_o/mA cm^{-2}*	Slope/Ω $sec^{-\frac{1}{2}}$
	23°C		23°C
Electrode area 3.46 x 10^{-2} cm^2			
0.0099	12	31.0	3000
0.0053	20	18.5	5000
0.0002	9	41.0	3600
0.0001	12	31.0	4000

Measurements were also made with the electrode polarised negative with respect to the equilibrium potential (up to 40 mV - ve of E^o). No change in the results was observed.

In the range of temperature investigated, 0 - 50°C, no significant change of Δ with temperature was found. This agreed with a previous investigation of this system (120).

Figure 55 shows the impedance results represented as a complex plane diagram (30). The linearity of the plot indicates that the reaction is fast and there appears to be no measureable charge transfer resistance.

11.2. (b) Double Impulse Measurements

A typical η_D vs i plot is shown in Figure 56. Values of R_D, shown in Table 17, obtained from the slopes of these plots were found to

*Footnote where $i_o = \frac{RT}{ZF\Delta}$

FIG.55 Polycrystalline Cd in NaOH.
Complex plane transformation.

0·009 mol l^{-1} Cd^{2+}, total $[OH^-]$ 7mol l^{-1} with NaOH, electrode area $3{\cdot}46 \times 10^{-2}$ cm^2, electrode/electrolyte contact time 40 min, 23 °C.

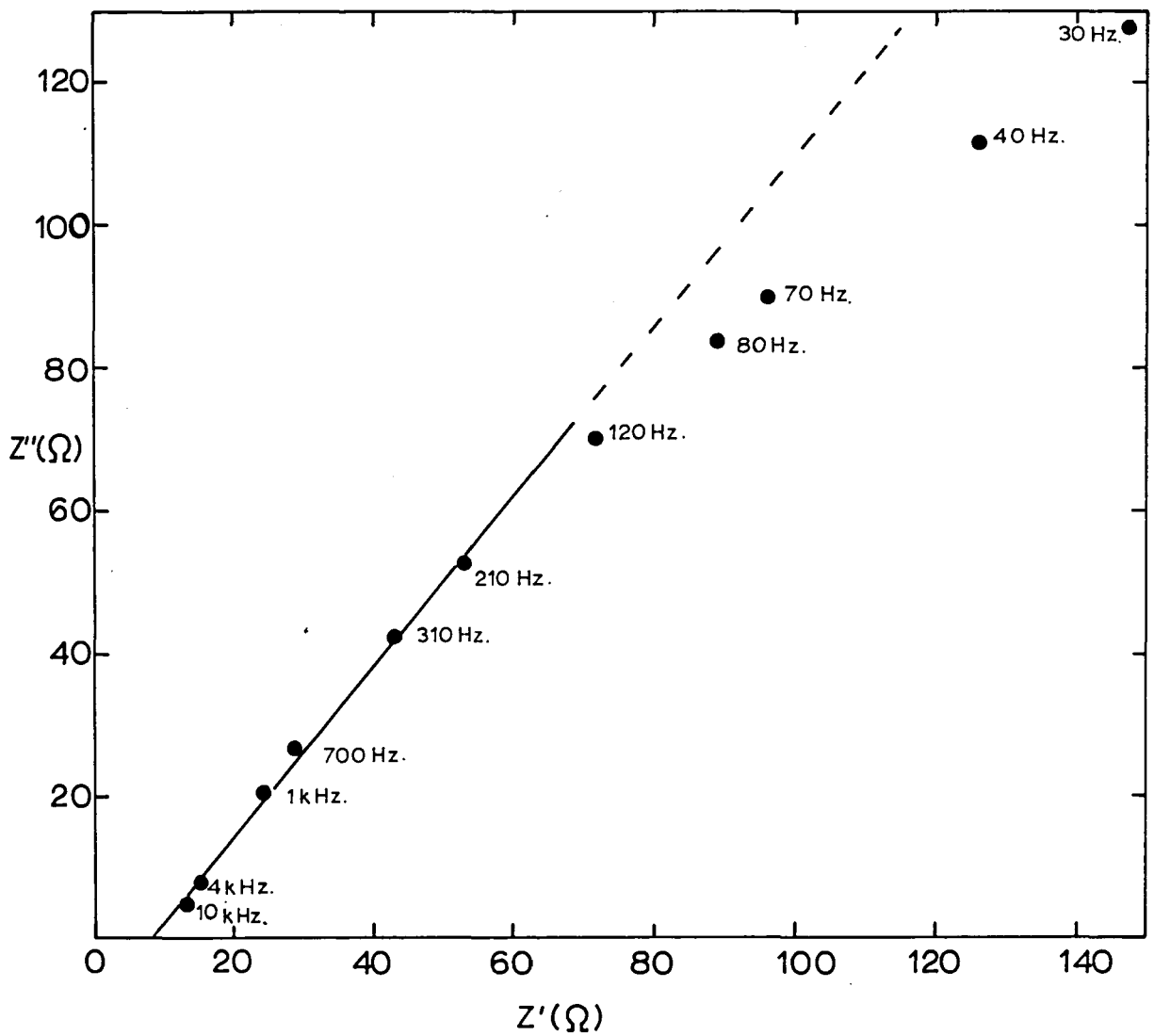

FIG. 56 Polycrystalline Cd in NaOH.

Typical η_D-i data from double impulse results.

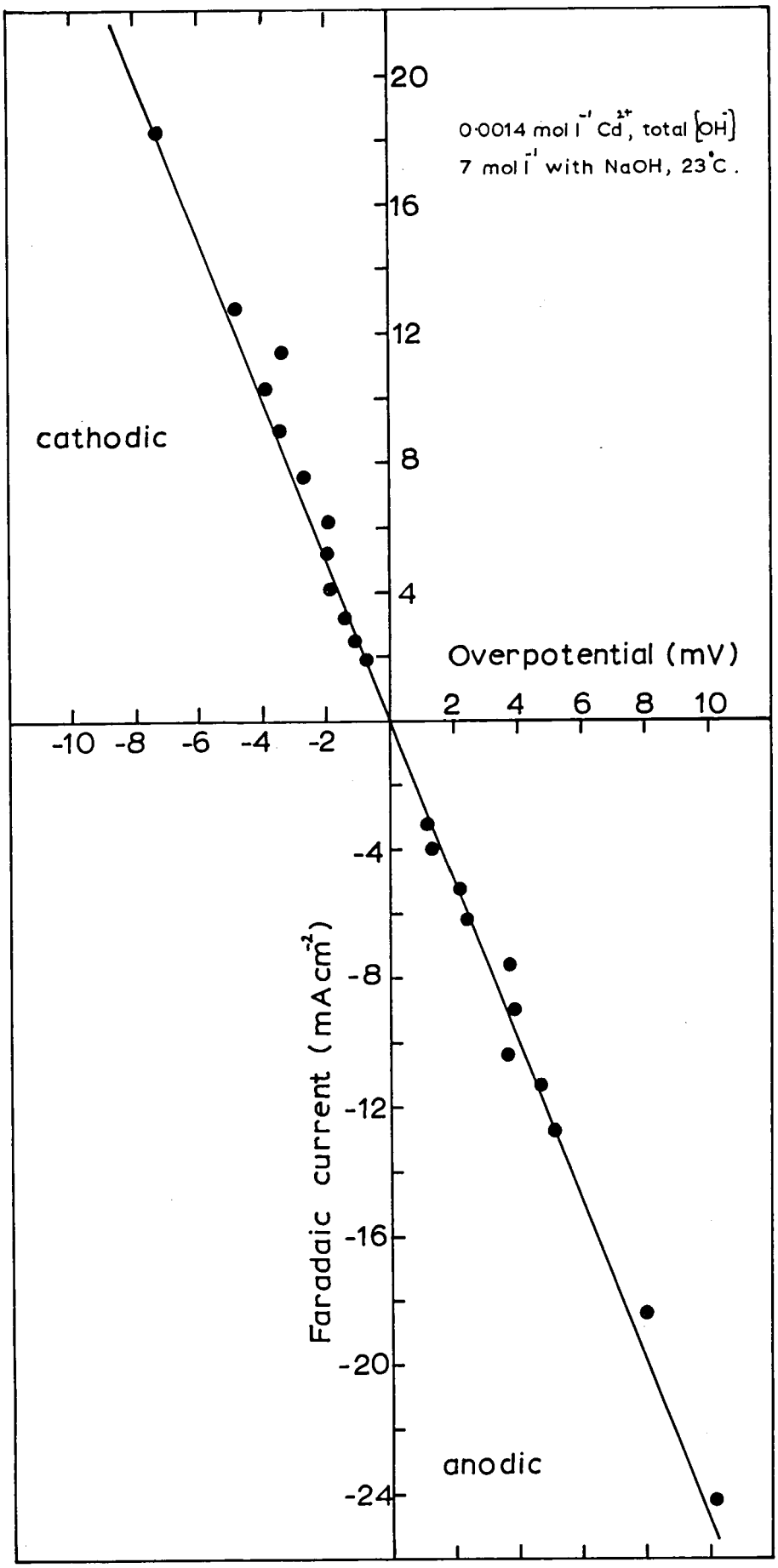

be independent of $[Cd^{2+}]$.

TABLE 17.

$[Cd^{2+}]$/mol l^{-1}	R/Ω cm^2	i_o/mA cm^{-2}*
0.0099	0.49	26.0
0.0014	0.41	31.0
0.0001	0.40	32.0

11.3. DISCUSSION

11.3. (a) Time Dependence of Impedance Plots

Figure 57 shows that the slope of the impedance plots is proportional to the intercept Δ. Thus the effective area of the surface is reduced with time of contact of the electrode with the electrolyte as the hydroxide (or oxide) film grows. The film growth is confirmed by the fact that the capacitance decreases with the time contact. The value of the Warburg coefficient calculated theoretically, and based on the superficial electrode area, was found to be ~ 40 times less than the value obtained from the experimental data (from the first available measurements). Clearly the active area of the electrode is only a fraction of the total area available.

11.3. (b) The Charge Transfer Process

The apparent charge transfer process is found to be considerably faster in alkali than in perchlorate electrolyte (Chapter 10). The complex

---

*Footnote where $i_o = \frac{RT}{ZFR_D}$

FIG. 57 Polycrystalline Cd in NaOH.
Change in Δ with slope of impedance plots.

0·0053 mol l^{-1} Cd^{2+}, total $[OH^-]$ 7 mol l^{-1} with NaOH, 23°C.

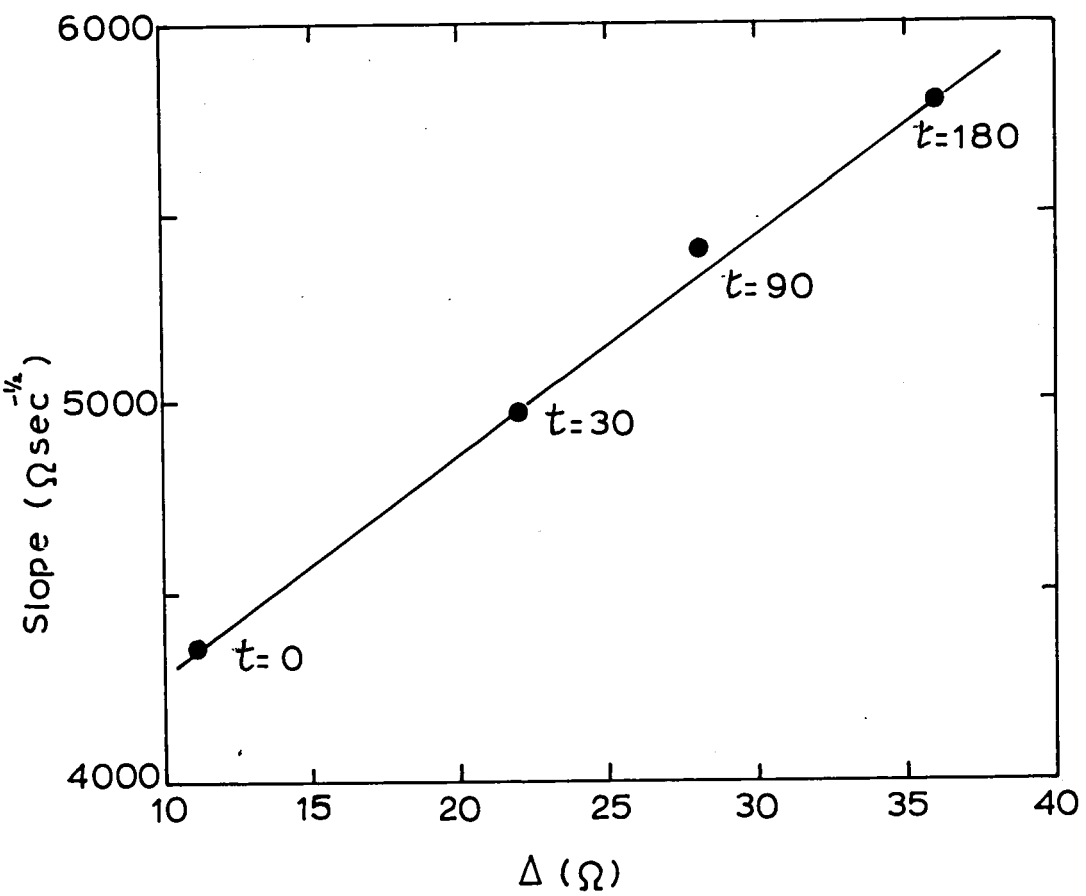

plane presentation of the results (Figure 55) confirms that the charge transfer process is very rapid. The exchange current densities from double impulse results obtained after 0.5μ sec of reaction agreed well with exchange current density measurements obtained in the faradaic impedance measurements. This further substantiates the absence of relaxation in the frequency range up to the equivalent of 1 M Hz and consequently reinforces the view that charge transfer is the rate-controlling process.

Negative polarisation of the electrode with respect to the equilibrium potential produced no change in the results. Negative polarization of the electrode would tend to prevent the adsorption of negative species at the interphase. However, in the present case no change was observed and hence the adsorption must be strong. The high concentration of electrolyte may pack the interphase with OH^- ions to such an extent that negative polarisation has no effect.

The exchange process is shown to be independent of $[Cd^{2+}]$ by both the impedance and the double impulse results. In the presence of the large excess concentration of supporting electrolyte it is possible that a complexed or neutral species is transferred. Cadmiate species in alkaline solutions are unknown (121) (cf. zincates and plumbates). The stable species in aqueous solution is $Cd(OH)_2$ (121). GERISCHER (42) has suggested that the species transferred most favourably are those with low electric charge and small co-ordination number. For example in the overall reaction (122):

$$Zn(CN)_4^{2-} + 2e = Zn(Hg) + 4CN^- \qquad [33]$$

the charge transfer process was found to be:

$$Zn(OH)_2 + 2e = Zn(Hg) + 2OH^- \qquad [34]$$

The transfer of a species such as $Cd(OH)_2$ explains why the process is much more rapid in alkaline solution.

The deviation from linearity on the impedance spectra observed at the lower end of the frequency range is interesting. The most likely cause is a frequency dispersion effect which results if different areas of the electrode have different capacitances (123). Such a situation is enhanced in the presence of adsorption to form a hydroxide (oxide) film.

11.3. (c) The Electrical Analogue

The presence of adsorption necessitates the inclusion of an extra capacitance, C_{ads}, into the electrical analogue. (Figure 58 a). The value of the capacitance abstracted by the computer match is much too large for a true double layer capacitance, and is probably a total capacitance represented by C_L and C_{ads} in parallel (Figure 58 b). Hence the capacitance C_o is obtained from the computer match. This is represented as parallel component across the faradaic impedance and hence straight line impedance plots result. Similar types of impedance plots were obtained by COOPER and PARSONS (124) for the reduction of bromine at a platinum electrode. In this case the adsorption capacitance was included in the electrical analogue in parallel across the Warburg impedance only (Figure 58 c). Those authors recommended subtracting C_L and C_{ads} separately, hence obtaining the RANDLES (21) circuit. However, it was reported difficult to assess C_{ads} with any degree of confidence.

FIG. 58 Electrical analogues for systems involving adsorption.

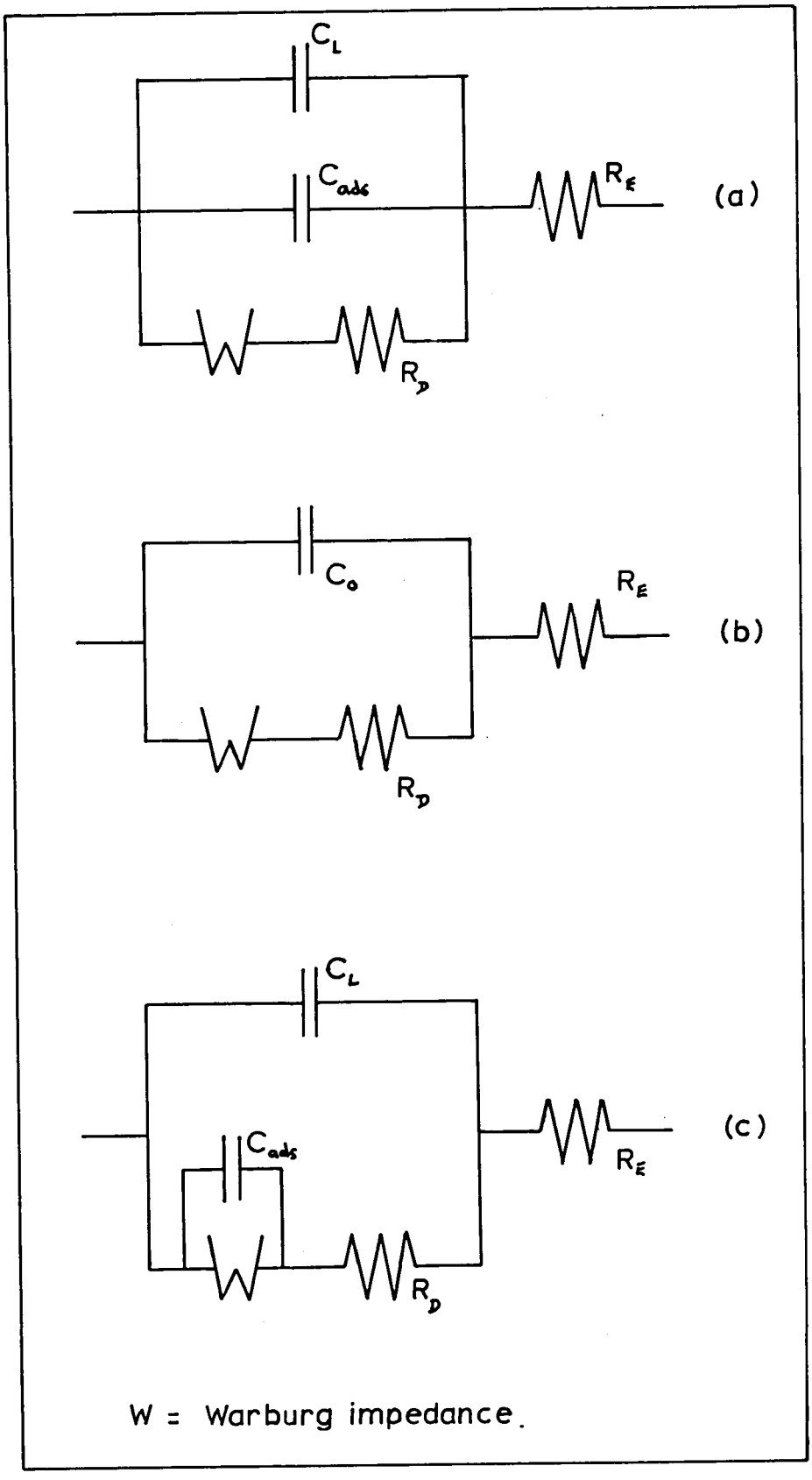

W = Warburg impedance.

11.3. (d) The Effect of Temperature

The lack of variation of the results with change in temperature is unusual. The control of the reaction by film growth obviously obscures any variation in the rate of the charge transfer process with temperature. The enthalpy of activation of the charge transfer process for polycrystalline zinc in alkaline solution was found ~ 12 kJ mol^{-1}. This is much smaller in magnitude than the values observed for systems free from strong adsorption (Chapters 6, 7, 10). The lower value expected for ΔH_D indicates that the change of the rate of the charge transfer process with temperature would be minor and thus easily obscured.

11.3. (e) The Nature of the Surface Film

It was not possible in this study to identify the chemical nature of the surface film. Previous work in this laboratory (125) has shown no evidence for the formation of CdO. However, it should be noted that the absence of CdO lines in X-ray diffraction patterns excludes only the presence of crystalline CdO, not of the amorphous compound. Although $Cd(OH)_2$ is favoured as the more thermodynamically stable species, the formation of CdO as the initial product at the electrode cannot be completely eliminated since it is not unusual for unstable intermediates to be generated at the electrode surface.

CHAPTER 12

FINAL DISCUSSION

12.1. METAL ELECTRODE/AQUEOUS SOLUTION INTERPHASES

12.1. (a) Equilibration Processes

In contrast to the behaviour of mercury and amalgam electrodes, on the introduction of a solid metal electrode into an electrolyte electrochemical measurements are frequently observed to be time dependent. It is suggested that the pretreatment (mechanical polishing, electrochemical polishing or chemical etching, for example) of a solid metal electrode probably produces a surface of different metallurgical configuration from that corresponding to an equilibrated electrode. Thus the initial electrode activity observed is probably due to a rearrangement of the surface to produce a surface of minimum surface energy. For differential capacitance studies (no exchanging ion present) surface rearrangement can only be achieved by the self diffusion of metal atoms on the electrode surface. It can be seen from the measurements on the metals involved in this work that copper (in adsorption free systems) shows considerably less initial electrode activity than cadmium and antimony*. This may be related to the crystal structure and lattice dimensions of the metals. The unit cell dimensions and types of crystal structures for some metals are shown in Table 18.

---

*Footnote: During the course of the investigation the differential capacitance of antimony in aqueous solution was also studied, see APPENDIX 3.

TABLE 18.

Metal	Structure	Cell Dimensions/Å	E°/V	E_z/V
Antimony	Rhomb	a = 4.5064	0.152 (Sb/Sb_2O_3)	~ -0.15
Cadmium	h.c.p.	a = 2.979 c = 5.617	-0.403	-0.7 to -0.9
Copper	f.c.c.	a = 3.6153	0.337	~ -0.1
Lead	f.c.c.	a = 4.9495	-0.126	-0.56
Silver	f.c.c.	a = 4.085	0.799	-0.7
Zinc	h.c.p.	a = 2.664 c = 4.945	-0.763	-0.93

Of the metals shown in Table 18, the systems having the least significant time dependencies are copper and silver, i.e. those metals with the smallest crystal cell dimensions and the more symmetrical face centred cubic crystal structure. It should be noted, however, that in electrolytes giving rise to some anionic adsorption (not strong, such as copper in sulphate electrolytes) the process of equilibration is considerably lengthened. This is likely to be due to hindrance of the "recrystallisation" of the surface, thus resulting in a longer time period to produce a more ordered surface. However, when strong adsorption is present (e.g. copper, cadmium, zinc and lead in alkaline solution) there is very little time variation. Obviously in these cases the adsorption "saturates" the surface and effectively produces an ordered layer. Hence diffusion of atoms on the surface "beneath" the adsorbed layer does not significantly effect the measurements.

It is also significant that the exchange processes at cadmium and

zinc (in simple electrolytes) have both proved difficult to study. Both metals have low melting points and hexagonal close packed crystal structures. The lattice energy is reflected in the melting point of the metals and therefore one expects that rearrangement of the surface will be more rapid in these cases than for example copper. A possible explanation for the observed behaviour may be connected with the presence of a cleavage plane in the metal. Zinc has the 0001 cleavage plane and it is therefore likely that in this case that the surface is undergoing continuous modification to achieve this latter plane. Consequently a considerable time dependency is observed in contrast to copper which has no cleavage plane and ultimately achieves a surface minimum free energy but having several crystal planes present. Although cadmium does not possess a cleavage plane the metallurgical similarity to zinc leads one to expect cadmium to exhibit a similar behaviour. It is likely therefore, that the cadmium surface also is striving to attain a particular orientation in order to achieve equilibrium and thus is undergoing continuous surface modification.

12.1. (b) The Potential of Zero Charge

Studies of the differential capacitance at solid metal electrodes are restricted by the limited potential regions available for study. Usually the potential region is limited at the negative extreme by the process of hydrogen evolution and at the positive extreme by either the process of lattice dissolution into solution or oxide formation.

Table 18 shows that the equilibrium potential, E^{o}, for solid metals is usually more positive than E_z (other metals for example: Tin, E^{o} =

-0.136 V, E_z = -0.43 V, Thallium E^o = 0.34 V, E_z = -0.6 V). Thus at the equilibrium potential the electrode has a positive charge with respect to the bulk of the electrolyte. It is to be expected therefore that anionic adsorption may occur and the exchange process at the electrode will be complicated by this factor. In contrast, exchange reactions at amalgam electrodes are not as likely to be complicated by adsorption since the electrode bears a negative charge with respect to the solution, i.e. E^o is more negative than E_z for mercury (-0.165 V). There has been considerably less information on the interphase and p.z.c. at solid metal electrodes. There are also few methods for study available for which a reliable theory exists. (Methods other than differential capacitance studies include mechanical properties, measurements of adsorption, double layer repulsion.) Thus a certain degree of uncertainty must be attached to any reported measurements.

However, the importance of an 'a priori' study of the potential of zero charge and possibilities of adsorption at the interphase has been shown in the case of copper in aqueous solution. The study of the structure of the interphase indicated that there may be adsorption in the case of sulphate electrolyte and this observation was manifested in the substantially different kinetic behaviour in solutions with and without anionic adsorption. In the particular treatment of the impedance results used in this study a value of C_L is subtracted from the measured series combination of R_{xs} and C_{xs} in order to evaluate the electrical analogue of the electrode system. A prior knowledge of the capacitance in the supporting electrolyte may be used as supporting evidence that the correct value of C_L has been used in the computation.

12.2. CHARGE TRANSFER

RANDLES (126) discussed the mechanism of charge transfer in terms of the Franck-Condon principle and of potential energy curves. Tunnelling of electrons has been discussed by HUSH (127) and MARCUS (128 - 130). The theory considers that the solvent sheath at the interphase undergoes fluctuations and during the "openings" thus appearing, the electrons tunnel through. In general LEVICH (131) agrees with the theories of HUSH (127) and MARCUS (128, 129) but notes the assumption that no account is taken of the electronic structure of the electrode. MARCUS (128 - 129) assumes that the electron is transferred to a definite energy level in the electrode which is understood to be the Fermi level. Although the theory of LEVICH (131) considers a continuous spectrum of energies in the metal, it is noted in this article that the same physical concepts underlie both this latter work and that of MARCUS (128, 129). It has been noted by BOCKRIS (132) however, that the tunnelling theory is really only satisfactory for the cathodic discharge process. Overpotential-time curves are usually symmetrical near the equilibrium and hence the mechanism of charge transfer must be similar for anodic and cathodic processes.

It is difficult to envisage a model in which a metal atom detaches itself from the metal lattice, transfers charge outside the solvent layer and then an electron tunnels back to the metal.

Consecutive electron transfers: For two consecutive one-electron transfer reactions:

$$O + e = X \quad (a) \qquad [35]$$

$$X + e = R \qquad (b) \qquad [36]$$

VETTER (133) has shown that:

$$i = 2\,\frac{e^{-(\alpha_a + \alpha_b)f\eta} - e^{(2-\alpha_a-\alpha_b)f\eta}}{\frac{1}{i_b^o}e^{(1-\alpha_a)f\eta} + \frac{1}{i_a^o}e^{-\alpha_b f\eta}} \qquad [37]$$

where $f = \frac{RT}{F}$ [38]

if $i_a^o \to \infty$ or $i_b^o \to \infty$, in the anodic and cathodic ranges, extrapolation of Tafel plots to $\eta = 0$ yields $2i_b^o$ or $2i_a^o$ respectively.

The charge transfer at low overpotentials is given by:

$$-\left(\frac{\partial\eta}{\partial i}\right)_{i \to o} = \frac{1}{4f}\left(\frac{1}{i_a^o} + \frac{1}{i_b^o}\right) \qquad [39]$$

The Cu(II)/Cu exchange has been considered as two one-electron transfers:

$$Cu^{2+} + e = Cu^{+} \qquad [40]$$

$$Cu^{+} + e = Cu \qquad [41]$$

with step [41] considered as the fast step. If the exchange current of step [41] is significantly larger in magnitude than [40], then equation [39] may be written as:

$$-\left(\frac{\partial\eta}{\partial i}\right)_{i \to o} = \frac{1}{4f}\left(\frac{1}{i_a^o}\right) \qquad [42]$$

In both cases of the Cu(II)/Cu exchange in nitrate and sulphate electrolyte, the value of:

$$-\left(\frac{\partial\eta}{\partial i}\right)$$

obtained from low overpotential measurements does not agree with that obtained from equation [42], using a value of i_a^o obtained from extrapolation of both anodic and cathodic Tafel plots. It may therefore, be concluded that the charge transfer mechanism at low overpotential is not similar to that at high overpotential.

The assymmetry of the Tafel plots indicates that the mechanism may be interpreted as a two-step reaction at higher over-potentials but there is not evidence for such a reaction at low overpotentials.*

CONWAY and BOCKRIS (134) have calculated free energies of various alternative paths in order to establish the most likely path of the metal deposition reaction. Using Morse functions, energy barriers

---

*Footnote: Relaxation on the impedance curves cannot be interpreted as two consecutive one-electron transfers. Relaxations occurring in the audio range of frequency are connected with the inability of the process to follow the applied a.c. Such processes in the present experiments are concentration changes on the electrode or in solution. It is extremely unlikely that two separate electron transfers which are electronic transitions will be relaxed in the frequency range employed.

separating the various transition states along the path were calculated for both the cases of deposition as adatoms and adions. In addition to preferring consecutive electron transfers the authors estimated the most likely path to be transfer of an ion to a plane surface site, diffusion to a step site, diffusion along the step to a kink site, and finally incorporation into the lattice accompanied by electron transfer. However, calculations by HUSH (127) and MOTT and WATTS-TOBIN (135) show that direct electron transfer between the metals surface and a hydrated ion should not be ignored. Moreover the method used by CONWAY and BOCKRIS (134) involves calculating energies and entropies at metastable positions.

12.3. NATURE OF THE ADSPECIES

It is difficult to decide the degree of ionic character which the bond between the adspecies and the surface has after charge transfer has occurred. BOCKRIS and CONWAY (134, 136) have compared calculations for adsorbed atoms and for adions, i.e. adspecies which are assumed to retain a dipolar character with respect to an electron in the metal surface. The calculations favour the formation of an adion and made a rough estimate of 50% for the degree of ionic character for silver. Similarly GERISCHER (137) has estimated a partial ionic charge of 30 - 40% for silver.

Although rough estimates can be made on a theoretical basis it is difficult to envisage how experimental data can distinguish between the two cases. There is little difference between the concept of a neutral atom on the surface and a partially ionic species associated with an elec-

tron in the surface. The estimates available indicate that the ionic character is not total and it may therefore vary according to the environment of the adspecies on the surface.

12.4. THE OVERALL ELECTRODE PROCESS

Two overall mechanisms have been suggested. The first scheme may be considered as the following steps:

a) Ion in double layer
b) Diffusion through solution
c) Ion in double layer opposite kink site in lattice
d) Charge transfer at kink
e) Adspecies at kink site.

The second type of overall scheme may be considered as follows:

a) Ion in double layer
b) Charge transfer to planar surface
c) Adspecies at surface
d) Diffusion across surface
e) Adspecies at kink.

Considerable evidence (138) has been presented to support the mechanism involving diffusion on the surface. However, it should be noted that this latter process in many circumstances is not rate controlling. A mechanism involving movement on the surface to a kink site would result

in the hydration sheath of the discharged species being discarded in stages whereas direct transfer to a kink site would necessitate a major loss of associated water molecules in one stage. In the present work the second scheme is confirmed. The presence of relaxation in the impedance data results from the movement of adatoms on the surface. Values of the observed Warburg coefficients in the present experiments were somewhat larger than the calculated theoretical values. This observation supports the surface diffusion mechanism. There may be certain crystal faces on the surface which are unfavourable as sites for transfer and this results in the observed difference in values of the Warburg coefficient. If the diffusion in solution mechanism was considered then the experimental values of σ would be many times greater than the theoretical values since the number of kink sites on the surface would only represent a very small fraction of the total area.

12.5. SURFACE DIFFUSION OR DIRECT TRANSFER TO KINK SITES

The mean free path of the diffusion of atoms on the surface is given by the Einstein equation:

$$X_s = \left(D_s \tau_s\right)^{\frac{1}{2}} \qquad [43]$$

where D_s is the surface diffusion coefficient and τ_s is the mean lifetime of an adsorbed atom on the surface. The diffusion coefficient is given by:

$$D_s = d^2 \nu e^{-U_s/RT} \qquad [44]$$

where U_s is the activation energy between two neighbouring equilibrium positions on the surface at a distance d from each other, and υ is a frequency factor. VERMILYEA (139) has shown that τ_s is given by the equation:

$$\tau_s = a^{-(1-\alpha)}\, \upsilon^{-1} \exp \frac{\Delta Ga^*}{RT} \exp\left[\frac{-(1-\alpha)zF}{RT}\right]\eta \qquad [45]$$

where a is the activity of ions in solution and ΔGa^* is the free energy of activation for anodic charge transfer. If the mean free path for surface diffusion, X_s, is much greater than the distance between kink sites, X_o, then surface diffusion will not be rate controlling since other processes in the overall exchange will be slower. If $X_s \ll X_o$, again surface diffusion will not be the rate controlling process and direct charge transfer to a kink site may become energetically more favourable. BURTON, CABRERA and FRANK (140) have shown that for the case of a metal in contact with vapour:

$$X_o = \frac{d}{2} e^{\frac{\Delta Gv}{RT}} \qquad [46]$$

where ΔGv is the free energy of activation for vaporisation of the metal.

Values of X_s and X_o may therefore be compared in order to predict whether the mechanism of the overall electrode reaction involves surface diffusion. It should be noted however that the only data available for estimating both X_s and X_o apply to solid metal/vapour interphases. Thus any conclusions must therefore be qualitative. An estimate of X_o

may be obtained from [46] using L_e, the heat of activation for evaporation of the metal.

Values of X_s can only be estimated approximately. Such values of D_s that are available (141) apply to metal/vapour systems for elevated temperatures only and may be estimated as ~ 10^{-10} to 10^{-12} cm^2 sec^{-1}. Clearly use of the diffusion coefficient for the metal ion in aqueous solution (~ 10^{-6} cm^2 sec^{-1}) is also unsatisfactory. In view of the probably partially hydrated state of the species involved it seems likely that the next suitable choice for D_s lies between these two values, i.e. ~10^{-8} cm^2 sec^{-1}. There is also difficulty in assessing a value for τ_s. Since

$$\tau_s = \frac{1}{\omega_{max}} \qquad [47]$$

the experiments in this investigation show that τ_s is ~ 10^{-4} - 10^{-5} sec. As a generalisation therefore X_s for most metals is likely to be ~ 100 - 1000 Å.

Table 19 shows a comparison for a wide range of metals of X_o (d is assumed to be ~ 1-2 Å) and X_s.

The data are also shown in diagram form on Figure 59.

In many cases, in view of the large degree of uncertainty in the estimations, X_s is of the same order as X_o and no conclusions can be made. It should be noted that many of the metals having $X_o >> X_s$ possess the body centred cubic crystal lattice.

In the ordered lattice the co-ordination number is 8; whereas for the hexagonal close packed and face centred cubic lattices the co-ordination number is 12. It is likely therefore that adatoms are less stable on

TABLE 19

Metal	Crystal Structure	L_e/kJ mol^{-1}	X_o	
Cd	h.c.p.	100	15 d	
Zn	h.c.p.	121	30 d	
Mg	h.c.p.	128	37 d	$X_o << X_s$
Tl	f.c.c.	167	140 d	
Bi	Rhom.	172	170 d	
Ag	f.c.c.	252	2.6×10^3 d	
Be	h.c.p.	310	2.7×10^4 d	
Au	f.c.c.	344	6×10^4 d	
Cu	f.c.c.	342	5.3×10^4 d	$X_o \sim X_s$
In	tetrag.	232	1.33×10^3 d	
Mn	cubic	232	1.26×10^3 d	
Sn	b.c.rect.	296	1.17×10^4 d	
Co	h.c.p.	425	9.2×10^5 d	
Cr	b.c.c.	400	3.4×10^5 d	
Fe	b.c.c.	400	3.77×10^5 d	
Mo	b.c.c.	590	2.5×10^8 d	$X_o >> X_s$
Ni	f.c.c.	376	1.66×10^5 d	
Pt	f.c.c.	500	1.29×10^7 d	
Re	h.c.p.	715	1.56×10^{10} d	
Rh	f.c.c.	715	1.56×10^{10} d	
V	b.c.c.	460	2.8×10^6 d	

the b.c.c. metals, i.e. they have a much lower co-ordination number.

However, there is no data available for the simple exchange processes, Me/Me^{z+}, for these metals. The majority of reported investigations have been concerned with active-passive transitions.

FIG. 59 Schematic representation of X_0 for some metals.

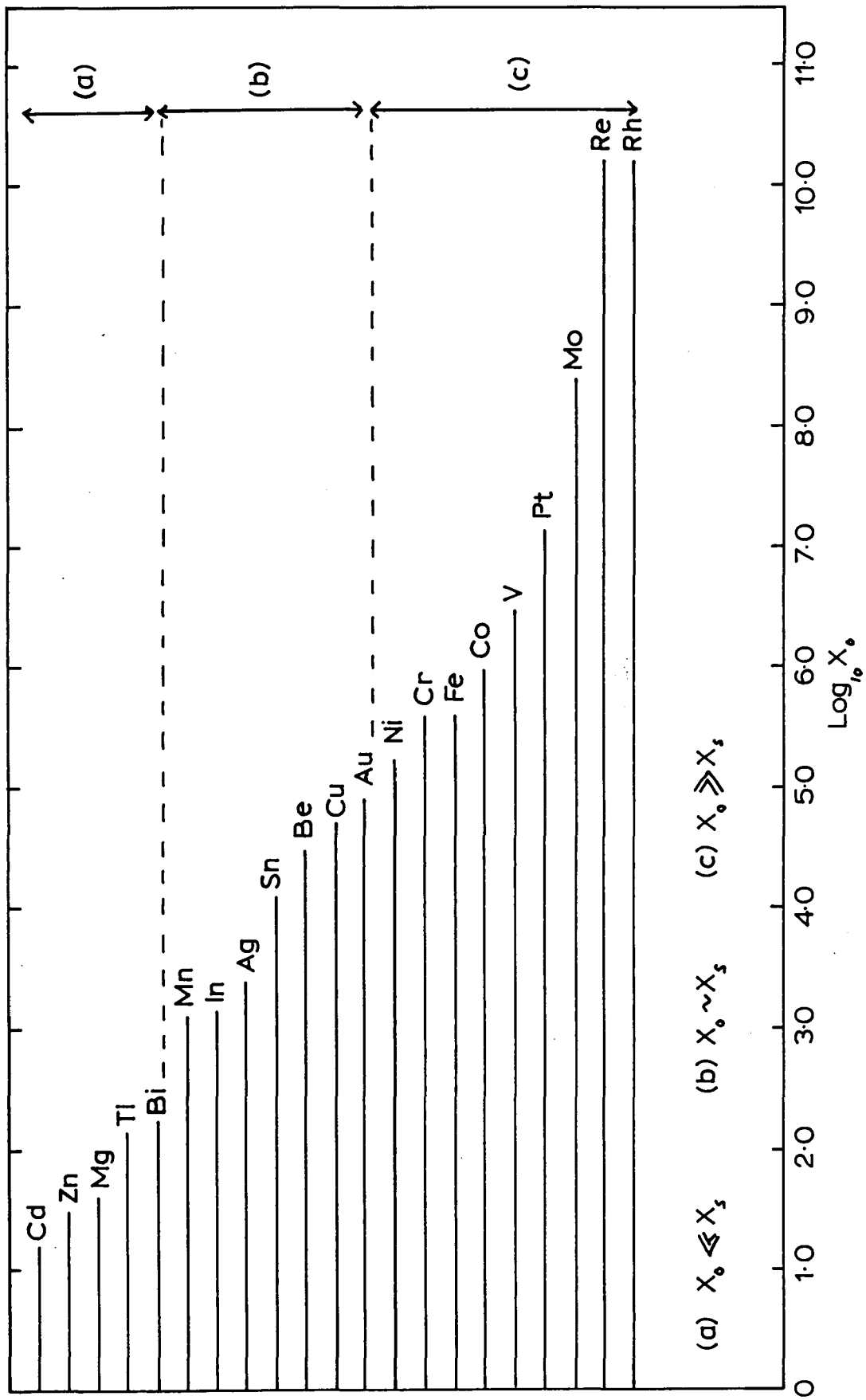

This may also explain why manganese shows as a discrepancy in Table 19. An experimental investigation by HEUSLER and BERGMANN (142) has shown that the exchange process at a solid manganese electrode proceeds directly via the kink sites whereas estimations of X_s and X_o indicate that surface diffusion possibly occurs. Manganese however, has a simple cubic structure, co-ordination number 6, and adatoms would be less stable than ever in the case of b.c.c. metals.

12.6. FURTHER WORK

1. The investigation of the copper electrode system should be extended to commercially more significant systems. The effect of organic additives on the structure of the double layer and on the electrode processes should be investigated.

2. As consequence of the investigation of the double layer structure at polycrystalline cadmium, the kinetics of the Cd/Cd(II) exchange in NaF electrolyte should be studied.

3. There is clearly a gap in the literature with respect to the exchange processes at metal having the b.c.c. structure. It would be extremely interesting to investigate these metals with particular attention to the possibility of the exchange process occurring via adspecies.

REFERENCES

1. A.N. FRUMKIN and M.A. PROSKURNIN, Trans. Faraday Soc., 31 (1935) 110.
2. A.N. FRUMKIN, J. Electrochem. Soc., 107 (1960) 461.
3. A.N. FRUMKIN, Svensk. Kemisk Tidschrift, 77 (1965) 300.
4. A.N. FRUMKIN, J. Res. Inst. Catalysis, Hokkaido Univ., 15 (1967) 61.
5. D. LARKIN, Ph.D Thesis, Loughborough Univ., (1968).
6. H. HELMHOLTZ, Wied. Ann., 7 (1879) 377.
7. A. GOUY, J. Phys., 9 (1910) 457.
8. D.L. CHAPMAN, Phil. Mag., 25 (1913) 475.
9. O. STERN, Zeit. Elektrochem., 30 (1924) 508.
10. D.C. GRAHAME, Chem. Rev., 41 (1947) 441.
11. D.C. GRAHAME, J. Amer. Chem. Soc., 71 (1949) 2975.
12. D.C. GRAHAME, J. Chem. Phys., 18 (1950) 903.
13. S. LEVINE, G.M. BELL and D. CALVERT, Can. J. Chem., 40 (1962) 518.
14. C.A. BARLOW and J.R. MACDONALD, "Advances in Electrochemistry and Electrochemical Engineering, Vol. 6", Ed. P. DELAHAY, Interscience, New York, (1967) p.1.
15. R. PARSONS, 2nd Australian Conference on Electrochemistry, Butterworths (1970) p.23.
16. T. ERDEY-GRUZ and M. VOLMER, Zeit. Physik. Chem., 150A (1930) 203.
17. J. HORIUTI and M. POLANYI, Acta Physicochim. U.S.S.R., 52 (1935) 505.
18. J. TAFEL, Zeit. Physik. Chem., 50 (1905) 641.
19. R.A. MARCUS, J. Phys. Chem., 67 (1963) 853.
20. K.J. VETTER, Zeit. Physik. Chem., 194 (1956) 284.

21. J.E.B. RANDLES, Disc. Faraday Soc., 1 (1947) 11.

22. E. WARBURG, Ann. Physik, 67 (1899) 493.

23. H. GERISCHER, Zeit, Physik. Chem., 158 (1951) 286.

24. H. GERISCHER, Zeit. Physik. Chem., 201 (1952) 55.

25. W. LORENZ, Zeit. Physik. Chem., 19 (1959) 377.

26. M. FLEISCHMANN, S.K. RANGARAJAN and H.R. THIRSK, Trans. Faraday Soc., 63 (1967) 1251.

27. M. FLEISCHMANN, S.K. RANGARAJAN and H.R. THIRSK, Trans. Faraday Soc., 63 (1967) 1256.

28. A. BEWICK and H.R. THIRSK, "Modern Aspects of Electrochemistry, No. 5", Ed. J. O'M. BOCKRIS and B.E. CONWAY, Butterworths, London, (1969), Ch. 4.

29. S.K. RANGARAJAN, J. Electroanal. Chem., 17 (1968) 61.

30. J.H. SLUYTERS, Recueil, 79 (1960) 1092

31. R. de LEVIE, Electrochim. Acta., 10 (1965) 395.

32. R. de LEVIE and L. POSPISIL, J. Electroanal. Chem., 22 (1969) 277.

33. W.A. ROITER, E.S. POLUJAN and W.A. JUZA, Acta Physicochim., U.S.S.R., 10 (1939) 389.

34. W.A. ROITER, E.S. POLUJAN and W.A. JUZA, Acta Physicochim., U.S.S.R., 10 (1939) 845.

35. L. GIERST and A.L. JULIARD, J. Phys. Chem., 57 (1953) 701.

36. P. DELAHAY and T. BERZINS, J. Amer. Chem. Soc., 75 (1953) 2486.

37. W. LORENZ, Zeit. Elektrochem., 58 (1954) 912.

38. H.J.B. SAND, Zeit. Physik. Chem., 35 (1900) 641.

39. Z. KARAOGLANOFF, Zeit. Elektrochem., 12 (1906) 5.

40. T. BERZINS and P. DELAHAY, Zeit. Elektrochem., 59 (1955) 792.

41. H. GERISCHER, Zeit Elektrochem., 59 (1955) 604.

42. H. GERISCHER, Anal. Chem., 31 (1959) 33.

43. H. GERISCHER and M. KRAUSE, Zeit. Physik. Chem., 10 (1957) 264.

44. S. GLASSTONE, K.J. LAIDLER and H. EYRING, "The Theory of Rate Processes", McGraw-Hill, New York, (1941) Chap. 10.

45. M.I. TEMKIN, Zhur. Fiz. Khim., 22 (1948) 1081.

46. G. BARKER, "Modern Electroanalytical Methods", Ed. G. CHARLOT, Elsevier, Amsterdam (1958).

47. B. HAGUE, "Alternating Current Bridge Methods", Pitman, London, (1962), Chap. 4.

48. J.E.B. RANDLES, Trans. Faraday Soc., 50 (1954) 1246.

49. H.A. LAITINEN and J.E.B. RANDLES, Trans. Faraday Soc., 51 (1955) 54.

50. E.A. UKSHE and A.I. LEVIN, Dokl. Akad. Nauk SSSR, 105 (1955) 119.

51. D.N. STAICOPOLUS, J. Electrochem. Soc., 108 (1961) 900.

52. B. JAKUSZEWSKI and Z. KOZLOWSKI, Roczniki Chem., 36 (1962) 1873.

53. B. JAKUSZEWSKI and Z. KOZLOWSKI, Lodz. Towarz. Nauk., Wydzial III, Acta. Chim., 9 (1964) 25.

54. A.I. LEVIN, E.A. UKSHE and N.S. BRILINA, Dokl. Akad. Nauk. SSSR, 88 (1953) 697.

55. M. BONNEMAY, G. BRONOEL, P.J. JONVILLE and E. LEVANT, Compt. Rend., 260 (1965) 2562.

56. M.A.V. DEVANATHAN and B.V. TILAK, Chem. Rev., 65 (1965) 635.

57. P.J. HILLSON, Trans. Faraday Soc., 56 (1954) 385.

58. J. O'M BOCKRIS and B.E. CONWAY, J. Chem. Phys., 28 (1958) 707.

59. I.M. PEARSON and G.F. SCHRADER, Electrochim. Acta, 13 (1968) 2021.

60. R. de LEVIE, J. Chem. Phys., 47 (1967) 2509.

61. R. PAYNE, J. Electroanal. Chem., 19 (1968) 1.

62. G.M. DERIAZ, Ph.D. Thesis, Birmingham University (1951)

63. W. LORENZ, Zeit. Physik. Chem., 19 (1959) 377.

64. Z.A. TKACHIK, K.M. GORBUNOVA and E.S. SEVAST'YANOV, Elektrokhimiya, 5 (1969) 351.

65. S.I. BREZINA, N.V. GUDIN and R.L. AKHMETOVA, Elektrokhimiya, 5 (1969) 1481.

66. Z.A. TKACHIK, K.M. GORBUNOVA, and E.S. SEVAST'YANOV, Elektrokhimiya, 5 (1969) 1125.

67. O.R. BROWN and H.R. THIRSK, Electrochim. Acta, 10 (1965) 383.

68. A. ICHIKAWA and S. HARUYAMA, J. Electrochem. Soc., Japan, 34 (1966) 21

69. S. HARUYAMA, J. Electrochem. Soc., Japan., 34 (1966) 85

70. E. MATTSSON and J. O'M BOCKRIS, Trans. Faraday Soc., 55 (1959) 1586.

71. J. O'M BOCKRIS and H. KITA, J. Electrochem. Soc., 109 (1962) 928.

72. J. O'M BOCKRIS and M. ENYO, Trans. Faraday Soc., 58 (1962) 1187.

73. H. SEITER and H. FISCHER, Zeit. Elektrochem., 63 (1959) 2491.

74. E. MATTSSON and R. LINDSTROM, C.I.T.C.E. VI, (1954) Butterworths, London, (1955), 263.

75. T. HURLEN, Acta Chem. Scand., 15 (1961) 630.

76. H.H. BAUER, J. Electroanal. Chem., 16 (1968) 419.

77. G.W. TINDALL and S. BRUCKENSTEIN, Anal. Chem., 40 (1968) 1051.

78. G.W. TINDALL and S. BRUCKENSTEIN, Anal. Chem., 40 (1968) 1402.

79. G.W. TINDALL and S. BRUCKENSTEIN, Anal. Chem., 40 (1968) 1637.

80. M.W. BREITER, Trans. Faraday Soc., 65 (1969) 2197.

81. S.C. BARNES, G.G. STOREY and H.J. PICK, Electrochim. Acta, 2 (1960) 195

82. T. HURLEN, Acta Chem. Scand., 15 (1961) 621.

83. M.C. SNEED, J.L. MAYNARD and R.C. BRASTED, "Comprehensive Inorganic Chemistry", D. Van Nostrand Co., New York, (1954) p.65.

84. F.A. COTTON and G. WILKINSON, "Advanced Inorganic Chemistry", Interscience Pub., New York, London, 2nd ed., (1966) p.206.

85. K.I. MACDONALD, Unpublished Data.

86. B.E. CONWAY, E. GILEADI, H. ANGERSTEIN-KOZLOWSKA, J. Electrochem. Soc., 112 (1965) 341.

87. T.I. BORISOVA and B.V. ERSHLER, Zhur. Fiz. Khim., 24 (1950) 337.

88. T.I. BORISOVA, B.V. ERSHLER and A.N. FRUMKIN, Zhur. Fiz. Khim., 22 (1948) 925.

89. N.A. HAMPSON and D. LARKIN, J. Electrochem. Soc., 114 (1967) 933.

90. V. Ya. BARTENEV, E.S. SEVAST'YANOV and D.I. LEIKIS, Elektrokhimiya, 4 (1968) 745.

91. V. Ya. BARTENEV, E.S. SEVAST'YANOV and D.I. LEIKIS, Elektrokhimiya, 5 (1969) 1491.

92. V. Ya. BARTENEV, E.S. SEVAST'YANOV and D.I. LEIKIS, Elektrokhimiya, 5 (1969) 1502.

93. R.J. BRODD, J. Res. Nat. Bur. Std., 65A (1961) 275.

94. K.E. HEUSLER and L. GAISER, J. Electrochem. Soc., 117 (1970) 762.

95. T.A. EDISON, British Pat., 20906 (1900).

96. J.T. CRENNEL and F.M. LEA, "Alkaline Accumulators", Longmans, Green and Co., London (1928).

97. S.A. ROZENTSVEIG, B.V. ERSHLER, E.L. STRUM and M.M. OSTANIA, Trudy. Soveshehaniya Elektrokhim. Akad. Nauk., S.S.S.R., Otdel. Khim. Nauk., 1950 (1953) 571.

98. K. HUBER, J. Electrochem. Soc., 100 (1953) 376.

99. P.E. LAKE and E.J. CASEY, J. Electrochem. Soc., 105 (1958) 52.

100. E. LANGE and R. OHSE, Naturwiss., 45 (1958) 437.

101. G.J. CROFT, J. Electrochem. Soc., 106 (1959) 278.

102. R. OHSE, Zeit. Elektrochem., 64 (1960) 1171.

103. S.U. FALK, J. Electrochem. Soc., 107 (1960) 661.

104. S. YOSHIZAWA and Z. TAKEHARA, Electrochim. Acta., 5 (1961) 240.

105. A.J. SALKIND and J.C. DUDDY, J. Electrochem. Soc., 109 (1962) 356.

106. M.W. BREITER and J.L. WEININGER, J. Electrochem. Soc., 113- (1966) 651.

107. M. FLEISCHMANN, K.S. RAJAGOPOLAN and H.R. THIRSK, Trans. Faraday Soc., 59 (1963) 741.

108. Y. OKINAKA, Ext. Absr. Battery Div. Electrochem., Soc., 11 (1966) 129.

109. M.W. BREITER and W. VEDDER, Trans. Faraday Soc., 63 (1967) 1042.

110. R.D. ARMSTRONG, E.H. BOULT, D.F. PORTER and H.R. THIRSK, Electrochim. Acta., 12 (1967) 1245.

111. J.P.G. FARR and N.A. HAMPSON, Electrochem. Technology, 6 (1968) 10.

112. M.A.V. DEVANATHAN and S. LAKSHMANAN, Electrochim. Acta., 13 (1968) 667.

113. Y. OKINAKA, J. Electrochem. Soc., 117 (1970) 289.

114. L.A. L'VOVA, D.K. GRACHEV and V.A. PANIN, Elektrokhimiya, 5 (1969) 627.

115. A. HAMELIN and G. VALETTE, Compt. Rend. 269C (1969) 1020.

116. Ya. KOLOTYRKIN, C.I.T.C.E. IX, (1958), Butterworths, London, p.406 Trans. Faraday Soc., 55 (1959) 455.

117. J.P.G. FARR and N.A. HAMPSON, J. Electroanal. Chem., 13 (1967) 433.

118. N.A. HAMPSON and D. LARKIN, J. Electroanal. Chem., 18 (1968) 401.

119. J.T. CLARK and N.A. HAMPSON, J. Electroanal. Chem., 26- (1970) 307.

120. N.A. HAMPSON, Unpublished data.

121. "Stability Constants", Special Publication, No. 17, The Chemical Society, (1964).

122. H. GERISCHER, Zeit, Physik. Chem., 202 (1953) 302.

123. L. RAMALEY and C.G. ENKE, J. Electrochem. Soc., 112 (1965) 947.

124. W.D. COOPER and R. PARSONS, Trans. Faraday Soc., 66 (1970) 1698.

125. J.P.G. FARR and N.A. HAMPSON, Electrochem. Technology, 6 (1969) 10.

126. J.E.B. RANDLES, Trans. Faraday Soc., 48 (1952) 828.

127. N.S. HUSH, J. Chem. Phys., 28 (1958) 962.

128. R.A. MARCUS, Can. J. Chem., 37 (1959) 155.

129. R.A. MARCUS, Ann. Rev. Phys. Chem., 15 (1964) 155.

130. R.A. MARCUS, Electrochim Acta., 13 (1968) 995.

131. V.G. LEVICH, "Advances in Electrochemistry and Electrochemical Engineering, Vol. 4," ed. P. DELAHAY, Interscience, New York, London, (1966), Chap. 5.

132. J. O'M BOCKRIS, "Proc. First Australian Conference on Electrochemistry", ed. J.A. FRIEND and F. GUTMANN, Permagon, New York, London (1965), p.691.

133. K.J. VETTER, Zeit. Naturf., 7a (1952) 328.
Zeit. Naturf., 8a (1953) 823.

134. B.E. CONWAY, and J. O'M BOCKRIS, Electrochim. Acta, 3 (1961) 340.

135. N.F. MOTT and R.J. WATTS-TOBIN, Electrochim. Acta, 4 (1961) 79.

136. B.E. CONWAY and J. O'M BOCKRIS, Proc. Roy. Soc. London, 248 (1958) 394.

137. H. GERISCHER, Zeit. Elektrochem., 62 (1958) 256.

138. For review articles see:

a) J. O'M BOCKRIS and A. DAMJANOVIC, "Modern Aspects of Electrochemistry, Vol. 3", ed. J. O'M BOCKRIS and B.E. CONWAY, Butterworths, London (1964), p.224.

b) J. O'M BOCKRIS and G. RAZUMNEY, "Fundamental Aspects of Electrocrystallisation", Plenum Press, New York, (1967).

138. c) A. BEWICK and H.R. THIRSK, "Modern Aspects of Electrochemistry, Vol. 5", ed. J. O'M BOCKRIS and B.E. CONWAY, Butterworths, London (1969), p.291.

139. D.A. VERMILYEA, J. Chem. Phys., 25 (1956) 1254.

140. K. BURTON, N. CABRERA and F.C. FRANK, Phil. Trans., A 243 (1951) 299.

141. See for example: C. SMITHELLS, "Metals Reference Book", Butterworths, London (1967).

142. K.E. HEVSLER and M. BERGMANN, Electrochim. Acta., 15 (1970) 1887.

143. R. PARSONS, "Modern Aspects of Electrochemistry, No. 1", ed. J. O'M BOCKRIS and B.E. CONWAY, Butterworths, London (1954), Chapter 3.

144. J. O'M BOCKRIS, S.D. ARGADE and E. GILEADI, Electrochim. Acta, 14, (1969) 1259.

145. R.S. PERKINS and T.N. ANDERSEN, "Modern Aspects of Electrochemistry, No. 5", ed. J. O'M BOCKRIS and B.E. CONWAY, Butterworths, London (1969), Chapter 3.

146. N.A. HAMPSON and D. LARKIN, Electrochim. Acta, 15- (1970) 581.

147. H. WU and C. LIN, Hua Hsueh Hsueh Pao, 29 (1963) 95.

148. R.A. ALEKSEEVA, V.A. KUZNETSOV and M.I. TALANOVA, Elektrokhimiya, 4 (1968) 95.

149. M. POURBAIX, "Atlas of Electrochemical Equilibria in Aqueous Solutions Pergamon, London, New York, (1966) p.52.

150. A.J. BETHUNE and N.A.S. LOUD, "Encyclopaedia of Electrochemistry", ed. C.A. HAMPEL, Reinhold Pub., New York, (1964).

151. H.E. HARING and K.G. COMPTON, Trans. Electrochem. Soc., 68 (1935) 283

152. H.W. SALZBERG and A.J. ANDREATCH, J. Electrochem. Soc., 101 (1954) 528

LIST OF SYMBOLS

C_L	total double layer capacitance
$C_{diff.}$	diffuse layer capacitance
$C_{comp.}$	compact layer capacitance
C_d	capacitive component of faradaic impedance due to diffusion in solution
C_K	capacitive component of faradaic impedance due to adatom flux
C_R	equivalent capacitive component of faradaic impedance
C_{ads}	adsorption capacitance
C_{xs}	experimental capacitive component in measured series combination
D_i	diffusion coefficient of species i
D_s	surface diffusion coefficient
E_z	potential of zero charge
E_R	rational potential
F_o	standard adatom flux
ΔH_D	enthalpy of activation for charge transfer
ΔH_K	enthalpy due to total crystallisation process
ΔH_{ad}	enthalpy of adsorption of adatoms
ΔH_{diff}	enthalpy of activation for diffusion of adatoms on the surface
I_o	standard exchange current
R_E	resistance of electrolytic system
R_D	resistance component of faradaic impedance due to charge transfer
R_d	resistive component of faradaic impedance due to diffusion in solution

R_k	resistive component of faradaic impedance due to adatom flux
R_R	equivalent resistive component of faradaic impedance
R_{xs}	experimental resistive component in measured series combination
V_g^o	adatom flux
X_s	mean free path for surface diffusion
X_o	mean path between kink sites
d	atomic diameter, distance of closest approach, jump distance for adatom diffusion
i	current density
i_o	exchange current density
i_a	anodic current density
i_c	cathodic current density
	electrode charge
α	charge transfer coefficient
Δ	difference between in-phase and out-of-phase component of faradaic impedance
η_D	charge transfer overpotential
η_Ω	ohmic overpotential
η_d	overpotential due to diffusion in solution
σ	Warburg coefficient
Γ_o	surface adatom population
ω	angular frequency
τ_s	mean lifetime of adatoms on surface
υ	surface vibrational frequency

APPENDIX 1

ANALYSES OF ELECTROLYTES

PREPARATION OF CHARCOAL

A.1. (a) Analysis For Cadmium in $NaClO_4$ Electrolyte

A known volume of electrolyte was diluted to 50 ml and buffered to pH 10. The solution was then titrated with a standard solution of the disodium salt of E.D.T.A. using Erichrome Black indicator. The end point was detected as a colour change from purple to a clear blue.

A.1. (b) Analysis For Cadmium in NaOH Electrolyte

A known volume of the electrolyte was taken and then neutralised using H_2SO_4. The concentration of cadmium was then established polarographically using a Cambridge Polarograph.

A.1. (c) Analysis For Copper

10 - 20 ml of the copper solution was buffered to pH 10 dropwise until the solution colour turned to blue and the precipitate first formed had dissolved. The solution was then diluted to 50 ml. The solution was then titrated against a standard solution of the disodium salt of E.D.T.A. using Murexide indicator. The end point was detected as a colour change from yellow-green to deep violet.

A.1. (d) Analysis of Perchlorate, Nitrate and Fluoride Electrolytes

In all cases the sodium (or potassium) content was determined and the anion concentration then determined.

A series of standards (of the appropriate electrolyte) in the range 5 - 50 p.p.m. was made up. Using a flame photometer (E.E.L.) a calibration graph was constructed. The electrolyte to be analysed was diluted to about 25 p.p.m. and the concentration thus determined.

A.1. (e) Analysis of Sulphuric Acid and Sodium Hydroxide Electrolytes

Electrolytes were analysed by conventional acid - base titration methods.

A.1. (f) Preparation of Charcoal

Granular gas adsorption charcoal was extracted in a Soxhlet apparatus with constant boiling hydrochloric acid. The acid was changed weekly and the extraction was continued until the acid remained colourless. Generally this procedure took about 3 months. The charcoal was then washed with water (also replaced weekly) until the washings showed no positive test for chloride ion.

APPENDIX 2

SERIES-PARALLEL CIRCUIT TRANSFORMATIONS

COMPUTOR PROGRAM FOR CIRCUIT TRANSFORMATIONS

Successive series parallel circuit transformations used for computation of faradaic impedance components.

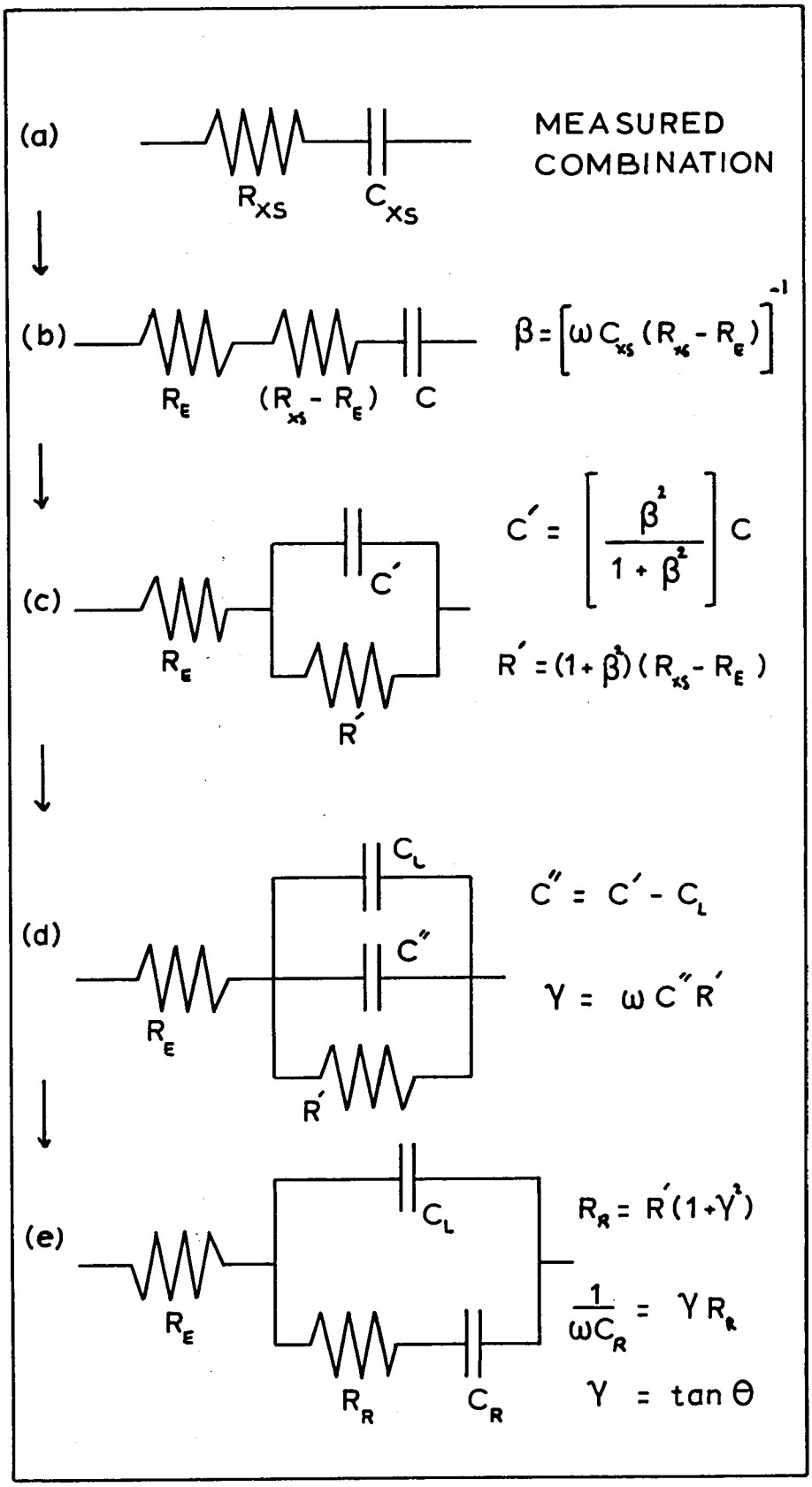

```
    SHORT LIST
    SEND TO 'ED,ICLA-DEFAULT.AXXX=
    PROGRAM'H075=
    INPUT1,CR0
    OUTPUT2,LP0
    TRACE 0
    END
    MASTER COMPUTATION
    REAL LOGF
    DIMENSION F1'50=, RXS1'50=, CXS1'50=
101 READ '1,20=      N
 20 FORMAT'I4=
 25 DO 21 K,1,N
201 READ '1,202=     M,NHEAD
202 FORMAT'2I4=
204 DO 900I,1,M
105 READ '1,1=       F1'I=, RXS1'I=, CXS1'I=
  1 FORMAT 'F4.0,F8.1,E11.4=
900 CONTINUE
    DO 901 J,1,NHEAD
103 READ '1,2=       RC,CL
  2 FORMAT 'F6.1,E11.5=
 26 WRITE'2,3=       RC,CL
  3 FORMAT  '6H RC , F7.1,5X5HCL , E12.5=
    WRITE'2,40=
 40 FORMAT  '///2X1HF7X3HRXS10X3HCXS10X4HBETA5X5HGAMMA6X2HRR8X2HGR7X3HR
   1RW//=
    CON1,2.*3.1415926
    DO 10 I,1,M
    RXS,RXS1'I=
    CXS,CXS1'I=
    F,F1'I=
    RA,RXS-RC
    W,CON1*F
    IF'W*CXS*RA=45,10,45
 45 BETA,1./'W*CXS*RA=
    T1,BETA*BETA
    T2,1.+T1
    RDASH,T2*RA
    CDASH,T1/T2*CXS
    C2DASH,CDASH-CL
    GAMMA,W*C2DASH*RDASH
    RR,RDASH/'1.+GAMMA*GAMMA=
    GR,GAMMA*RR
    RRW,1./SQRTF'W=
    WRITE'2,5=       F,RXS,CXS,BETA,GAMMA,RR,GR,RRW
  5 FORMAT'F7.0,2XF8.1,2XE12.4,1XF9.4,1XF8.4,1XF9.1,1XF10.4,1XF9.6=
```

```
   10 CONTINUE
      WRITE(2,300)
  300 FORMAT (1H1)
  901 CONTINUE
   21 CONTINUE
      STOP
      END
      FUNCTION EXPF(X)
      EXPF=EXP(X)
      RETURN
      END
      REAL FUNCTION LOGF(X)
      LOGF=ALOG(X)
      RETURN
      END
      FUNCTION ABSF(X)
      ABSF=ABS(X)
      RETURN
      END
      FUNCTION SQRTF(X)
      SQRTF=SQRT(X)
      RETURN
      END
      FUNCTION SINF(X)
      SINF=SIN(X)
      RETURN
      END
      FUNCTION COSF(X)
      COSF=COS(X)
      RETURN
      END
      FUNCTION ATANF(X)
      ATANF=ATAN(X)
      RETURN
      END
      FINISH
```

APPENDIX 3

THE DIFFERENTIAL CAPACITANCE OF POLYCRYSTALLINE ANTIMONY IN AQUEOUS SOLUTION

The structures of certain electrode/electrolyte interphases have been correlated with the properties of the electrode materials (3,4, 143-146). It is clearly desirable to extend our knowledge to all types of electrode. Data has been slowly accumulating as a result of many investigations. However, there still exists a number of metals for which data is lacking. Antimony may be included among these.

WU and LIN (147) have reported differential capacitance results for antimony in 0.01 NHCl. Using an a.c. bridge method, at frequencies 1000 to 5000 Hz, they estimate the p.z.c. to be -0.19 $\pm$ 0.02 V (N.H.E.), which corresponded to a deep minimum in the C_L vs E curve. ALEKSEEVA et al (148) have also studied the differential capacitance of antimony-gallium alloys in a eutectic LiCl/KCl melt. At a frequency of 50 Hz, for antimony, a capacitance minimum of 30μ F cm^{-2} at -0.18 V was observed.

The antimony/aqueous solution interphase is complicated by oxide (or hydroxide) films under conditions of high pH, and even in acid solutions, oxide films may be present at positive potentials (149, 150). The following reactions are known to occur in acid solutions:

	Reaction	E_h^o	
SbH_3 (g) $\longrightarrow$	Sb + $3H^+$ + 3e	-0.51 V	[48]
$2Sb + 3H_2O \longrightarrow$	Sb_2O_3 + $6H^+$ + 6e	+0.152 V	[49]

$$Sb_2O_4 + H_2O \longrightarrow Sb_2O_5 + 2H^+ + 2e \qquad +0.479\ V \qquad [50]$$

$$2SbO^+ + 3H_2O \longrightarrow Sb_2O_5 + 6H^+ + 4e \qquad +0.581\ V \qquad [51]$$

It is therefore clear that the antimony/aqueous solution interphase may be studied in a small range of potential around 0.0 V (N.H.E.)

EXPERIMENTAL

The preparation of electrode and electrolytes has been described in Section 3.1. The electrical circuit has been described in Section 3.2. The electrolytic cell has been described in 5.1. (a).

Electrode Pretreatment

The electrode was mechanically polished on carborundum paper using bidistilled water as a lubricant, and the electrode freed from SiC particles by etching. Various chemical etches were used; a 5 sec etch in concentrated HCl or a 4 sec etch in concentrated HNO_3 were found to give reproducible results. Longer etches in HNO_3 and electropolishing in $HClO_4$ were found to produce a film on the electrode surface.

RESULTS

Figure 60 shows characteristic faradaic current vs potential curves for HNO_3, H_2SO_4 and H_3PO_4 electrolytes. This indicates an experimentally accessible polarisable region for H_2SO_4 and H_3PO_4 from -0.05 to

FIG. 60 Polycrystalline Sb.
Faradaic current-potential curves.

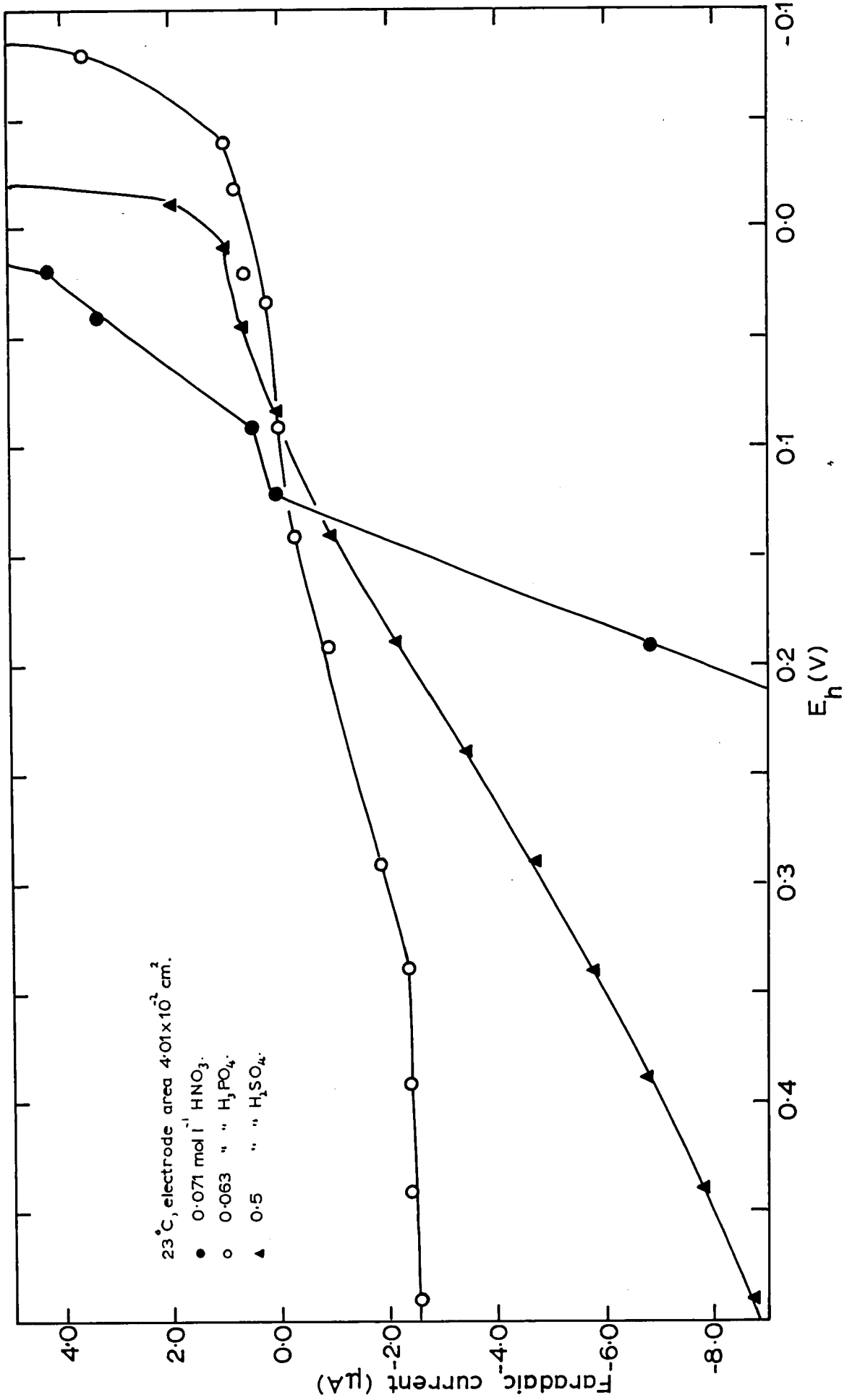

+0.4 V. For H_2SO_4 and H_3PO_4 electrolytes over the range +0.35 to 0.5 V there was little change in the curve before a significant increase in faradaic current density was observed. The curve for HNO_3 shows an initial increase in faradaic current; however, at more positive potentials the curve was similar to those observed for the other electrolytes. Experimentally it was found that stable impedance readings could be taken at potentials more negative than -0.05 V; the ultimate limit was defined by the process of gas evolution at ~ -0.5 V.

Chemically etched electrodes were generally satisfactory. Both HNO_3 and HCl (30%) gave consistent results, although for more dilute solutions there was evidence that stability was reached in a shorter period of time of electrode/electrolyte contact using HCl etches.

The times of electrode/electrolyte contact required to give stable values of electrode impedance for H_2SO_4 and H_3PO_4 electrolytes were from 2 h for the more concentrated solutions to $7\frac{1}{2}$ h for the more dilute solutions. Generally for HNO_3 electrolytes, less than half the time for H_2SO_4 and H_3PO_4 electrolytes was required to reach equilibrium.

Electrodes forced to potentials at the extremes of the experimental polarisable region (+0.3 to -0.45 V) required some time to revert to equilibrium. Hysteresis at the positive limit of potential was greater than at the negative limit; in both cases ~ 20 min was required for the impedance measurements to return to the initial values. Hysteresis became more pronounced in dilute solutions and the effect was particularly marked where capacitance changes were large for small deviations in potential.

Black-grey films were observed when the electrode was forced to potentials more positive than +0.3 V in relatively concentrated (~ 0.05 mol l^{-1}) H_2SO_4 electrolytes. Visible films were not observed in H_3PO_4

electrolytes and the more dilute H_2SO_4 electrolytes. Films were also produced in HNO_3 electrolytes; when the potential was forced to ~ 0.95 V a substantial film was observed (Figure 61).

Figures 62, 63 and 64 show typical differential capacitance curves for polycrystalline antimony in H_2SO_4, HNO_3 and H_3PO_4 electrolytes. The variation of R_E with potential is also shown for each electrolyte. A maximum in capacitance occurs in the range 0.05 to 0.15 V. A minimum is also observed from -0.05 to -0.25 V in all cases.

Some frequency dispersion was observed; however this was no more than expected for a polycrystalline metal surface.

DISCUSSION

Figure 60 indicates that in the experimentally accessible region the electrode behaviour is not ideal. Although the negative limit of the experimental region is well defined (sharp increase in faradaic current), it is difficult to decide the positive limit since no abrupt increase in the current density is observed.

A sharp peak is observed in the capacitance curves (Figures 62, 63 and 64) at ~ 0.1 V. This may be an adsorption peak preceding the formation of an antimony oxide, Sb_2O_3 (150). At these potentials, capacitances were observed to be unstable with time. This is consistent with the formation of a surface film and may account for the fact that the magnitude of the capacitance peak does not decrease with electrolyte concentration as expected, although the general shapes of the curves followed the expected trend.

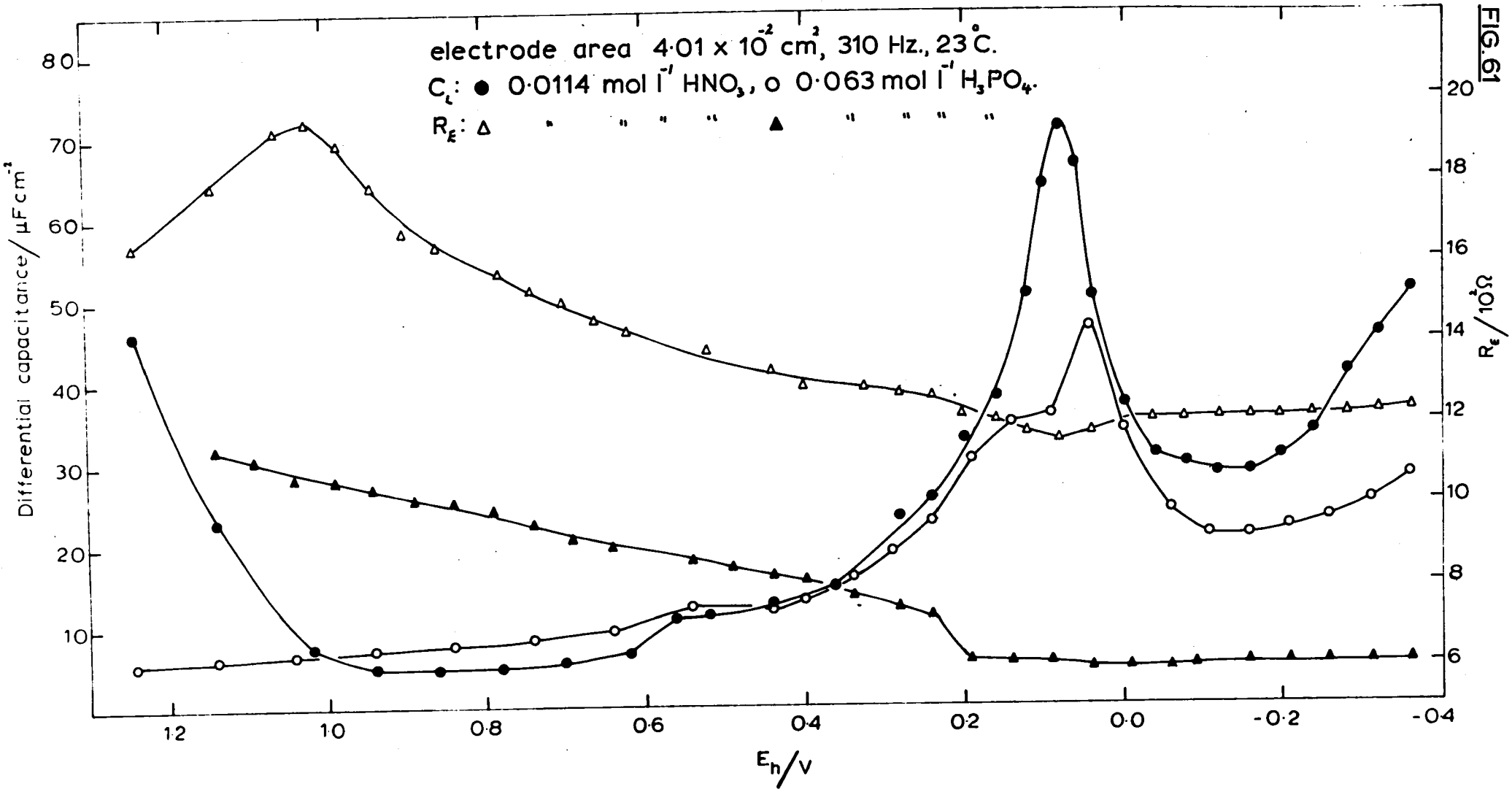
electrode area 4·01 x 10⁻² cm², 310 Hz., 23°C.
C_L: ● 0·0114 mol l⁻¹ HNO₃, o 0·063 mol l⁻¹ H₃PO₄.
R_E: Δ " " " " ▲ " " " "
Differential capacitance/μF cm⁻²
R_E/10³Ω
E_h/V
80
70
60
50
40
30
20
10
20
18
16
14
12
10
8
6
1·2
1·0
0·8
0·6
0·4
0·2
0·0
-0·2
-0·4

FIG. 61

FIG.62 Polycrystalline Sb in H_2SO_4.

Differential capacitance curves.

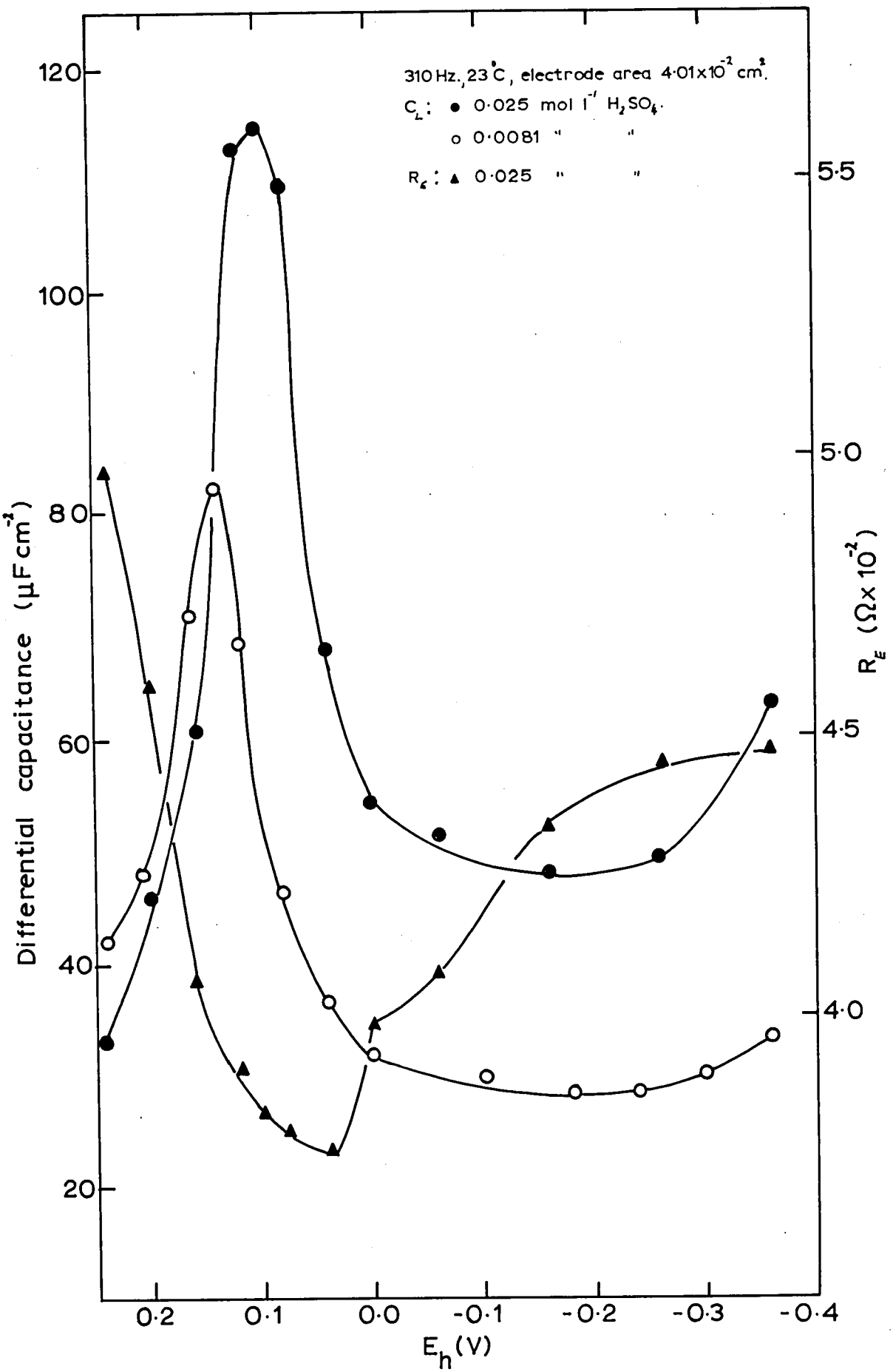

FIG.63 Polycrystalline Sb in HNO_3.
Differential capacitance curves.

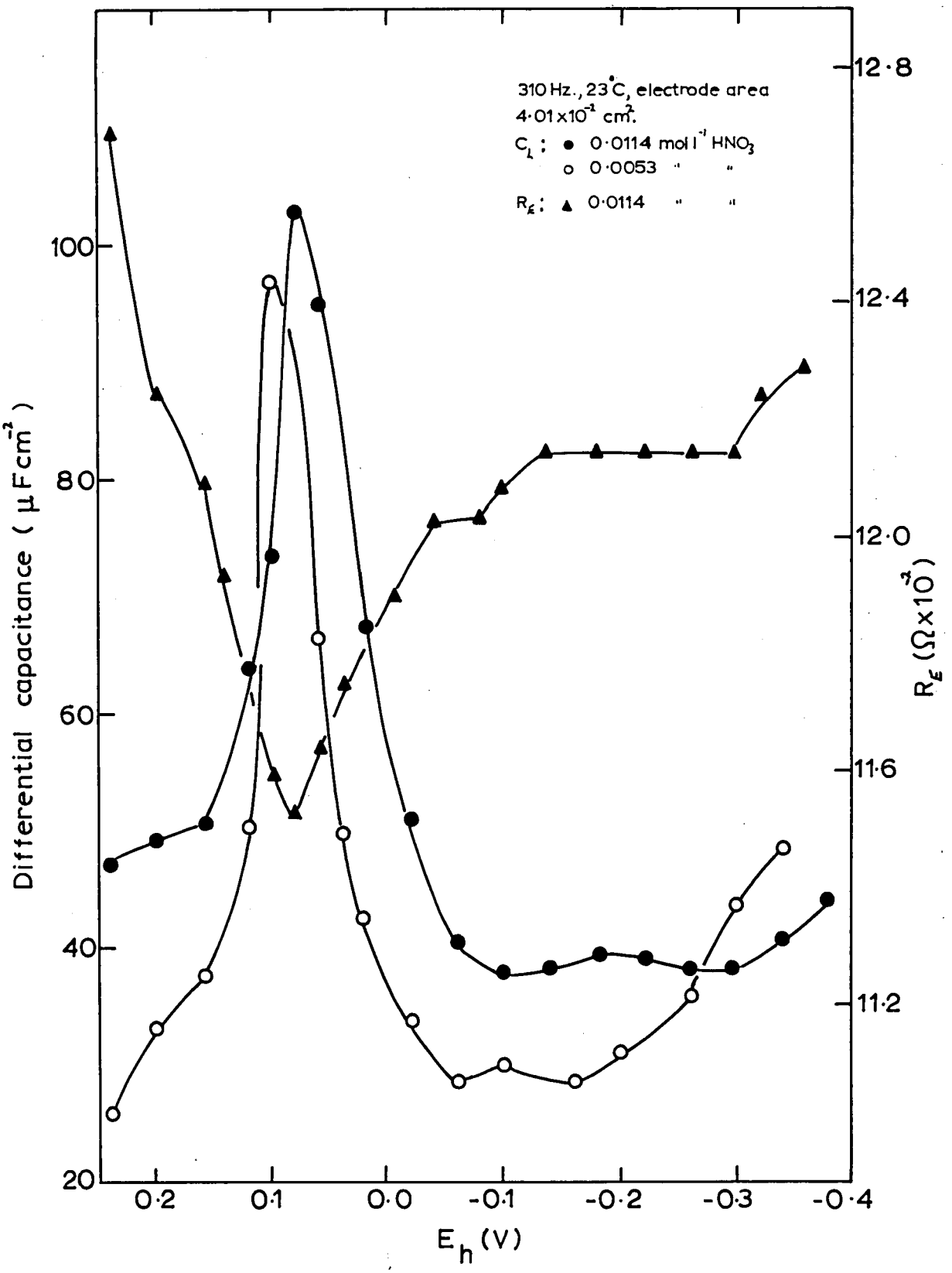

FIG. 64 Polycrystalline Sb in H_3PO_4.
Differential capacitance curves.

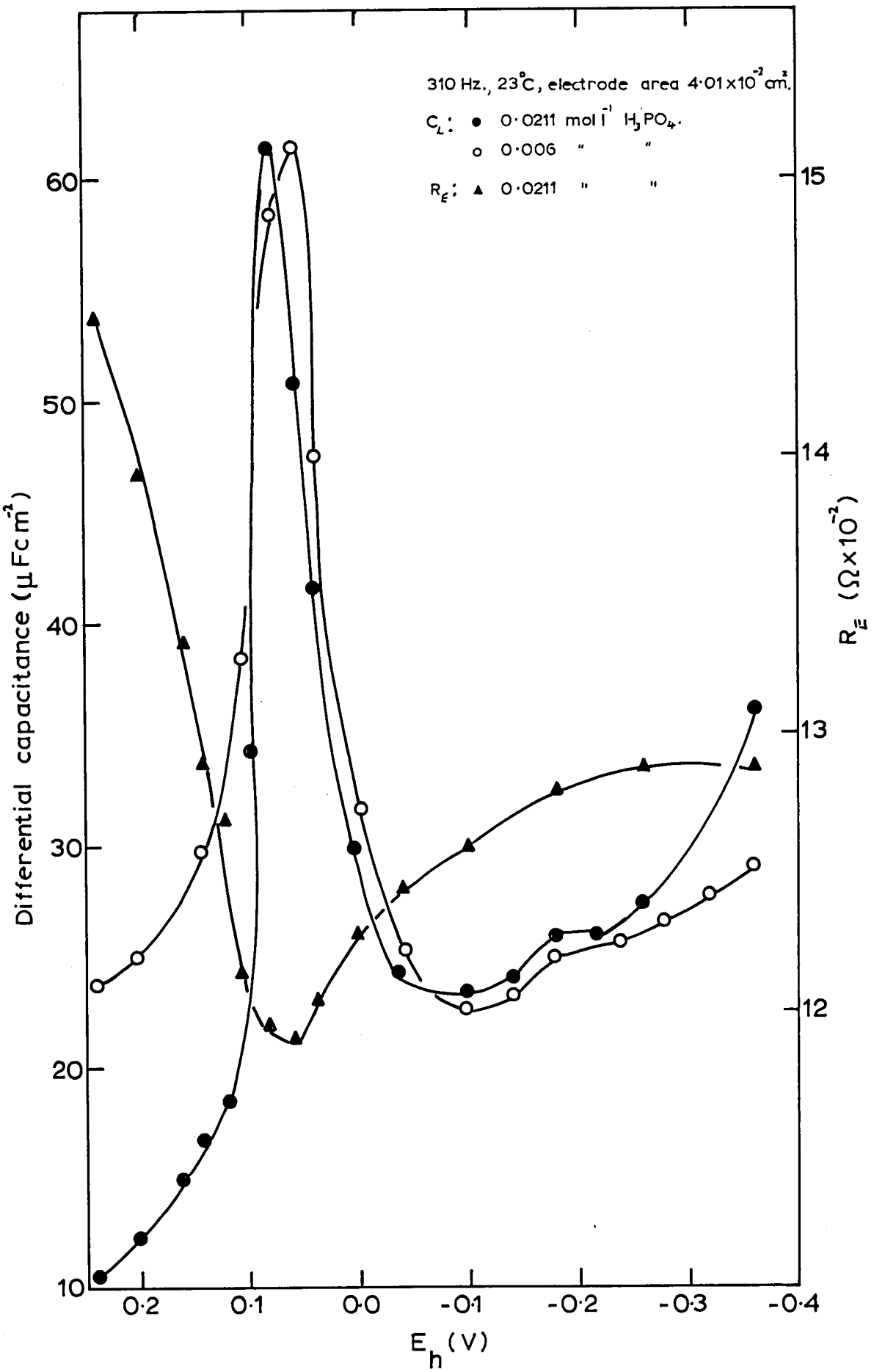

Studies of lead-acid battery systems (151, 152) have shown that stibine is evolved from antimony during cathodic polarisation at the potential corresponding to hydrogen evolution and occurs simultaneously with the process of hydrogen evolution. In all cases a rapid increase in capacitance is observed at -0.4 to -0.5 V and it is not possible to detect any change in electrode capacitance which could be ascribed to SbH_3 formation.

Previous work (147, 148) indicates that the p.z.c. should occur at ~ -0.18 V. In all capacitance curves observed a broad minimum was obtained. It is therefore likely, as discussed by FRUMKIN (2) that the p.z.c. is masked by a minimum which represents a transition from preferential anion to preferential cation adsorption. Consequently the p.z.c. can only be estimated as -0.15 ± 0.1 V.

It is interesting to note that only in HNO_3 electrolytes, at ~ 0.9 to 1.0 V the capacitance rises after a gradual decrease. Inspection of the electrode showed a substantial black film on the surface. This feature was not observed in H_2SO_4 and H_3PO_4 electrolytes. In these electrolytes the interphase may be complicated by adsorption to form complex species at the surface.